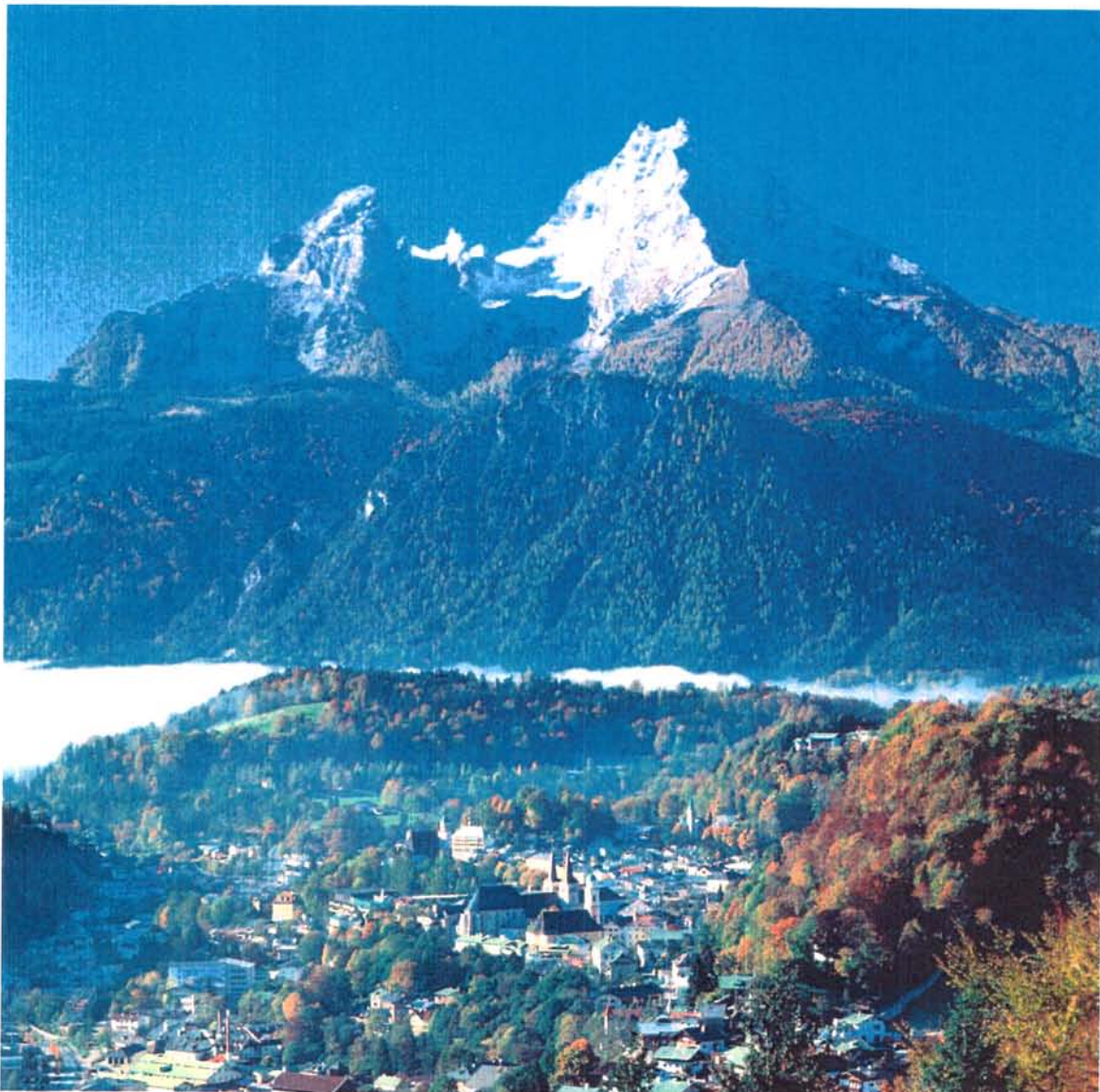Proceedings of the

5th INTERNATIONAL SYMPOSIUM ON VIBRATIONS OF CONTINUOUS SYSTEMS

Berchtesgaden at Lake Königssee, Germany
July 25-29, 2005

CONTENTS

Biographical Sketches

PREFACE

The International Symposium on Vibrations of Continuous Systems is a forum for leading researchers from across the globe to meet with their colleagues and present both old and new ideas on the field. Each participant has been encouraged to either present results of recent, significant research or to reflect on some aspect of the vibration of continuous systems which is particularly interesting, unexpected, or unusual. This latter type of presentation – of which there are several in the program – was proposed to encourage participants to draw on understanding obtained through – in many cases – decades of research.

The Fifth ISVCS takes place July 25-29, 2005. Its location is one of the most beautiful places in Germany – Lake Königssee in the heart of the Alpine National Park of Berchtesgaden. Here, one finds Germany's second highest mountain, Mount Watzmann at 2713 m, Germany's most picturesque lake with the Pilgrimage Church of St. Bartholomew, and many beautiful villages, with Berchtesgaden as the central one.

The Berchtesgaden area boasts some of the most stunning mountain panoramas in the German Alps. There are spectacular mountain gorges and inspiring mountain landscapes inviting the visitor to enjoyable longer hikes and nice shorter walks which are essentially level. The villages show local esprit with the typical German "Gemütlichkeit", while Mount Obersalzberg documents some history from the 1930's until the Second World War. The Eagle's Nest or Kehlsteinhaus gives the visitor an overwhelming panoramic view of the Berchtesgaden area.

These Proceedings contain 29 summaries of the presentations to be made at the Symposium and short biographical sketches submitted by many of the participants.

Editor
Ali H. Nayfeh

Reviewing Editors
Stuart Dickinson
Jim Hutchinson
Fred Williams
Jörg Wauer

General Chairman
Arthur W. Leissa

On Rotating Ring Dynamics: Instabilities under Harmonic Velocity Perturbation

Samuel F. Asokanthan[1*] and Jihyun Cho[2]

[1,2]Department of Mechanical and Materials Engineering,
The University of Western Ontario, London, ON, Canada, N6A 5B9

*Corresponding Author: Tel.: 1-519-661-2111 (ex.88907), Fax: 1-519-661-3020, E-mail: sasokanthan@eng.uwo.ca

Introduction

Dynamic stability behaviour of a rotating ring when subjected to harmonic perturbation in the input angular rate is investigated and closed form stability conditions are obtained via an analytical approach. Bickford and Reddy [1] investigated the problems concerned with in-plane vibrations of a rotating ring. In their study, effects of extensional and shear deformation and of rotary inertia on the natural frequency variations were investigated. For higher rotational speeds and for higher bending modes, the effects of shear deformation and rotary inertia were shown to be significant. Recently, Huang and Soedel [2] investigated the in-plane vibration behaviour of rotating rings. They performed a detailed study on the influence of rotational speed and an elastic support on the natural frequencies and mode shapes. In addition, a general solution for forced vibration was formulated. Also, effects on the response due to Coriolis acceleration have been examined. In the recent past, owing to the possible use of ring structures as part of vibratory angular rate sensors, there has been a renewed interest in studying the dynamic characteristics of rotating flexible rings (see e.g., Putty and Najafi [3]). Eley et al. [4] considered the Coriolis coupling effect between the in-plane and the out-of-plane motions due to the input angular rate about three mutually perpendicular axes with the intent of applying their findings to the design of dual axis angular rate sensors.

In the present study, the angular speed of a rotating ring is considered to be subjected to periodic fluctuations of small intensity. Investigation of these effects on the ring dynamics can be considered essential for the use of rings in many practical dynamic applications. To the best of the authors' knowledge, there has been no study performed on the stability of a rotating ring subjected to harmonic perturbation in input angular speed. However, stability of systems that are of similar class has been performed in the past. Tan et al. [5] performed a stability analysis for a rotating beam subjected to an input speed perturbation using the method of multiple scales, while Van Doorn and Asokanthan [6] used the method of averaging for studying the stability of a rotating dual-spin spacecraft.

Equation of Motion

The ring used for the present study is assumed to possess isotropic and homogeneous material properties, and the transverse shear deformation effects are considered negligible in accordance with the thin ring assumption. Figure 1 illustrates the ring supported internally with eight springs which has radial and circumferential stiffness, k_r and k_θ, respectively. A body fixed frame, $X - Y - Z$, has been used for representing the angular motion of the ring with respect to the inertial frame 'R', and the locations of the neutral surface elements in the rotational coordinates can be defined by introducing curvilinear surface coordinates α_1, α_2, α_3. In the figure, r represents the mean radius of the ring, and u_r and u_θ represent, respectively, the transverse and circumferential displacements. E and ρ represent, respectively, the Young's modulus and density of the material. The area moment of inertia of the ring cross section about its neutral axis is expressed as $I = bh^3 / 12$, where h, b represent, respectively, the radial and axial thicknesses.
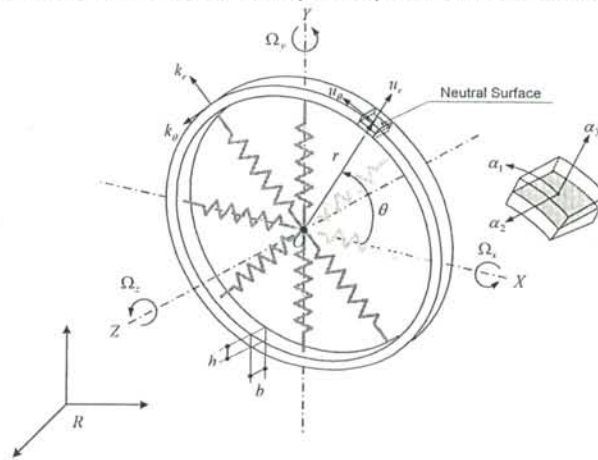

Figure 1. Schematic of a rotating ring with support springs

Considering that the ring is rotating about the Z – axis with a certain angular rate, $\Omega(t)$, the equations that govern the in-plane motion of the ring can be derived using the Hamilton's principle:

$$-\frac{EA}{br^2}(u''_\theta + u'_r) - \frac{EI}{br^4}(u''_\theta - u'''_r) + \rho h \Omega^2(-2u'_r - u''_\theta) + k_\theta u_\theta + \rho h \left(\ddot{u}_\theta + \dot{\Omega}u_r + 2\Omega\dot{u}_r\right) = 0,\tag{1}$$

$$\frac{EA}{br^2}(u'_\theta + u_r) - \frac{EI}{br^4}(u'''_\theta - u''''_r) + \rho h \Omega^2(2u'_\theta - u''_r) + k_r u_r + \rho h \left(\ddot{u}_r - \dot{\Omega}u_\theta - 2\Omega\dot{u}_\theta\right) = 0.\tag{2}$$

The rotational rate Ω is assumed to be time-dependent in this study, and as a result the equations of motion include terms that contain the angular acceleration term $\dot{\Omega}$. The second flexural modes are chosen for investigating natural frequency variation with the input angular rate and for performing stability analysis. It is known that these modes are generally adopted for typical angular rate sensor applications (see e.g., Putty and Najafi [3]). From Equations (1) and (2), the general expression for the discretized equation can be written in terms of the generalized coordinate vector $\mathbf{q} = [q_1 \; q_2]^T$

$$\mathbf{M}\ddot{\mathbf{q}} + \mathbf{G}\dot{\mathbf{q}} + \mathbf{K}\mathbf{q} = \mathbf{0},\tag{3}$$

and the system matrices can be derived as follows:

$$\mathbf{M} = \begin{bmatrix} 1 & 0 \\ 0 & 1+\delta m \end{bmatrix}, \quad \mathbf{G} = \begin{bmatrix} 0 & -2\Omega\gamma \\ 2\Omega\gamma & 0 \end{bmatrix}, \quad \mathbf{K} = \begin{bmatrix} \kappa_1 + \kappa_2\Omega^2 & -\dot{\Omega}\gamma \\ \dot{\Omega}\gamma & \kappa_1 + \kappa_2\Omega^2 \end{bmatrix},\tag{4}$$

where $\mathbf{M}$ is the mass matrix in which a mass mismatch term δm is added to represent the ring asymmetry, $\mathbf{G}$ is the skew-symmetric gyroscopic matrix which results from Coriolis acceleration and $\mathbf{K}$ is the stiffness matrix. The approximated parameters γ, κ_1 and κ_2 are constant values that depend on the mode number n and the physical properties of a ring. Further details of derivation of the equations can be found in the paper by Huang and Soedel [2]. The support springs are considered to possess significantly low stiffness and hence assumed not to have significant effects on the ring dynamics. In the present study, the damping effects are also ignored for simplicity. For the purpose of investigating the stability behaviour of a rotating ring subjected to periodic perturbation in the angular rate, the input angular rate is assumed to take the form:

$$\Omega(t) = \overline{\Omega}(1 + \mu\cos\nu t), \quad 0 < \mu \ll 1\tag{5}$$

where $\overline{\Omega}$ is the amplitude of the input angular rate, μ represents the small dimensionless amplitude of fluctuation, and ν represents the frequency of the imposed periodic excitation. Since the input angular rate is assumed to be a periodic function of time, the system can be regarded as a parametrically excited system, the excitation being harmonic.

Dynamic stability analysis

Owing to the speed-dependent gyroscopic coupling and system stiffness, it is known that bifurcations of natural frequencie can take place. In order to illustrate this effect, the second flexural mode is considered and the variations of the corresponding natural frequencies with input angular rate are depicted in Fig. 2. As a result of an assumed mass mismatch, δm, of 0.01%, it can be observed that the natural frequencies associated with a non-rotating ring system (i.e., input angular rate is zero) are not identical. It may be noted that this natural frequency variation with the input angular rate as described above is essential for stability investigation since it is known that the instability regions near certain combinations and multiples of these system natural frequencies are of significance in this class of systems (see e.g., Van Doorn and Asokanthan [6]).
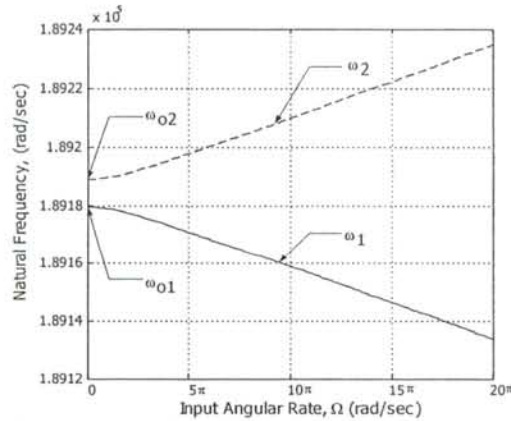

Figure 2. Natural frequency variations for a rotating ring with non-zero mass mismatch

Before performing any analytical stability analysis, it is first necessary to decouple the equation of motion, which are coupled via the gyroscopic and stiffness terms. A contact transformation is used in the present paper to decouple the system, and for this purpose, the equations are formulated in the Hamiltonian form (see e.g., Van Doorn and Asokanthan [6]). Then, the coordinates of the decoupled system are transformed to amplitude and phase variables a, ϕ, so that an asymptotic method such as the method of averaging may be applied. The closed-form stability conditions are obtained via the method of averaging and plotted in the excitation frequency-amplitude space $(v - \mu)$ as shown in Figure 3. The hatched parts represent the unstable regions and the clear parts illustrate the stable regions.
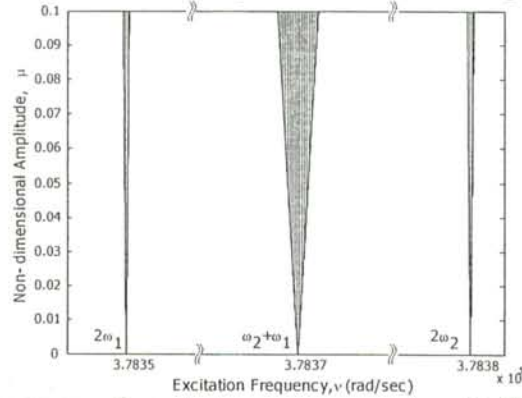
Figure 3. Instability regions: undamped with non-zero mass mismatch; ▨ unstable regions

It can be seen that the instability region associated with the sum-type combination resonance, $v = \omega_2 + \omega_1$, is relatively larger than the regions associated with the sub-harmonic resonances, $v = 2\omega_1, 2\omega_2$. Also, it may be noted that with the presence of some mass mismatch in the system, no instability region is found to exist for the difference-type combination resonance, $v = \omega_2 - \omega_1$. However, It is also observed from this analysis (not shown in this paper) that when the ring is assumed to be perfect, i.e., $\delta m = 0$, instability regions are found only in the case of the sum and difference-type of combination resonance. The instability regions become wider as input angular rate increases or when the difference between non-rotational natural frequencies increases.

Conclusions

Dynamic stability analysis for a ring-type structure subjected to base rotation with periodic perturbations is performed. The angular motion of the ring affects not only the gyroscopic coupling but also the system stiffness. The method of averaging has been employed for deriving the instability conditions in closed-form. These conditions predict the onset of instability behaviour characterised by exponential growth in response amplitudes, and are illustrated by plotting the instability regions in the excitation frequency-excitation amplitude space. If the mass mismatch in the ring is considered, instability regions are observed when the excitation frequencies are near the sub-harmonic or sum-type combination resonance frequencies. In the case of no mass mismatch, instability regions are observed when the excitation frequencies are near the sum and difference-type combination resonance frequencies. The understanding of the instability behaviour as predicted in the present study is expected to result in a better insight into the dynamic behaviour associated with applications that utilise rotating rings.

References

[1] W. B. Bickford and E. S. Reddy, "On the in-plane vibrations of rotating rings", *Journal of Sound and Vibration* 101(1), (1985), pp. 13-22.
[2] S. C. Huang and W. Soedel, "Effect of Coriolis acceleration on the free and forced in-plane vibrations of rotating rings on elastic foundation", *Journal of Sound and Vibration* 115(2), (1987), pp. 253-274.
[3] M. W. Putty and K. Najafi, "A micro machined vibrating ring gyroscope", *Solid-State Sensor and Actuator Workshop*, Hilton Head, South Carolina, 1994.
[4] R. Eley, C. H. J. Fox and S. McWilliam, "Coriolis coupling effects on the vibration of rotating rings", *Journal of sound and vibration* 238(3), (2000), pp. 459-480.
[5] T. H. Tan, H. P. Lee, G. S. B. Leng, "Dynamic stability of a radially rotating beam subjected to base excitation", *Computer Methods in Applied Mechanics and Engineering*, 146, (1997), pp. 265-279.
[6] E. Van Doorn and S. F. Asokanthan, "Attitude stability of dual-spin asymmetric spacecraft" *The Journal of the Astronautical Sciences*, Vol. 44, No. 2, (1996).

A Unified Formulation to Assess Various Theories for the Free Vibrations Analysis of Homogeneous and Multilayered Plates

Erasmo Carrera
Aerospace Department, Politecnico di Torino,
e.mail: carrera@polito.it

Flat panels are typical structural components employed in automotive, ship and aerospace vehicles. These panels are usually constituted by traditional homogeneous metallic materials. However, non- homogeneous multi-layered materials have been recently used to build large partions of these vehicles. Examples of multilayered panels are laminated structures constituted by anisotropic composite materials, sandwich panels, layered structures used in thermal protections and intelligent structural systems embedding piezo-layers. The free vibrational response of flat panels often represent a key topic for the structural analyst. Many classical plate theories have been proposed for traditional homogeneuos plates [1]. Refinements of these classical theory have been proposed to laminated structures [2]. However, amendments are needed in classical and refined theories for the accurate evaluation of the response of multilayered structures. Among them, the fulfillment of both continuity of displacement (the so called Zig-Zag effect, ZZ) and transverse shear and normal stresses (the so called interlaminar continuity, IC) at the interface between two adjacent layers are such necessary amendments [3]. In [4] these requisites were referred to by the acronyms C_z^0–requirements which state that both displacements and transverse stress components are C^0–continuous functions in the thickness coordinate z. An exhaustive overview of these subjects is given in the article by Noor, Burton and Bert [5].

Comprehensive modeling of homogenoeus and multilayered plates is developed in this paper to assess the free vi-bration response of homogeneous and multilayered plates:

– Classical theories formulated on the basis of the Principle of Virtual Displacement (PVD) (with only displacement variables) and advanced mixed models related to the application of the Reissner Mixed Variational Theorem (RMVT) [4] (with displacement and transverse stress variables) are considered.

– Both Layer-Wise (LW) and Equivalent Single Layer (ESL) models have been addressed. Those theories which pre-serve the number of variables independent of the number of layers are herein denotes by ESLM, while those theories in which the same variables are independent in each layer are denoted by LWM.

– Linear up-to fourth order thickness expansions are discussed.

– The evaluations of transverse normal strain effects have been conducted by comparing constant, linear and higher order distributions of transverse displacement components in the plate thickness directions.

All these modelings have been derived in a unified manner by referring to the Unified Formulation (UF) that has been developed by the author in earlier works and recently detailed in [6]. The availability of this large number of model-ings permits one to furnish a quite exhaustive assessment of available plate theories in the free vibration analysis of homogeneous and multilayered plates.

The numerical investigation has been restricted to those lamination schemes (orthotropic layers), geometries (rectangular) and boundary conditions (simply supported) that permit analytical solutions in closed form. An example of plate theories assessment is presented in Tables 1, which is related to a cross-ply laminated composite plates. Acronyms have been used to denote different theories: L and E, denote LW and ESL variables descriptions, respectively; M and D, denote formulations based on RMVT and PVD, respectively; Z and C denote inclusion of Zig-Zag Effects and IC, respectively; 1,2,3,4 denote the order of the expansion used in the thickness layer/multilayer direction; d denotes results that discard transverse normal strains ϵ_{zz}. Comparison of frequency predictions based upon the implemented two-dimensional models reveals that the unified formulation is able to furnish both results (such as LM4) which are in excellent agreement with the ones based on 3-D elasticity theory and results related to Classical Lamination Theory (CLT) and First order Shear Deformation Theory (FSDT). A number (31) of additional theories have been considered between LD4 and CLT analysis. These 31 additional theories are able to evaluate the approximations of the considered two dimensional analyses (such as order of the expansion, ZZ effect and IC inclusion etc.). Some conclusions from Table 1 are listed below. – The possibility of describing *a priori* interlaminar continuous transverse normal stress makes the mixed theories more attractive with respect to other available modelings. – A very accurate description of the vibrational response of anisotropic, thick and very thick plates requires layer-wise description. – Any refinements of classical models are meaningless, unless the effects of interlaminar continuous transverse shear and normal stresses are both taken into account in a multilayered plate theory.

References

[1] Leissa A W, 1969, Vibration of Plates. NASA-SP-160, Washington DC.

[2] Qatu M S, 2004, Vibration of laminated shells and plates, Elsevier Academic Press, 2004, Oxford

[3] Carrera E, 2003, Historical Review of Zig-Zag theories for multilayered plates and shells, *Applied Mechanics Review*, vol 56, pp 287–308.

[4] Carrera E, 2001, Developments, ideas and evaluations based upon the Reissner's mixed theorem in the modeling of multilayered plates and shells, *Applied Mechanics Review*, vol 54, pp 301–329.

[5] Noor A K, Burton S, Bert C W, 1996, Computational model for sandwich panels and shells. *Applied Mechanics Review*, vol 49, pp 155-199.

[6] Carrera E, 2003, Theories and Finite Elements for multilayered plates and shells: A Unified compact Formulation with numerical assessment and benchmarking. Archives of Computational Methods in Engineering, State of the art reviews, vol 10, pp 215-296

a/h	2	4	10	20	100
Theories based on RMVT					
					Layer-Wise Models
LM4	5.260	9.224	15.148	17.626	18.753
LM3	5.259	9.224	15.148	17.626	18.753
LM2	5.247	9.220	15.148	17.626	18.753
LM1	5.143	9.103	15.087	17.604	18.752
			Equivalent Single Layer Models including ZZ and IC		
EMZC3	5.370	9.371	15.224	17.625	18.754
EMZC2	5.847	9.846	15.455	17.737	18.758
EMZC1	5.782	9.768	15.423	17.759	18.814
			... discarding transverse normal strains		
EMZC3d	5.374	9.377	15.263	17.714	18.827
EMZC2d	5.850	9.863	15.504	18.801	18.831
EMZC1d	5.782	9.771	15.433	17.773	18.830
			ESLM results that discard ZZ and include IC		
EMC4	5.361	9.367	15.224	17.653	18.754
EMC3	5.365	9.364	15.221	17.652	18.754
EMC2	5.781	9.757	15.387	17.709	18.757
EMC1	5.572	9.522	15.260	17.703	18.826
Theories based on PVD					
					Layer-Wise Models
LD4	5.260	9.224	15.148	17.626	18.753
LD3	5.262	9.224	15.148	17.626	18.753
LD2	5.277	9.236	15.152	17.626	18.753
LD1	5.414	9.473	15.335	17.703	18.761
			Equivalent Single Layer Models including ZZ		
EDZ3	5.390	9.388	15.232	17.655	18.754
EDZ2	5.920	9.938	15.522	17.763	18.760
EDZ1	5.926	9.956	15.563	17.817	18.819
			.. .. discarding transverse normal strains		
EDZ3d	5.393	9.394	15.271	17.717	18.827
EDZ2d	5.927	9.960	15.572	17.829	18.833
EDZ1d	5.927	9.595	15.572	17.829	18.833
			Classical Equivalent Single Layer Models		
ED4	5.380	9.384	15.232	17.655	18.754
ED3	5.392	9.389	15.232	17.655	18.754
ED2	5.920	9.938	15.522	17.763	18.759
ED1	5.927	9.960	15.573	17.829	18.833
			.. .. discarding transverse normal strains		
ED4d	5.393	9.394	15.271	17.717	18.827
ED3d	5.393	9.394	15.271	17.717	18.827
ED2d	5.927	9.960	15.573	17.829	18.833
FSDT	5.927	9.960	15.573	17.829	18.833
CLT	15.892	17.977	18.725	18.840	18.877

Table 1: Circular frequency parameter $\omega\sqrt{\frac{a^4\rho}{E_T h^2}}$ of Simply supported square plates Cross-ply symmetric laminates 0/90/90/0 (layers of equal thickness). Mechanical properties of the layers: $\frac{E_L}{E_T} = 40$, $\frac{G_{LT}}{E_T} = \frac{G_{Lz}}{E_T} = .50$, $\frac{G_{TT}}{E_T} = .60$, $\nu_{LT} = \nu_{Lz} = \nu_{TT} = 0.25$.

Stability and Vibration of a Nonlinear Beam with Subcritical Axial Speed

Li-Qun Chen

Department of Mechanics, Shanghai University, Shanghai 200436, China

Modeling and analysis of transverse vibration are of considerable interest in the study of axially moving beams. Thurman and Mote derived a nonlinear mode for coupled longitudinal and transverse vibration of axially moving beams [1]. They reduced the governing equation for transverse motion by neglecting the coupling. Wickert [2] supposed that the influence of longitudinal inertia could be neglected (the quasi-static stretch assumption) to establish a decoupled transverse equation of motion. This assumption, which has been widely used, means that the dynamic tension component is a function of time alone. This investigation treats stability and nonlinear frequencies of axially moving beams with the emphasis on the comparisons of the two models.

A uniform axially moving beam, with linear density ρ, elastic modulus E, cross-sectional area A, cross-sectional area moment of inertial I and initial tension P_0, travels at the constant axial transport speed c between two boundaries separated by distance L. Consider only the bending vibration described by the transverse displacement $U(X,T)$ at the longitudinal coordinate X and time T. Newton's second law of motion yields

$$\rho\left(U,_{TT} + 2cU,_{TX} + c^2 U,_{XX}\right) = \left[(P_0 + A\sigma)U,_X\right],_X - (EIU,_{XX}),_{XX} \tag{1}$$

where the axial disturbed stress $\sigma(X,T) = E\varepsilon_L(X,T)$ and ε_L is the Lagrangian strain accounting for geometric nonlinearity due to small but finite stretching of the beam. The replacement of the exact value $A\sigma$ by the averaged value of the disturbed tension $\int_0^L A\sigma\,dX\Big/L$ leads to the model based on the quasi-static stretch assumption. The dimensionless equations for the two models are respectively

$$u,_{tt} + 2\gamma u,_{tx} + \left(\gamma^2 - 1\right)u,_{xx} + k_f^2 u,_{xxxx} = \frac{3}{2}\varepsilon k_1^2 u,_{xx}\, u,_x{}^2 \tag{2}$$

$$u,_{tt} + 2\gamma u,_{tx} + \left(\gamma^2 - 1\right)u,_{xx} + k_f^2 u,_{xxxx} = \frac{1}{2}\varepsilon k_1^2 u,_{xx} \int_0^1 u,_x{}^2\, dx \tag{3}$$

Eq. (2) can be derived from the governing equation for coupled longitudinal and transverse vibration under the assumption that $u^4 \ll u^2$ (Eqs. (15) and (16) in [1]) by considering the transverse vibration only and setting all longitudinal variables to zero. Eq. (3) has been obtained through uncoupling the governing equation for coupled longitudinal and transverse vibration under the quasi-static stretch assumption (Eq. (30) in [2]). In traditional derivation, Eq. (3) seems more exact than Eq. (2) because it is the transverse equation of motion in which the longitudinal displacement field is taken into account. However, the derivation here indicates that Eq. (2) can be reduced to Eq. (3) based on the quasi-static stretch assumption.

For beams with pinned or clamped ends, it has been proven that the following quantities [3]

$$I_1 = \int_0^1 \left[4u_{,t}^2 + 4(1-\gamma^2)u_{,x}^2 + 4k_f^2 u_{,xx}^2 + \varepsilon k_1^2 u_{,x}^4 \right] dx$$

$$I_2 = \int_0^1 \left[4u_{,t}^2 + 4(1-\gamma^2)u_{,x}^2 + 4k_f^2 u_{,xx}^2 + \varepsilon k_1^2 u_{,x}^2 \int_0^1 u_{,x}^2 dx \right] dx$$

(4)

are constants for the models corresponding to Eqs. (2) and (3) respectively. Using the conserved quantities defined by Eq. (4), one can prove that, if $\gamma < 1$, there exists a positive number M such that

$$\|u(x,t)\| \le M \left[\|a(x)\| + \|a^2(x)\|^2 + \|b(x)\| \right], \quad \|u(x,t)\| \le M \left[\|a(x)\| + \|a(x)\|^2 + \|b(x)\| \right]$$

(5)

for solutions to Eqs. (2) and (3) with the initial conditions $u(x,0)=a(x)$ and $u_{,t}(x,0)=b(x)$. Inequality (5) means that the vibration caused by a small initial disturbance is small. Therefore, based on both models, the straight configuration of an axially moving beam is stable in the Lyapunov sense.

To calculate the frequencies of nonlinear free vibration about the straight configuration, the method of multiple scales is directly applied to Eqs. (2) and (3). They have the same order-ε^0 equation with the solution $u_0(x,t)=\alpha_n(\varepsilon t)e^{i(\omega_n t+\beta_n(\varepsilon))}\phi_n(x)+cc$, where ω_n and $\phi_n(x)$ are respectively the n-th natural frequency and complex mode function of the corresponding linear homogeneous system [4], and cc represents complex conjugate to the previous term. Here the internal resonance is not considered, and u_0 includes only the n-th mode vibration to calculate the n-th nonlinear frequency. The solvability condition of order-ε^1 yields

$$\frac{d\alpha_n}{dt} = 0, \quad \alpha_n \frac{d\beta_n}{dt} = -\frac{1}{4}\varepsilon \kappa_n^1 \alpha_n^3$$

(6)

where κ_n^J is the imaginary part of

$$\kappa_n = \frac{3\int_0^1 \bar{\phi}_n \bar{\phi}_n'' \phi_n'^2 dx + 6\int_0^1 \bar{\phi}_n \phi_n'' \phi_n' \bar{\phi}_n' dx}{4\left(i\omega_n \int_0^1 \bar{\phi}_n \phi_n dx + \gamma \int_0^1 \bar{\phi}_n \phi_n' dx\right)} k_1^2, \quad \kappa_n = \frac{\int_0^1 \bar{\phi}_n \phi_n'' dx \int_0^1 \bar{\phi}_n'^2 dx + 2\int_0^1 \phi_n' \bar{\phi}_n' dx \int_0^1 \bar{\phi}_n \phi_n'' dx}{4\left(i\omega_n \int_0^1 \bar{\phi}_n \phi_n dx + \gamma \int_0^1 \bar{\phi}_n \phi_n' dx\right)} k_1^2$$

(7)

for Eqs. (2) and (3) respectively. Integration of Eq. (6) gives the n-th nonlinear frequency

$$\omega_n^{NL} = \omega_n + \frac{1}{4}\varepsilon \kappa_n^1 a_{0n}^2$$

(8)

where a_{0n} is a constant determined by the initial conditions. Eq. (8) indicates that the nonlinear characteristic of the vibration is represented by κ_n^1, while there is no nonlinear effect when $\kappa_n^1=0$. Fig. 1 shows the change of the nonlinear characteristic κ_n^1 varies with the axial speed γ, where the dashed line and the solid line represent the results for Eqs. (2) and (3) respectively. In all calculations, $k_f=1.0$ and $k_1=0.8$. The linear critical axial speeds for the first two modes are respectively $\gamma_{1cr}=2.7045$ and $\gamma_{2cr}=5.2728$. For both models, the nonlinear characteristic increases with the growth of the axial speed, and it increases dramatically for the speed approaching the critical speed. Besides, the higher order mode has the larger nonlinear characteristic. From Eq. (8), it can be concluded that the difference between the nonlinear frequency and linear natural frequency increases with the axial speed and the order of the mode. For the same parameters, the nonlinear characteristic of Eq. (2) is larger than that of Eq. (3). Therefore, averaging the tension along the beam makes the nonlinearity weaker. Fig. 2 shows the relationship between nonlinear frequencies and amplitudes, given by Eq. (8), at different axial speed for $\varepsilon=0.005$. In the figures, the dashed and solid lines represent the results for Eqs. (2) and (3) respectively. The two models yield almost the same results for small axial speed. The

difference of the two models increases with the axial speed; it increases especially rapidly when the axially speed is near the critical speed.
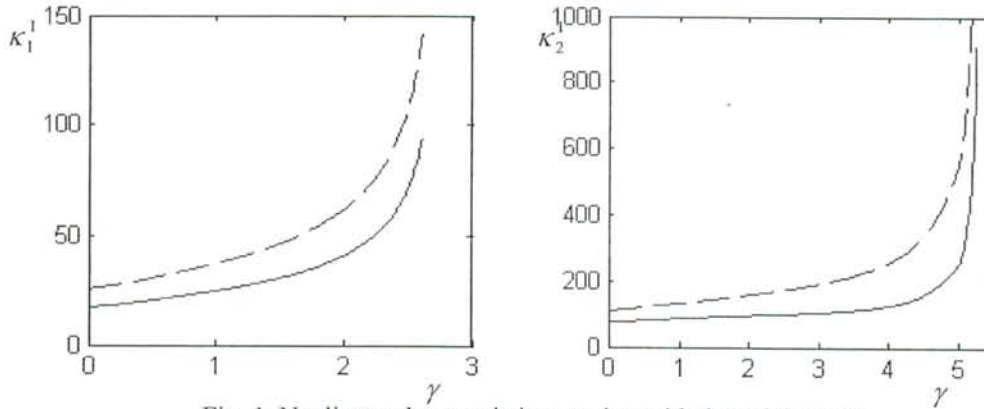
Fig. 1. Nonlinear characteristics varying with the axial speed
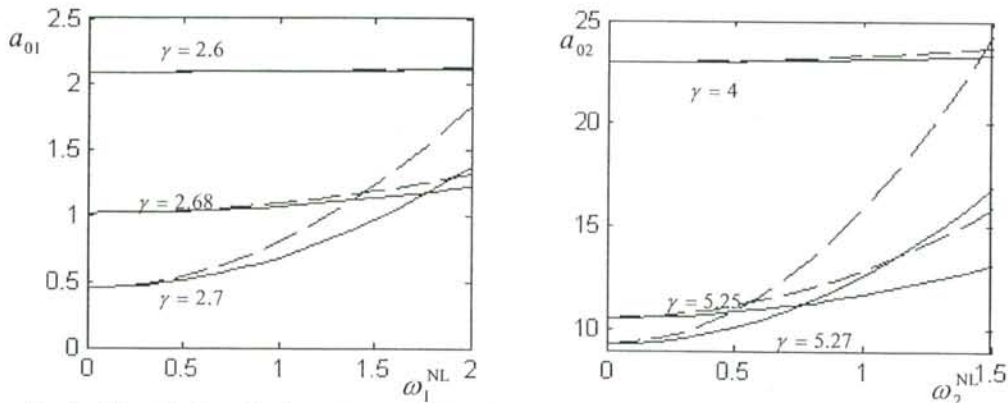
Fig. 2. The relationship between nonlinear frequencies and amplitudes at different axial speed

In conclusions, this presentation investigates two models of nonlinear free vibration of an axially moving beam. The stability is proven for both models. The nonlinear frequencies of two models are calculated via the method of multiple scales. Numerical results show that both models have the same tendencies to change with related parameters, and give essentially the same results for small axial speed. However, the difference increases when the axial speed grows.

1   Thurman A.L., Mote C.D.Jr. Free, periodic, nonlinear oscillation of an axially moving strip, *ASME Journal of Applied Mechanics* **36**(1969): 83-91

2   Wickert J.A. Non-linear Vibration of a traveling tensioned beam, *International Journal of Non-Linear Mechanics* **27**(1992): 503-517

3   Chen L.Q, Zu J.W. Energetics and conserved functional of moving materials undergoing transverse nonlinear vibration. *ASME Journal of Vibration and Acoustics* **126**(2004): in press

4   Wickert J.A., Mote C.D.Jr. Classical vibration analysis of axially moving continua, *ASME Journal of Applied Mechanics* **57**(1990): 738-744

Three-dimensional natural frequency analysis of piezoelectric shells of revolution by the Ritz method

Piotr CUPIAL

Cracow University of Technology, Institute of Applied Mechanics,
Al. Jana Pawla II-go 37, 31-864 Krakow, Poland. Email: cupial@mech.pk.edu.pl

Piezoelectric shells find several applications, e.g. in measurements and mechatronics. One such application is the use of cylindrical shells in ultrasonic micromotors. A number of approximate piezoelectric shell theories are available in the literature, but their accuracy is still under investigation and additional research into this subject is still of much importance. Below, a summary is given of the extension of the approach used to the three-dimensional analysis of elastic shells described by A.W. Leissa and J.-H. Kang in reference [1], to the study of piezoelectric 3-D shells of revolution.

An orthonormal co-ordinate system (α, θ, ζ) is used to describe the geometry of the shell of revolution, where α is measured along the meridional direction of the shell middle surface, θ is the circumferential- and ζ- the normal direction. The extension of the variational formulation of the elastic free-vibration problem to a piezoelectric shell is given by (more details about the variational principle of piezoelectricity can be found in reference [2]):

$$\int_{\alpha_1}^{\alpha_2} \int_0^{2\pi} \int_{-h/2}^{h/2} [-\rho\omega^2 (U_\alpha \delta U_\alpha + U_\theta \delta U_\theta + U_\zeta \delta U_\zeta) + \sigma_\alpha \delta\varepsilon_\alpha + \sigma_\theta \delta\varepsilon_\theta + \sigma_\zeta \delta\varepsilon_\zeta + \sigma_{\theta\zeta} \delta\gamma_{\theta\zeta} + \sigma_{\alpha\zeta} \delta\gamma_{\alpha\zeta} +$$
$$+ \sigma_{\alpha\theta} \delta\gamma_{\alpha\theta} - D_\alpha \delta E_\alpha - D_\theta \delta E_\theta - D_\zeta \delta E_\zeta] \rho_\zeta r_\zeta \, d\alpha d\theta d\zeta = 0 \tag{1}$$

The components of the strain tensor appearing in equation (1) have been derived using the general tensor formulation in curvilinear co-ordinates discussed in reference [3]. The final form of these expressions is as given in references [1] and [4]. In equation (1), $D_\alpha, D_\theta, D_\zeta$ stand for the components of the electric displacement vector, and $E_\alpha, E_\theta, E_\zeta$ are the components of the electric field vector, which are related to the electrostatic potential in the following way:

$$E_\alpha = -\frac{1}{\rho_\zeta} \frac{\partial\phi}{\partial\alpha}, \quad E_\theta = -\frac{1}{r_\zeta} \frac{\partial\phi}{\partial\theta}, \quad E_\zeta = -\frac{\partial\phi}{\partial\zeta} \tag{2}$$

ρ_ζ and r_ζ are defined using the principal radii of curvature, similar as in references [1] and [4]:

$$\rho_\zeta = (R_1 + \zeta), \quad r_\zeta = (R_2 + \zeta)\sin\alpha \tag{3}$$

A shell poled in the normal direction is considered, and the constitutive equations (assuming the orthorhombic symmetry class *mm2*) have the following form:

$$
\begin{Bmatrix} \sigma_\alpha \\ \sigma_\theta \\ \sigma_\zeta \\ \sigma_{\theta\zeta} \\ \sigma_{\alpha\zeta} \\ \sigma_{\alpha\theta} \end{Bmatrix} = \begin{bmatrix} c_{11} & c_{12} & c_{13} & 0 & 0 & 0 \\ c_{12} & c_{22} & c_{23} & 0 & 0 & 0 \\ c_{13} & c_{23} & c_{33} & 0 & 0 & 0 \\ 0 & 0 & 0 & c_{44} & 0 & 0 \\ 0 & 0 & 0 & 0 & c_{55} & 0 \\ 0 & 0 & 0 & 0 & 0 & c_{66} \end{bmatrix} \cdot \begin{Bmatrix} \varepsilon_\alpha \\ \varepsilon_\theta \\ \varepsilon_\zeta \\ \gamma_{\theta\zeta} \\ \gamma_{\alpha\zeta} \\ \gamma_{\alpha\theta} \end{Bmatrix} - \begin{bmatrix} 0 & 0 & e_{31} \\ 0 & 0 & e_{32} \\ 0 & 0 & e_{33} \\ 0 & e_{24} & 0 \\ e_{15} & 0 & 0 \\ 0 & 0 & 0 \end{bmatrix} \cdot \begin{Bmatrix} E_\alpha \\ E_\theta \\ E_\zeta \end{Bmatrix},
$$

$$
(4)
$$

$$
\begin{Bmatrix} D_\alpha \\ D_\theta \\ D_\zeta \end{Bmatrix} = \begin{bmatrix} 0 & 0 & 0 & 0 & e_{15} & 0 \\ 0 & 0 & 0 & e_{24} & 0 & 0 \\ e_{31} & e_{32} & e_{33} & 0 & 0 & 0 \end{bmatrix} \cdot \begin{Bmatrix} \varepsilon_\alpha \\ \varepsilon_\theta \\ \varepsilon_\zeta \\ \gamma_{\theta\zeta} \\ \gamma_{\alpha\zeta} \\ \gamma_{\alpha\theta} \end{Bmatrix} + \begin{bmatrix} k_{11} & 0 & 0 \\ 0 & k_{22} & 0 \\ 0 & 0 & k_{33} \end{bmatrix} \cdot \begin{Bmatrix} E_\alpha \\ E_\theta \\ E_\zeta \end{Bmatrix}.
$$

In all results discussed below, the displacements and electric potential are approximated by polynomial functions. The following material properties, typical of a piezoelectric ceramic, have been used:

$$
c_{11} = c_{22} = 13.2 \cdot 10^{10} \, (\frac{N}{m^2}), \quad c_{12} = 7.1 \cdot 10^{10} \, (\frac{N}{m^2}), \quad c_{13} = c_{23} = 7.3 \cdot 10^{10} \, (\frac{N}{m^2}), \quad c_{33} = 11.5 \cdot 10^{10} \, (\frac{N}{m^2}),
$$

$$
c_{44} = c_{55} = 2.6 \cdot 10^{10} \, (\frac{N}{m^2}), \quad c_{66} = 3.0 \cdot 10^{10} \, (\frac{N}{m^2}), \quad e_{15} = e_{24} = 10.5 (\frac{C}{m^2}), \quad e_{31} = e_{32} = -4.1 (\frac{C}{m^2}),
$$

$$
e_{33} = 14.1 (\frac{C}{m^2}), \quad k_{11} = k_{22} = 7.124 \cdot 10^{-9} \, (\frac{F}{m}), \quad k_{33} = 5.841 \cdot 10^{-9} \, (\frac{F}{m}), \quad \rho = 7.5 \cdot 10^3 \, (\frac{kg}{m^3}).
$$

To demonstrate the approach, the results will be discussed for a cylindrical shell of constant thickness. Table 1 shows the convergence of the non-dimensional frequencies of a cylindrical shell with the radius-to-length ratio $R/L = 0.5$ and the thickness-to-length ratio $h/L = 0.01$. The shell ends are mechanically restrained and 'electrically unrestrained' (open-circuit condition, for which no potential is prescribed at any point). In the numerical analysis, an efficient algorithm to solve the generalized eigenvalue problem has been used and the need of matrix inversion has been avoided. Additionally, the above electrical boundary condition is more difficult to analyze than the case with a prescribed potential, since electrostatic potential can only be determined up to an arbitrary constant. This fact has been taken into account in the algorithm.

Table 1. Non-dimensional frequencies $\bar{\omega} = \omega \dfrac{L}{2} \sqrt{\dfrac{\rho}{c_{11}}}$ of a cylindrical shell.

K1=K2= K3=K4	Circumferential wave number n						
	0	1	2	3	4	5	6
2	0.7538	0.5742	0.4707	0.4299	0.4164	0.4189	0.4350
4	0.7489	0.4896	0.3246	0.2343	0.1900	0.1867	0.2181
6	0.7489	0.4853	0.3164	0.2269	0.1855	0.1845	0.2171
8	0.7489	0.4849	0.3151	0.2253	0.1842	0.1836	0.2166
10	0.7489	0.4849	0.3150	0.2252	0.1840	0.1835	0.2165
12	0.7489	0.4848	0.3149	0.2250	0.1839	0.1834	0.2165
14	0.7489	0.4848	0.3148	0.2249	0.1838	0.1833	0.2164
16	0.7489	0.4848	0.3148	0.2249	0.1838	0.1833	0.2164

The same number of polynomials (K1=K2=K3=K4) has been used to approximate the displacements and the electrostatic potential with respect to the axial co-ordinate. Quadratic approximation has been found to be accurate enough in the ζ-coordinate. It has also been displayed that the use of linear approximation for the tangential displacements practically leaves the results in Table 1 unchanged, but quadratic terms for the normal displacement and potential are non-negligible.

In order to verify the results, Table 2 gives a comparison with the finite element analysis (FEA) results obtained using the coupled-field capability of the finite element code ANSYS. Solid brick elements have been used, with a linear approximation of the mechanical and electric fields within the element. To achieve the necessary accuracy, a fine mesh had to be used and the results shown were obtained with 160 elements along the circumferential direction, 40 elements in the axial direction and 3- in the radial direction.

Table 2: Comparison of the lowest frequencies for a cylindrical shell with
$$R = 5 \cdot 10^{-2}[m], L = 10 \cdot 10^{-2}[m], h = 10^{-3}[m]$$

Ritz method	2450 [Hz] (n=5)	2457 [Hz] (n=4)	2891 [Hz] (n=6)	3001 [Hz] (n=3)	3645 [Hz] (n=7)
FEA (ANSYS)	2461 [Hz]	2464 [Hz]	2910 [Hz]	3011 [Hz]	3678 [Hz]
(Ansys-Ritz)/Ritz*100%	0.4%	0.3%	0.7%	0.3%	0.9%

Even better agreement than that shown in Table 2 has been found for thick cylinders.

For vibrating piezoelectric continua piezoelectric coupling takes place through the piezoelectric constants e_{ij} in constitutive equations (4). Proper approximate shell theories should be able to correctly model this effect. The coupling depends on the values of material constants, shell geometry and the mode under consideration. Table 3 shows the effect of the piezoelectric coupling for the shell, the results of which were given in Table 1. The results termed "without coupling" were obtained by setting all piezoelectric constants to zero.

Table 3. Effect of piezoelectric coupling on non-dimensional frequencies of a cylindrical shell

	Circumferential wave number n						
	0	1	2	3	4	5	6
Without coupling	0.7489	0.4719	0.3072	0.2178	0.1744	0.1690	0.1954
With coupling	0.7489	0.4849	0.3150	0.2252	0.1840	0.1835	0.2165
Relative change	0%	2.8%	2.5%	3.4%	5.5%	8.6%	10.8%

The approach has also been used successfully for other shell geometries including spherical shell sections and conical shells.

References

1. Leissa A.W. and Kang J.-H., Three-Dimensional Analysis of Thick Shells of Revolution, *Journal of Engineering Mechanics*, vol.125, 1999, 1365-1371.
2. Tiersten, H.F., *Linear Piezoelectric Plate Vibrations,* Plenum Press, New York, 1969.
3. Naghdi P.M., Foundations of Elastic Shell Theory, in *Progress in Solid Mechanics*, vol. IV, 1963, 1-90, North-Holland Publishing Company, Amsterdam.
4. Kang J.-H. and Leissa A.W., Three-Dimensional Field Equations of Motion, and Energy Functionals for Thick Shells of Revolution with Arbitrary Curvature and Variable Thickness, *Transactions of ASME, Journal of Applied Mechanics*, vol.68, 2001, 593-594.

Modal Data for a Layered Piezoelectric Cylinder and Their Applications*

Stanley B. Dong

Civil and Environmental Engineering Department
University of California
Los Angeles, California, 90095-1593, USA

Abstract

The spectral decomposition of the governing differential operator for layered piezoelectric circular cylinder yields a complete set of modal data. These data consist of all propagating modes as well as edge vibrations for the cylinder. Herein, these modal data are used to construct steady-state Green's functions and to explore the reflection of monochromatic waves arriving at the free end of the cylinder.

The structure is in the form of a right circular cylinder composed of any number of perfectly bonded layers, each of constant thickness and distinct piezoelectric properties. The cylinder may be hollow or solid, whose lateral surfaces are traction-free. The equations of motion are based on linear piezoelectricity theory, Using cylindrical coordinates (r, θ, z) and finite element modeling over the thickness, the displacement/electric field has form

$$\mathbf{V}(r, \theta, z, t) \equiv \mathbf{V_m} e^{i(k_m z + m\theta + \omega t)} \qquad (1)$$

where array $\mathbf{V_m}$ contains the nodal displacement components (u_r, u_θ, u_z) and electric potential ϕ. Upon inserting this field into the equations of motion, the following Hermitian system of equations is obtained.

$$\left[(\mathbf{K_1} + m^2 \mathbf{K_4} + m k_m \mathbf{K_5} + k_m^2 \mathbf{K_6} - \omega^2 \mathbf{M}) + i(m \mathbf{K_2} + k_m \mathbf{K_3}) \right] \mathbf{V_m} = 0 \qquad (2)$$

with $\mathbf{K_1}, \mathbf{K_4}, \mathbf{K_5}, \mathbf{K_6}, \mathbf{M}$ and $\mathbf{K_2}, \mathbf{K_3}$ as symmetric and antisymmetric matrices, respectively. In this problem, circumferential mode number m is always assigned. Thus, this is a two parameter eigenproblem where modal data can be extracted by using either axial wave number k_m or squared circular frequency ω^2 as the eigenvalue parameter.

For ω^2 as the eigenvalue, Eq. (2) takes the form

$$\left[(\mathbf{K_1} + m^2 \mathbf{K_4} + m k_m \mathbf{K_5} + k_m^2 \mathbf{K_6}) + i(m \mathbf{K_2} + k_m \mathbf{K_3}) \right] \mathbf{V_m} = \omega^2 \mathbf{M} \mathbf{V_m} \qquad (3)$$

This algebraic eigenproblem is Hermitian so that only real ω^2's are admitted. The eigendata extracted from Eq. (3) define all of the propagating modes in the cylinder.

If k_m acts as the eigenvalue parameter, then Eq. (2) becomes a quadratic eigenproblem.

$$\left[\left(\mathbf{K_1} + m^2\mathbf{K_4} - \omega^2\mathbf{M} + im\mathbf{K_2}\right) + k_m\left(m\mathbf{K_5} + i\mathbf{K_3}\right) + k_m^2\mathbf{K_6}\right]\mathbf{V_m} = 0 \qquad (4)$$

With real ω^2 assigned, the solution provide eigenvalues k_m's and associated right eigenvectors $\phi_\mathbf{m}$'s. Both real and complex conjugate pairs are possible. Real eigendata portray monotonically decaying wave forms in the z-direction from the origin of coordinates, while complex eigendata give decaying sinusoids. Because Eq. (4) can be reduced to a first order system involving a non-symmetric matrix, in addition to right eigenvectors, there is a system of left eigenvectors $\psi_\mathbf{m}$ associated with the same eigenvalues k_m's.

Steady-state Green's functions are based on forced response to a time harmonic load. The general form of this response was obtained by instating the load $\tilde{\mathbf{f}}_m$ after a Fourier transform is effected to quell the z-dependence. A subsequent inverse Fourier transform recovers the axial dependence. The solution form can be written in terms of two groups of axial wave numbers, k_m^+ and k_m^-, according to traveling and decaying motions from the origin along the positive and negative z-directions.

$$\bar{\mathbf{V}}_\mathbf{m}(z) = i \sum_{k_{mn} \in k_m^+} \frac{\boldsymbol{\Psi}_{mn}^T \tilde{\mathbf{f}}_m}{B_{mn}} \phi_{mn} e^{ik_{mn}z} + i \sum_{k_{mn} \in k_m^-} \frac{\boldsymbol{\Psi}_{mn}^T \tilde{\mathbf{f}}_m}{B_{mn}} \phi_{mn} e^{ik_{mn}z} \qquad (5)$$

Green's function is based on the load or electric charge as a point source. Because of convergence (or lack thereof) in the modal expansion of any point source, the source is replaced by a uniform load or charge acting over a very small surface area. To represent this source, a double modal summation is needed, i.e., In the θ and axial directions. While such a representation of a point source requires a huge number of terms, the structural response on the other hand converges with substantially fewer terms. Green's functions for point loads and point charges are constructed on this basis and their convergence of both their kinematic and force-type quantities is shown.

In wave reflection in a semi-infinitely long cylinder, a steady-state monochromatic wave is assumed to arrive at the free end cross-section $z = 0$ from afar, i.e., at $z = +\infty$. The reflected wave is represented by a basis of propagating modes and edge vibrations.

$$\bar{\mathbf{V}}_\mathbf{m}^{re} = \sum_{n=1}^{N} a_N \phi_{mn} e^{i(k_{mn}z - m\theta - \omega t)} \qquad z \geq 0 \qquad (6)$$

For a traction-free end, this condition prescribes that the combination of incoming and reflected wave fields yields no surface traction on a point-wise basis over the free end, i.e.,

$$\mathbf{R}^{in} + \mathbf{R}^{re} = 0 \qquad (7)$$

where $\mathbf{R}$ denotes the relevant traction components and electric potential and superscripts *in* and *re* refer to the incident and reflected fields. In our analysis, $\mathbf{R}$ is an array of the traction components and electric potential at the Gaussian points over the cylinder's end cross-section. The traction of reflected field is obtained by differentiating Eq. (6) to form the deformation measures and using the piezoelectric constitutive relation. In our investigations, Eq. (7) is solved on a least-squares basis using a finite number of modes. An energy flux calculation is also performed to assure the consistency of the unknown amplitudes of vibration. Reflections due to incoming axisymmetric ($m = 0$) and flexural ($m = 1$) waves were studied.

For incoming axisymmetric waves, there is a particular frequency which enables an end resonance condition. This phenomenon is characterized by extremely high amplitudes of end motions at a certain frequency *vis-a-vis* those of neighboring (i.e., slightly different) frequencies. End resonance was first observed experimentally by Oliver (1957) in a homogeneous, isotropic cylinder. A similar phenomenon can be predicted to occur in piezoelectric cylinders.

Instead of a passive reflection of incoming waves, it is possible to modify this event by imposing some voltage distribution over the free end, which is essentially a forced input. In fact, if this applied voltage is out-of-phase with that of the incoming wave, it is possible to extract electrical energy from it. This means of energy harvesting is intriguing.

References

1. BAI, H., TACIROGLU, E., DONG, S.B. AND SHAH, A.H., 2004, "Elastodynamic Green's Functions for a Laminated Piezoelectric Cylinder," *Int. J. of Solids and Structures*, **41**, 6335-6350.

2. BAI, H., SHAH, A.H., DONG, S.B. AND TACIROGLU, E., 2004, "End Reflections in Layered Piezoelectric Cylinder," submitted for publication.

3. OLIVER, J., 1957, "Elastic Wave Dispersion in a Cylindrical Rod by a Wide-band Short-duration Pulse Technique," *J. Acoust. Soc Amer*, **29**, 189-194.

4. SIAO, C.T., DONG, S.B. AND SONG, J., 1994, "Frequency Spectra of Laminated Piezoelectric Cylinders," *ASME J. Vib. and Acoust.*, **116**, 364-370.

Free Vibration of Variable Thickness Skew Plates

Moshe Eisenberger and Igor Shufrin

Faculty of Civil and Environmental Engineering

Technion-Israel Institute of Technology

Technion City 32000, Israel

Abstract

Accurate prediction of the free vibration behavior of skew plates is of fundamental importance in the design of structures such as swept wings and skew bridges. Although a large number of available papers dealing with free vibrations of skew plates with uniform thickness, the natural frequencies of skew plates with variable thickness have received little attention. In this work the free vibration of variable thickness skew plate is analyzed using classical plate theory. The solution is performed by the extended Kantorovich method [1] in conjunction with the exact element method [2].

Consider a thin isotropic skew plate with variable thickness $h(x, y)$ and arbitrary boundary conditions. The out of plane energy functional Π can be written in terms of the strain energy of bending, and the kinetic energy of free vibration as follows [3]:

$$\Pi = \frac{1}{2\cos^3(\theta)} \int_0^{L_x} \int_0^{L_y} \left(\begin{array}{c} Dw_{,xx}^2 + Dw_{,yy}^2 + 2D(1 + \sin^2(\theta) - \nu\cos^2(\theta))w_{,xy}^2 + \\ + 2D(\sin^2(\theta) + \nu\cos^2(\theta))w_{,xx}w_{,yy} - \cos^4(\theta)\omega^2\rho h w^2 \\ - 4D\sin(\theta)w_{,xx}w_{,xy} - 4D\sin(\theta)Dw_{,yy}w_{,xy} \end{array} \right) dxdy \quad (1)$$

where x, y are skew axes and θ is the external angle of the coordinate system. In accordance with common notation w is transverse deflection, D is the plate bending rigidity, ν is the Poisson ratio, ρ is the density and ω is the angular frequency.

According to the extended Kantorovich method the solution is assumed as follows:

$$w = \sum_{i=1}^{N} X_i(x)Y_i(y) = \{X\}^T\{Y\} \quad (2)$$

Also the plate thickness and rigidity are taken as

$$h(x, y) = H_0 H_x(x) H_y(y); \quad D(x, y) = D_0 D_x(x) D_y(y) \quad (3)$$

Then, assuming the solution in one direction *a priory*, for example $\{Y\}$, and substitution of (2) and (3) into (1), integration over y direction, assignment of the first variation to zero, and integration by parts lead to the system of ordinary differential equation of motion (4) and natural boundary conditions (5, 6) in the x direction.

$$D_x[\,S^{(1)}\,]\{X\}_{,xxxx} + \left(2D_{x,x}[\,S^{(1)}\,] + D_x\left([\,S^{(5)}\,] - [\,S^{(5)}\,]^T\right)\right)\{X\}_{,xxx} +$$

$$+\left(D_{x,xx}[\,S^{(1)}\,] + D_{x,x}\left(2[\,S^{(5)}\,] - [\,S^{(5)}\,]^T\right) + D_x\left([\,S^{(2)}\,] + [\,S^{(2)}\,]^T - [\,S^{(4)}\,]\right)\right)\{X\}_{,xx} +$$

$$+\left(D_{x,xx}[\,S^{(5)}\,] + D_{x,x}\left(2[\,S^{(2)}\,] - [\,S^{(4)}\,]\right) + D_x\left([\,S^{(6)}\,] - [\,S^{(6)}\,]^T\right)\right)\{X\}_{,x} +$$

$$+\left(D_{x,xx}[\,S^{(2)}\,] - D_{x,x}[\,S^{(6)}\,]^T + D_x[\,S^{(3)}\,] - \omega^2 H_x[\,S^{(7)}\,]\right)\{X\} = \{0\} \tag{4}$$

$$\{V\} = \left[\begin{array}{l} -D_x[\,S^{(1)}\,]\{X\}_{,xxx} - \left(D_{x,x}[\,S^{(1)}\,] + D_x\left([\,S^{(5)}\,] - [\,S^{(5)}\,]^T\right)\right)\{X\}_{,xx} + \\ -\left(D_{x,x}[\,S^{(5)}\,] + D_x\left([\,S^{(2)}\,] - [\,S^{(4)}\,]\right)\right)\{X\}_{,x} - \left(D_{x,x}[\,S^{(2)}\,] - D_x[\,S^{(6)}\,]^T\right)\{X\} \end{array}\right]\Bigg|_0^{L_x} \tag{5}$$

$$\{M\} = \left[D_x[\,S^{(1)}\,]\{X\}_{,xx} + D_x[\,S^{(2)}\,]\{X\} + D_x[\,S^{(5)}\,]^T\{X\}_{,x}\right]\Bigg|_0^{L_x} \tag{6}$$

where the S matrices result from integration over the y direction as follows:

$$[\,S^{(1)}\,] = \int_0^{L_y} D_y\{Y\}\{Y\}^T dy \;;\; [\,S^{(2)}\,] = \left(\sin^2(\theta) + \nu\cos^2(\theta)\right)\int_0^{L_y} D_y\{Y\}\{Y\}^T_{,yy} dy$$

$$[\,S^{(3)}\,] = \int_0^{L_y} D_y\{Y\}_{,yy}\{Y\}^T_{,yy} dy \;;\; [\,S^{(4)}\,] = 2\left(1 + \sin^2(\theta) - \nu\cos^2(\theta)\right)\int_0^{L_y} D_y\{Y\}_{,y}\{Y\}^T_{,y} dy$$

$$[\,S^{(5)}\,] = 2\sin(\theta)\int_0^{L_y} D_y\{Y\}\{Y\}^T_{,y} dy \;;\; [\,S^{(6)}\,] = 2\sin(\theta)\int_0^{L_y} D_y\{Y\}_{,yy}\{Y\}^T_{,y} dy$$

$$[\,S^{(7)}\,] = \cos^4(\theta)\int_0^{L_y} H_y\{Y\}\{Y\}^T dy \tag{7}$$

According to the exact element method [2], the natural frequency for the x direction is obtained as the frequency that causes a dynamic stiffness matrix be singular. The terms of the stiffness matrix are clamping actions at the both ends of the strip element (5, 6) due to unit displacement in one of the degrees of freedom when all other are restrained. The shape functions are given as an exact solution for the equations of motion (4) which is done using the power series method when the thickness variation is described in polynomial form as well. In the next step the obtained solution is used as specified *a priory*, while the solution in the second direction is calculated by another solution process. The iterations are repeated until the result converges to a desired degree.

Simple separation of variables with only one term in series (2) leads to a bad approximation. The use of additional terms improves the results significantly (see Table 1). Comparison with existing solutions shows the high accuracy of the current results, which are obtained for the plates with both uniform and variable thickness (see Table 2). Many examples are given

to demonstrate the accuracy and flexibility of this approach. The effect of the thickness variation on the natural frequencies of thin skew plates with different combinations of boundary conditions is investigated.

Table 1: Convergence of frequency parameter $\Omega^2 = \omega^2 L_y^4 \rho H_0 / D_0$ for a CCCC rhombic plate, $L_x/L_y = 1.0$, $\theta = 30°$, $\nu = 0.3$.

Number of terms	Mode				
	1	2	3	4	5
1	50.569	156.043	320.494	543.819	826.005
2	46.403	81.607	108.159	186.592	473.741
3	46.125	81.604	106.427	178.788	221.939
4	46.097	81.601	105.265	119.269	164.991
5	46.091	81.601	105.210	119.269	164.988
6	46.090		105.173		164.986
7	46.090		105.170		164.986
8			105.168		
9			105.167		

Table 2: Comparison of frequency parameter $\Omega^2 = \omega^2 L_y^4 \rho H_0 / D_0$ rhombic plate ($L_x/L_y = 1.0$) with linear thickness variation in both directions: $H_x = H_0 (1 - \beta_x x/L_x)$, $H_y = H_0 (1 - \beta_y y/L_y)$.

BC	θ	β_x	β_y	Mode					Reference
				1	2	3	4	5	
CCCC	45	0	0	65.645	106.498	148.315	157.241	196.774	Present
				65.643	106.495	148.312	157.236	196.773	[4]
	45	0.5	0	47.953	77.531	106.972	115.820	141.985	Present
				48.501	78.256	110.940			[5]
SSSS	60	0	0	63.772	104.971	148.167	196.301	200.074	Present
				64.818	104.955	148.320	196.294	210.658	[4]
	60	0.5	0	47.230	76.933	108.330	142.803	146.541	Present
				53.475	84.115	139.820			[5]
	60	0.5	0.5	34.745	55.445	77.805	102.505	113.168	Present
				39.308	62.676	94.284			[5]

References

1. Kerr A.D. 1969 An Extended Kantorovich Method for the Solution of Eigenvalue Problems. *International Journal of Solids and Structures, Vol. 5, 559-572.*

2. Eisenberger M. 1990 An Exact Element Method. *International Journal for Numerical Methods in Engineering, Vol. 30, 363-370.*

3. A.W. Leissa 1969 Vibration of Plates. *(NASA SP160) Washington, D.C.*

4. N.S. Bardell 1992 The Free Vibration of Skew Plate Using the Hierarchical Finite Element Method. *Journal of Computer and Structures 45, 841-847*

5. B. Singh, V. Saxena 1997 Transverse Vibration of Skew Plates with Variable Thickness. *Journal of Sound and Vibration 206(1), 1-13*

Free In-plane Vibration Analysis of Rectangular Plates with Elastic Support Normal to the Edges

D. J. Gorman
Professor Emeritus, Dep't of Mech. Eng., University of Ottawa
Ottawa, Canada K1N 6N5

Free in-plane vibration analysis of rectangular plates by the method of superposition was introduced at the Fourth Symposium on Vibrations of Continuous Systems [1]. Full length papers related to in-plane vibration of plates were subsequently prepared [2],[3]. These papers contained listings of a number of relevant publications in the literature. In the work described here the above analytical approach is extended to the case of vibration of plates with uniform elastic support acting perpendicular to the plate edges.

It was shown in reference [2] that the in-plane governing differential equations can be written in dimensionless form as,

$$a_{11}\frac{\partial^2 U}{\partial \xi^2} + \frac{a_{12}}{\phi}\frac{\partial^2 V}{\partial \xi \partial \eta} + \frac{a_{66}}{\phi}\left[\frac{\partial^2 V}{\partial \xi \partial \eta} + \frac{1}{\phi}\frac{\partial^2 U}{\partial \eta^2}\right] + \lambda^4 U = 0 \tag{1}$$

and,

$$a_{66}\left[\frac{\partial^2 V}{\partial \xi^2} + \frac{1}{\phi}\frac{\partial^2 U}{\partial \xi \partial \eta}\right] + \frac{a_{12}}{\phi}\frac{\partial^2 U}{\partial \eta \partial \xi} + \frac{a_{12}}{\phi^2}\frac{\partial^2 V}{\partial \eta^2} + \lambda^4 V = 0 \tag{2}$$

where ξ and η are dimensionless coordinates, and U and V are plate in-plane displacements in the ξ and η directions, respectively. ϕ is the ratio of plate edge lengths, b/a, and the dimensionless frequency of plate vibration $\lambda^2 = \omega a[\rho(1-\nu^2)/E]^{1/2}$, where ω is the circular frequency of vibration, ρ is the plate mass density, ν is the Poisson ratio, and E equals the Young's modulus. All other symbols are as defined in reference [2].

Dimensionless normal and shear stresses are written as,

$$\sigma_x^* = \frac{\partial U}{\partial \xi} + \frac{\nu}{\phi}\frac{\partial V}{\partial \eta}; \; \sigma_y^* = \nu\frac{\partial U}{\partial \xi} + \frac{1}{\phi}\frac{\partial V}{\partial \eta}; \; and \; \tau_{xy}^* = \frac{\partial U}{\partial \eta} + \phi\frac{\partial V}{\partial \xi}$$

Conditions to be satisfied at the boundaries are,

$$\sigma_y^*(\xi,\eta) = -K_1^* V(\xi,\eta), \; and \; \sigma_x^* = -K_2^* U(\xi,\eta)$$

$$where \, K_1^* = k_1 a(1-\nu^2)/E, \; and \; K_2^* = k_2 a(1-\nu^2)/E$$

Here k_1 and k_2 are the actual elastic edge stiffnesses per unit edge length, per unit edge deflection.

It is assumed that elastic stiffness coefficients are equal along opposite edges. The resulting symmetry permits us to examine one quarter of the plate only. Modes are defined as being symmetric about a plate central axis if displacement along the axis is zero and displacement normal to the axis is symmetrically distributed along it [2]. Conversely, if displacement normal to an axis is zero and that parallel to the axis is symmetrically distributed about it, the mode is said to have an anti-symmetric distribution with respect to the axis. Modes will be symmetric-symmetric, ie., have symmetric displacement distributions with respect to the plate central axes, anti-symmetric – anti-symmetric , or will possess symmetry with respect to one axis and anti-symmetry with respect to the other. Here, because of space limitations, we will restrict the written discussion to analysis of symmetric-symmetric modes, only. The quarter plate shown on the left hand side of Figure 1 is considered to be undergoing symmetric-symmetric mode in-plane free vibration. Using the superposition method the vibration is analyzed by superposition of the two forced vibration problems (building blocks) shown schematically on the right hand side. Each building block is driven by a distributed harmonic displacement enforced along one edge as indicated by the small line of arrows.

Displacements for the first building block are expressed in the form proposed by Levy as,

$$U(\xi,\eta) = \sum_{m=1,2}^{\infty} U_m(\eta)\cos emp\xi \tag{3}$$

and

$$V(\xi,\eta) = \sum_{m=1,2}^{\infty} V_m(\eta)\sin emp\xi \tag{4}$$

where emp=$(2m-1)\pi/2$.

It will be noted that the solution satisfies symmetric mode conditions along the η axis, and a condition of zero shear stress along the edge, $\xi=1$. Following standard procedures, the above series solutions are substituted in the governing differential equations. A pair of coupled ordinary differential equations are thereby obtained. Through judicious manipulating of this latter pair a fourth order homogeneous differential equation involving the quantity $V_m(\eta)$, only, is obtained. Solving the associated characteristic equation it is found that three forms of solution for $V_m(\eta)$ are possible, depending on the equation coefficients. The first form of solution is found to be,

$$V_m(\eta) = A_m \sinh\beta_m\eta + B_m \cosh\beta_m\eta + C_m \sin\gamma_m\eta + D_m \cos\gamma_m\eta \tag{5}$$

where A_m and B_m etc., are constants to be evaluated according to the boundary conditions. The quantities β_m and γ_m are as defined in reference [2]. The other two forms of solution involve either all trigonometric functions or all hyperbolic functions. Companion solutions for the quantities $U_m(\eta)$ are now also available.

Two of the constants of equation 5 are eliminated in order to satisfy conditions of symmetry along the ξ axis. A third is evaluated through enforcement of the condition of zero shear stress along the driven edge. Amplitude of the imposed harmonic displacement along the driven edge is expressed as,

$$V_m(\eta)|_{\eta=1} = \sum_{m=1,2}^{\infty} E_m \sin emp\xi \qquad (6)$$

Upon enforcing this latter boundary condition a complete solution for the building block response in terms of the driving coefficients, E_m, is available. The second building block of Figure 1 constitutes essentially a mirror image of the first. Solution for its response is readily extracted from that of the first through a transformation of axes as described in reference [2].

Upon superimposing of the building block solutions, one-upon-the-other, standard procedures are followed. Let there be K terms in each building block solution. The difference between the normal stress and the elastic forces along the edge, $\eta=1$, is expanded in an appropriate series of K terms. That of equation 6 is used here. Each coefficient in this new boundary series is set equal to zero thus giving rise to K homogeneous algebraic equations relating the 2K driving coefficients, E_m, F_n, etc. A second set of equations is obtained by enforcing equilibrium along the edge, $\xi=1$. The coefficient matrix of this combined set of equations becomes our eigenvalue matrix. Eigenvalues are those values of the parameter λ^2 which cause the determinant of this matrix to vanish.

It will be appreciated that certain limiting eigenvalues will be approached as the elastic spring constants are allowed to approach their limits of zero and infinity. It is found that convergence is rapid and correct limits are approached by each mode.
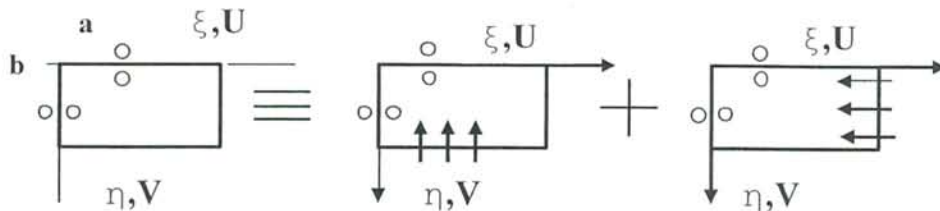
Figure 1. Schematic representation of building blocks employed in
Fully Symmetric mode analysis.

References

1) D. J. Gorman, 'On the free in-plane vibration of rectangular plates by the method of superposition', Proceedings of the Fourth International Symposium on Vibrations of Continuous Structures, Skiddaw Hotel, Keswick, Lakes District, England, July 7-11, 2003.
2) D. J. Gorman, 'Free in-plane vibration analysis of rectangular plates by the method of superposition', Journal of Sound and Vibration, Vol. 272, (2004), pp831-851.
3) D. J. Gorman, 'Accurate analytical type solutions for the free in-plane vibration of clamped and simply supported rectangular plates', Journal of Sound and Vibration (in press).

Remarks on an Annular Plate with Partial Elastic Bedding

Peter Hagedorn, Daniel Hochlenert, Florian Fischer
Technische Universität Darmstadt, Department of Applied Mechanics, Germany

Introduction

The motivation for the problem discussed in this note was the modelling of squeal in disk brakes. The squeal corresponds to self-excited vibrations of the brake system. The vibration pattern of a squealing brake is dominated to a good extent by the dynamic behavior of the brake disk, which for certain purposes can be modelled as an annular plate clamped at its inner boundary and undergoing transverse vibrations. This annular plate is in contact with the brake pads, which in the present note are approximated by elastic bedding acting over a sector of the plate. Understanding the details of the eigenmodes and eigenfrequencies of such a plate can help to construct squeal free brakes.

The present note is devoted to the calculation and discussion of the mode shapes of an annular plate with partial elastic bedding. Some of the results obtained by adding the elastic bedding to the plate were unexpected. They can however readily be understood intuitively and the phenomena will be discussed making use of simpler problems, namely a vibrating string with partial bedding and also of a simple two degree-of-freedom system.

Partially elastically bedded annular plate

An annular plate with partial elastic bedding is shown in figure 1. It is modelled as a KIRCHHOFF plate of constant thickness and clamped at its inner radius a and free at the outer radius b. The transverse displacement of the plate is described in polar coordinates by $w(r, \varphi, t)$. The polar coordinates are chosen such that the elastic bedding extends from $\varphi = -\varphi_0$ to $\varphi = \varphi_0$. The inner radius of the bedding is r_i and the outer radius r_a and the bedding constant is k, so that the equation of motion of the plate is

$$\rho h \frac{\partial}{\partial t^2} w(r, \varphi, t) + D \nabla^4 w(r, \varphi, t) + k K(r, \varphi) w(r, \varphi, t) = 0$$

with $K(r, \varphi) = 1$ in the area of the bedding and $K(r, \varphi) = 0$ elsewhere. The corresponding eigenvalue
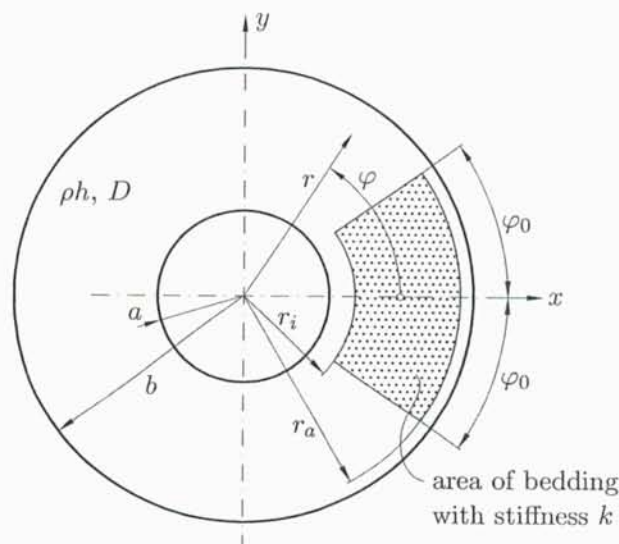

Figure 1: Annular plate with partial elastic bedding

problem can be solved in terms of BESSEL and trigonometric functions. For the calculation of a limited number of eigenmodes it turns out to be more convenient to use a RITZ discretization in the form

$$W(r,\varphi) = \sum_{n=1}^{N} \sum_{m=1}^{M} c_{n,m}(r-a)^{n+1} \cos\left((m-1)\varphi\right) + s_{n,m}(r-a)^{n+1} \sin\left((m-1)\varphi\right)$$

for the eigenfunctions. The eigenvalue problem of the discretized system was solved and the eigenvalues behave in the expected manner, i.e. all eigenfrequencies of the system increase with increasing bedding stiffness k. Understanding the changes in the mode shapes due to the bedding requires some additional thoughts. Figure 2 shows the normalized mode shapes for one nodal circle and 3 diameters. The region of the bedding is marked as a black area. The mode shapes are normalized to be 1 at $r=b$ and $\varphi=\pi$. One can see that the normalized mode shapes of the bedded plate may
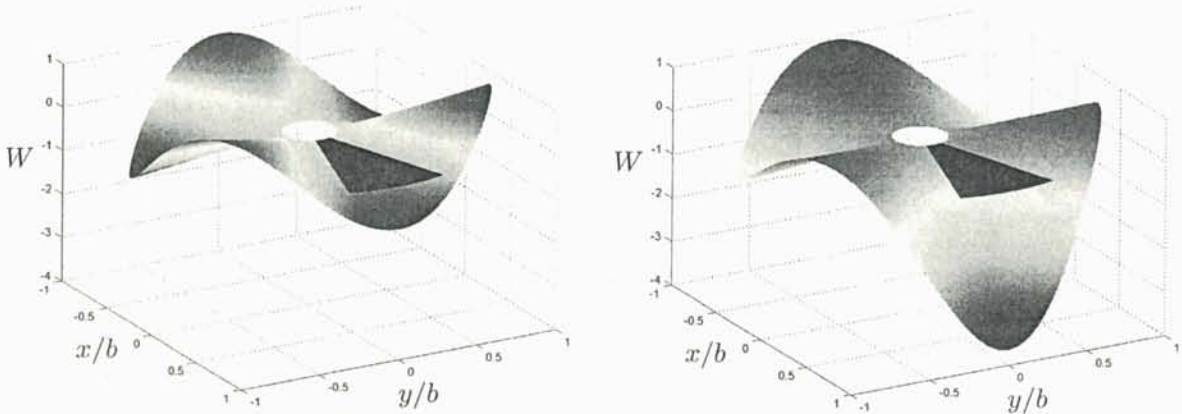

Figure 2: Normalized mode shapes without (left) and with (right) elastic bedding

have larger absolute values around $\varphi=0$ than the corresponding mode shapes of the plate without bedding. Similar results are obtained for other (not all) mode shapes. This is somehow surprising since the bedding and therefore additional stiffness is now present around $\varphi=0$. It does however become completely clear with some additional considerations, which we will carry out first for a bedded string and then for a 2 degree of freedom system.

Partially elastically bedded taut string

Since the mode shapes of the plate described above can not be calculated in closed form, we consider the simpler problem of a bedded string, for which we find similar results. Figure 3 shows a taut string (tension T, length L, mass per unit area ρh) which is partially elastically bedded (stiffness per unit length k, length of bedding b). The eigenfunctions of this system can be calculated by solving
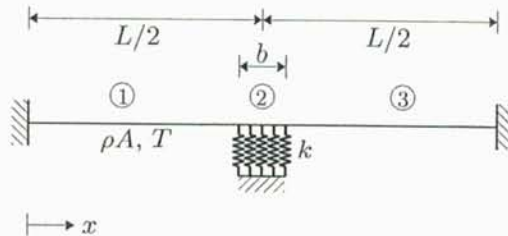

Figure 3: Taut string with partial elastic bedding

the wave equation in closed form separately in the three sections and matching the solutions with

continuity conditions. Figure 4 shows the analytically calculated fifth eigenfunction of the taut string for $b/L = 0.2$ and varying dimensionless stiffness of the bedding $k^* = kL^2/T$. The eigenfunctions are
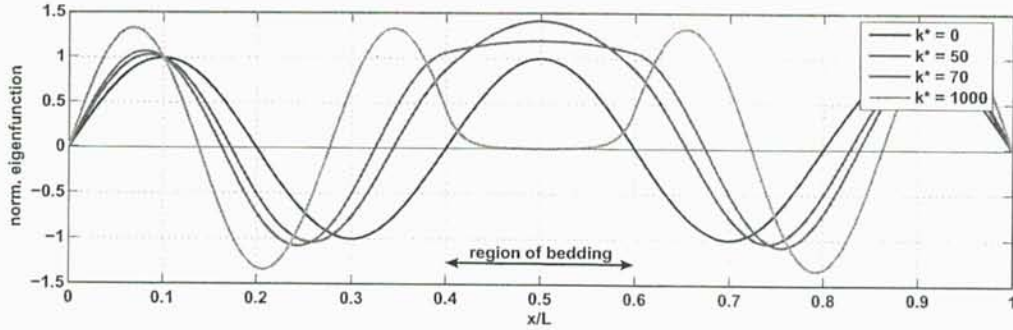

Figure 4: Fifth eigenfunction of the taut string for varying k^*

normalized to have the same values at $x/L = 0.1$ for different dimensionless stiffness of the bedding. The results show similar behavior compared to the partially bedded plate. The fifth eigenfunction clearly has a larger value around $x/L = 0.5$ for $k^* = 50$ and $k^* = 70$ than the corresponding eigenfunction of the string without bedding. It is obvious that for very large values of k^* there are eigenfrequencies of the type $\omega^2 = k/\rho A$, since the influence of the stiffness of the string in the bedded region then becomes negligible. By considering this problem of the bedded string we have therefore obtained a more intuitive understanding of the mode shapes of the bedded plate problem.

Two degree of freedom analogue

One may think that the phenomenon of increasing the normalized amplitude of the eigenfunctions at the location of additional bedding only occurs in continuous systems. However, similar results can be found with the two degree of freedom system shown in figure 5. The right spring with stiffness
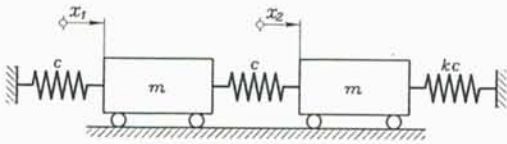
Figure 5: Two degree of freedom model
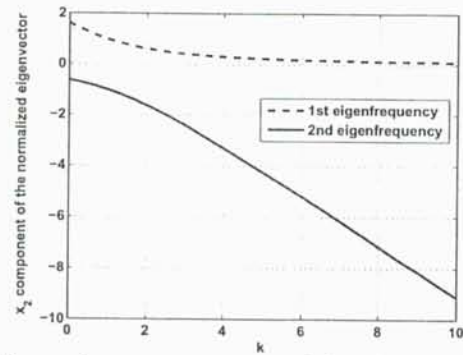
Figure 6: x_2-components of the eigenvectors

kc corresponds to an additional bedding which is attached to the system at the body 2, whose position is described by the coordinate x_2. Figure 6 shows the x_2 component of the eigenvectors of this system for varying k. The eigenvectors are normalized such that the x_1 component is 1. It is clear that the absolute value of the x_2 component of the eigenvector corresponding to the second eigenfrequency increases with increasing k. For k going to infinity there is in the limit an eigenvector $(0,1)$. The corresponding eigenvalue is simply $\omega^2 = kc/m$, as can be immediately and intuitively understood without carrying out any computations. Therefore the two degree of freedom model in this respect shows a similar qualitative behavior as the plate and the string.

IN-PLANE ANALYSIS OF VIBRATION AND STABILITY OF A LOADED ARCH WITH VARIABLE CURVATURE

C. S. Huang*, K. Y. Nieh**, and M. C. Yang*

*: Department of Civil Engineering, National Chiao Tung University, Hsinchu, Taiwan

**: Department of Civil Engineering, Tamkang University, Tamsui, Taiwan

INTRODUCTION

Curved beam structures have been often used in civil, mechanical, and aerospace engineering applications, for example, arch bridges, springs, and stiffeners in aircraft structures. Review articles (Laura and Maurizi, 1987; Chidamparam and Leissa, 1993) reveal that most of the research examines the vibrations of unloaded arches and rings, but rather few publications address the vibrations of loaded arches and rings, even though dynamic analyses of loaded arches are frequently needed in many engineering applications.

Most studies on the vibrations and stability of loaded circular arches considered cases with inextensional centerline or no shear deformation (i.e. Chidamparam and Leissa, 1995; Kang *et al.*, 1996). Recently, Huang *et al.* (2003) developed the governing equations for such an arch using the variational form presented by Washizu (1982) for the dynamical problems concerning an elastic body under initial stresses. The developed governing equations include not only the effect of initial axial force but also the effects of other initial stress resultants, such as shear force and moment due to initial loading. This study basically extends the authors' previous work on circular arches (Huang *et al.*, 2003) to arches with variable curvature. A series-based solution is established to investigate the effects of the opening angle, the ratio of the long-axis length to the short-axis length, and a slenderness parameter on the vibration frequencies and buckling loads of elliptic arches under uniformly distributed vertical forces.

GOVERNING EQUATIONS

The equations governing the free vibration of a loaded arch and the associated boundary conditions are developed according to the following variational principle given by Washizu (1982) for the dynamic problem of an elastic body with equilibrium initial stresses, $\sigma_{ij}^{(0)}$:

$$\delta \int_{t_1}^{t_2} \left\{ T - U - \iiint_V \sigma_{ij}^{(0)} \varepsilon_{ij}^{(H)} dV \right\} dt = 0, \tag{1}$$

where T and U are the kinetic and strain energies, given by

$$T = \iiint_V \frac{1}{2} \rho (\dot{\bar{v}}^2 + \dot{\bar{w}}^2) dV, \quad U = \iiint_V \frac{1}{2} \sigma_{ij} \varepsilon_{ij}^{(L)} dV, \tag{2}$$

ρ is the material density, and the dots denote the derivative with respect to time. In the strain components ε_{ij}, the superscript "L" represents infinitesimal strain parts, while the superscript "H" denotes high order terms. The term with $\sigma_{ij}^{(0)}$ represents the additional strain energy contributed by the initial static stresses.

As in Timoshenko first-order beam theory, the in-plane displacement components of an arch can be assumed to be

$$\bar{v}(r,\theta,t) = v(\theta,t) - z\psi(\theta,t) \quad \text{and} \quad \bar{w}(r,\theta,t) = w(\theta,t), \tag{3}$$

where v and w represent the tangential and radial displacements of the centroidal axis, respectively, and ψ is the angle of rotation of the centroidal axis due to bending only. Introduce the following definition of stress resultants:

$$(N, M) = \int_A \sigma_{\theta\theta}(1, z)\, dA, \quad Q = \int_A \sigma_{r\theta}\, dA, \quad (N^{(0)}, M^{(0)}, P^{(0)}) = \int_A \sigma_{\theta\theta}^{(0)}(1, z, z^2)\, dA, \text{ and}$$

$$(Q^{(0)}, T^{(0)}) = \int_A \sigma_{r\theta}^{(0)}(1, z)\, dA \cdot \tag{4}$$

The relationships between the stress resultants and the displacement components for an arch with h/R (where h and R are the thickness of arch and the radius of the centroidal axis, respectively) sufficiently less than unity are

$$N = EA\left(\frac{\partial v}{\partial S} + \frac{w}{R}\right), \quad M = EI\frac{\partial \psi}{\partial S}, \quad Q = \kappa GA\left(\frac{\partial w}{\partial S} - \frac{v}{R} - \psi\right), \quad P = EI\left(\frac{\partial v}{\partial S} + \frac{w}{R}\right), \text{ and } \quad T = \kappa GI\frac{\psi}{R} \tag{5}$$

where S is the arc length coordinate; E and G are elastic and shear moduli, respectively; A and I are the area and moment of inertia of the cross section, respectively; and κ is the correction factor for the shear force.

By performing the variation as indicated in eqn (1), the governing equations for the free vibrations of a statically loaded arch with the displacement field specified by eqns (3) are obtained and expressed as

$$N' + \frac{Q}{R} + (N^{(0)}v' + M^{(0)}\psi' + \frac{N^{(0)}}{R}w - Q^{(0)}\psi)' + \frac{N^{(0)}}{R}w' - \frac{1}{R^2}(N^{(0)}v + M^{(0)}\psi) = \rho A \ddot{v} \tag{6a}$$

$$Q' - \frac{N}{R} + (N^{(0)}w' - \frac{N^{(0)}}{R}v - \frac{M^{(0)}}{R}\psi)' - \frac{N^{(0)}}{R}v' - \frac{M^{(0)}}{R}\psi' + Q^{(0)}\frac{\psi}{R} - \frac{N^{(0)}}{R^2}w = \rho A \ddot{w}, \tag{6b}$$

$$M' + Q + (M^{(0)}v' + \frac{M^{(0)}}{R}w + P^{(0)}\psi')' + \frac{M^{(0)}}{R}w' + Q^{(0)}(v' + \frac{w}{R}) - \frac{M^{(0)}}{R^2}v - \frac{P^{(0)}}{R^2}\psi + (T^{(0)})'\psi = \rho I \ddot{\psi} \tag{6c}$$

where the primes denote derivatives with respect to S.

Substituting the relations between stress resultants and displacement components into the governing equations yields a set of three differential equations with complicated variable coefficients in terms of the displacement functions. The static solution is first found for determining the distribution of initial stress resultants caused by static loading. Then, the solutions for vibration frequencies and buckling loads are obtained by solving the proposed governing equations. A general analytical solution to the governing equations is obtained by decomposing the entire arch under consideration into several sub-domains and establishing a dynamic stiffness matrix for each sub-domain. The dynamic stiffness matrix is developed according to a series solution of the governing equations defined in the sub-domain.

RESULTS AND DISCUSSION

Consider an elliptic arch with $b/a = 0.5$ and $\mu = 20$ and subjected to uniform static vertical loads with intensity γ, where a and b are the long-axis length and short-axis length, respectively, and $\mu = 2a/\sqrt{I/A}$. Figure 1 exhibits the variation of $\overline{\kappa}(= \omega L^2 \sqrt{\rho A/EI}$, where $L = 2a$) with $\downarrow$ $(= \gamma L^3/EI)$ for a clamped arch with opening angle $\theta_0 = 60°$, considering various combinations of static stress resultants, namely $N^{(0)}$, $Q^{(0)}$, $M^{(0)}$, $P^{(0)}$, and $T^{(0)}$ in eqns (6a)-(6c). In the legend of the figure, the stress resultants inside parentheses are those considered in eqns (6a)-(6c) to obtain the results. The lable (ALL) indcates the results obtained by considering all the stress resultants in eqns

(6a)-(6c). Only the results for the first symmetric mode are shown. Traditionally, the static axial force $N^{(0)}$ is thought of as the most important factor that influences the vibration behavior of a preloaded beam. Figure 1 reveals considerable differences between the results obtained by considering all the static stress resultants in eqns. (6a)-(6c) and those obtained by considering $N^{(0)}$ only, especially in the region of small ⬉. Figure 2 plots the buckling loads as a function of opening angle. In the legend of the figure, S1 and A1 represent the buckling loads that correspond to the first symmetric and anti-symmetric modes, respectively. The buckling loads were determined by considering all initial stress resultants or $N^{(0)}$ only. Figure 2 also depicts the results of Nieh *et al.*(2002), based on the theory neglecting shear deformation and represented by $\varepsilon_{r\theta} = 0$ in the legend of the figure.
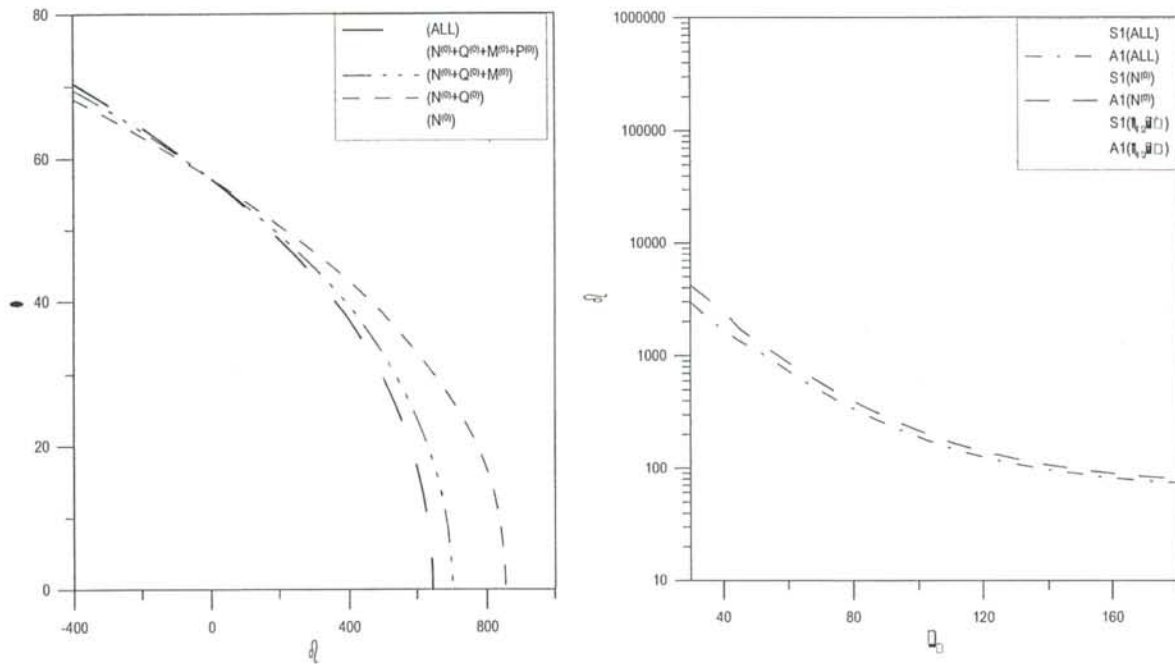

Fig.1 Variation of ⬉ with ⬇for an elliptic arch   Fig. 2 Variation of buckling loads withθ_0 for elliptic

with a/b=0.5, μ=20, and θ_0=60°   arches with a/b=0.5 and μ=20

REFERENCES

Chidamparam, P. and Leissa, A. W., Vibrations of planar curved beams, rings, and arches. *Applied Mechanics Reviews,* 1993, 46(9), pp.467-483.

Chidamparam, P. and Leissa, A. W., Influence of centerline extensibility on the in-plane free vibrations of loaded circular arches, *Journal of Sound and Vibration*, 1995, 183(5), pp. 779-795.

Huang, C. S., Nieh, K. Y., and Yang, M. C., In-plane free vibration and stability of loaded and shear-deformable circular arches, *International Journal of Solids and Structures*, 2003, 40, pp.5865-5886.

Kang, K. L., Bert, C. W., and Striz, A. G., Vibration and buckling analysis of circular arches using DQM, *Computers and Structures*, 1996, 60(1), pp.49-57.

Laura, P. A. A. and Maurizi, M. J., Recent research on vibrations of arch-type structures. *The Shock and Vibration Digest,* 1987, 19 (1), pp.6-9.

Nieh, K. Y., Huang, C. S., and Tseng, Y. P. An analytical solution for in-plane free vibration and stability of loaded elliptic arches, *Computer & Structures*, 2003, 81(13), pp.1311-1327.

Washizu, K. *Variational Methods in Elasticity & Plasticity*, 3rd ed., Pergamon Press, Oxford, 1982.

The Crosswise Series Superposition Method in Solid Mechanics

James R. Hutchinson

Department of Civil and Environmental Engineering, University of California, Davis

This paper is intended primarily as a tutorial on the crosswise series superposition method in solid mechanics. Its history will be outlined and some results from recent work-in-progress will also be presented. This method has been called by a number of different names in the past, including: Mathieu's method, the Fourier series method, the exact method, and the superposition method. Therefore, I have chosen to call it by another, and I hope, even more descriptive name. The method of solution has an interesting history in that it has been apparently been rediscovered a number of times. Mathieu [1] first applied the method in 1890 to plane strain problem of a rectangular plate loaded with normal stress distributed on the boundary. In 1933 Taylor [2] applied the method to the lateral buckling of a rectangular plate with four clamped edges subjected to "thrusts in its plane and perpendicular to its edges." For the numerical solution Taylor limited the solution to a square plate with equal thrusts along each edge. In 1936 Tomotika [3] solved the problem of the transverse vibration of a square plate clamped at four edges by the same method. In 1938 Timoshenko [4] used the method to solve the static problem of the bending of rectangular plates with clamped edges. Timoshenko limited his numerical work to the square plate with a uniform load. Timoshenko gave more of a physical description of the process than Taylor or Tomotika, but the solution steps were almost identical in all three papers. Tomotika did reference the work of Taylor, but Timoshenko did not mention either, even though his work was two years after Tomotika's and 5 years after Taylor's. Following Tomotika's work, a number of other researchers applied the method to rectangular plate vibrations. In 1944 Pickett [5] applied the method to plane stress problems in a rectangular domain, and to the problem of the axial compression of circular cylinders. In 1967 Hutchinson [6] applied the method to the problem to the axisymmetric vibrations of a solid elastic cylinder encased in a rigid container. I also wrote a number of follow-on papers on the vibrations of cylinders using the crosswise series superposition method. In 1976 Gorman [7] wrote the first of many papers, and two books, using this method for the vibration of rectangular plates. Other vibration problems such as Box Type Structures, Rectangular Parallelepipeds and Open Cylindrical Shells have also been solved using this method. Space limitations preclude my giving specific reference to these.

To describe the method I will consider Tomotika's problem of the rectangular plate, which is fixed on all four edges. As Tomotika did, I will limit the solution to the modes that are symmetric in both x and y. The governing differential equation is:

$$DV^4w + \rho\frac{\partial^2 w}{\partial t^2} = 0 \tag{1}$$

Assuming sinusoidal motion $w = W \cos \omega t$ and defining k^4 as $\rho\omega^2/D$ equation (1) becomes,

$$\left(\nabla^4 - k^4\right)W = 0 \tag{2}$$

Solution forms which are symmetric in both x and y can be written in the following form,

$$W = \cos\alpha x \cos\beta y \quad \text{where} \quad \alpha^2 + \beta^2 = \pm k^2 \tag{3}$$

The plate has dimensions $2a$ in the x direction and $2b$ in the y direction, with the origin at the center. The boundary conditions for this problem are that $W(a,y) = 0$, $W(x,b) = 0$, $W_x(a,y) = 0$, and $W_y(x,b) = 0$. As pointed out by Taylor Tomotika and Timoshenko, these boundary conditions do not allow for the satisfaction of both boundary conditions on two opposite edges. Therefore they chose to satisfy one boundary condition on each edge. Their choice was to satisfy the displacement boundary conditions identically. The total solution can be written as two infinite series.

$$W = \sum_{n=1}^{\infty} A_n \left[a_1 \cos\beta_1 y + a_2 \cos\beta_2 y \right] \cos\alpha_A x + \sum_{n=1}^{\infty} B_n \left[b_1 \cos\alpha_1 x + b_2 \cos\alpha_2 x \right] \cos\beta_B y \tag{4}$$

For the A series $\beta_1^2 = k^2 - \alpha_A^2$ and $\beta_2^2 = -k^2 - \alpha_A^2$, and for the B series $\alpha_1^2 = k^2 - \beta_B^2$ and $\alpha_2^2 = -k^2 - \beta_B^2$. The α_A are chosen so that the A series will satisfy $W(a,y) = 0$, the β_B are chosen so that the B series will satisfy $W(x,b) = 0$, the a_1 and a_2 are chosen so that the A series will satisfy $W(x,b) = 0$, and the b_1 and b_2 are chosen so that the B series will satisfy $W(a,y) = 0$. Thus, the choice can be made that,

$$\alpha_A = (2n-1)\pi/2a, \quad \beta_B = (2n-1)\pi/2b, \quad a_1 = \cos\beta_2 b, \quad a_2 = -\cos\beta_1 b, \quad b_1 = \cos\alpha_2 a, \quad b_2 = -\cos\alpha_1 a \tag{5}$$

At this point it is evident why the name crosswise was used to describe the method. One can view the A series as a Fourier series in x and the B series as a Fourier series in y; however, the A series coefficients are functions of y and the B series coefficients are functions of x. Each series, therefore, affects the other in a *crosswise* fashion. The slopes are given by the expressions,

$$W_{,x} = \sum_{n=1}^{\infty} A_n \left[-a_1 \cos\beta_1 y - a_2 \cos\beta_2 y \right] \alpha_A \sin\alpha_A x + \sum_{n=1}^{\infty} B_n \left[-b_1\alpha_1 \sin\alpha_1 x - b_2\alpha_2 \sin\alpha_2 x \right] \cos\beta_B y \tag{6}$$

$$W_{,y} = \sum_{n=1}^{\infty} A_n \left[-a_1\beta_1 \sin\beta_1 y - a_2\beta_2 \sin\beta_2 y \right] \cos\alpha_A x + \sum_{n=1}^{\infty} B_n \left[-b_1 \cos\alpha_1 x - b_2 \cos\alpha_2 x \right] \beta_B \sin\beta_B y \tag{7}$$

The slope boundary conditions are satisfied by applying orthogonality along each edge. Thus,

$$\int_0^b W_{,x}(a,y) \cos\beta_m y\, dy = 0 \quad \int_0^a W_{,y}(x,b) \cos\alpha_m x\, dx = 0 \quad \text{where } \beta_m = \frac{(2m-1)\pi}{2b}, \text{ and } \alpha_m = \frac{(2m-1)\pi}{2a} \tag{8}$$

This leads to the following matrix form,

$$\begin{bmatrix} [c_{11}] & [c_{12}] \\ [c_{21}] & [c_{22}] \end{bmatrix} \begin{Bmatrix} \{A\} \\ \{B\} \end{Bmatrix} = \begin{Bmatrix} \{0\} \\ \{0\} \end{Bmatrix} \tag{9}$$

where c_{11} and c_{22} are diagonal matrices and c_{12} and c_{21} are full matrices. The solution process is to search for the frequencies, which make the determinant of the C matrix zero. It should be noted that each series may be truncated with a different number of terms. This author has found it best to make the number of terms proportional to the aspect ratio. Thus if $b = 2a$ make $N_y = 2N_x$, where N_x is the number of terms in the A series and N_y is the number of terms in the B series.

There are a number of arbitrary choices that are made in this solution. There is the choice of the a's and b's. The a_1 and a_2 must only be in the *proportion* chosen, and likewise with the b_1 and b_2. The choice of which boundary conditions to satisfy identically and which to satisfy by orthogonality are even more arbitrary. For instance one could choose to satisfy the slope conditions identically and the displacement conditions by orthogonality. This could be done by taking,

$$\alpha_A = (n-1)\pi/a, \quad \beta_B = (n-1)\pi/b, \quad a_1 = \beta_2 \sin\beta_2 b, \quad a_2 = -\beta_1 \sin\beta_1 b \quad b_1 = \alpha_2 \sin\alpha_2 a, \quad b_2 = -\alpha_1 \sin\alpha_1 a \tag{10}$$

$$\int_0^b W(a,y) \cos\beta_m y\, dy = 0 \quad \int_0^a W(x,b) \cos\alpha_m x\, dx = 0 \quad \text{where } \beta_m = \frac{(m-1)\pi}{b}, \text{ and } \alpha_m = \frac{(m-1)\pi}{a} \tag{11}$$

It would also be possible to satisfy the displacement identically along one edge and the slope on the other, and the other two boundary conditions by orthogonality.

What is shown above is the basic process, but the various authors have expressed the process differently while going through the same steps. I described the process for satisfying the boundary conditions, which were not satisfied identically, as an application of orthogonality. Taylor, Tomotika, Timoshenko, and Gorman express it as a Fourier expansion. For instance those authors, in satisfying the condition $W_{,y}(x,b) = 0$ would say the A series is a Fourier cosine series so the B series needs to also be expanded as a Fourier cosine series, and each coefficient in the two-series expansion must vanish. This, of course, is exactly what the orthogonalization in equations (8) accomplishes. Another difference is that many of the authors, in recognition of the fact that the β's in the A series and the α's in the B series can be imaginary, split each series into two series so that everything will be real. I prefer to handle that detail at the programming level. The C matrix will contain expressions with $\alpha_1 \sin \alpha_1 a$ and $\cos \alpha_1 a$ with similar expressions for the other α's and β's. In the computer program I check if α_4^2 is positive or negative, if positive I return the sine and cosine as written, if negative,

$$\alpha_1 \sin \alpha_1 a \text{ is returned as } -|\alpha_1|\left(1 - e^{-2|\alpha_1|a}\right) \text{ and } \cos \alpha_1 a \text{ is returned as } \left(1 + e^{-2|\alpha_1|a}\right) \tag{12}$$

These expressions are the hyperbolic sine and cosine normalized by $2e^{-|\alpha_1|a}$. The reason for the normalization is to prevent computer overflow.

As mentioned above, Timoshenko explained the process in physical terms. He considered the moments along the boundary $y = b$ from the A series and the moments along the boundary $x = a$ from the B series as acting to force the slopes to zero. Gorman in his papers carries that process one step further. He shows "building blocks" corresponding to each of the series with the moments along their edges and considers the process as a superposition of these blocks. This process has some merit in visualizing plate problems, but does not lend itself well to the solid cylinder and rectangular parallelepiped formulations.

Pickett noted that he ran into convergence problems for the problem of the axial compression of circular cylinders. He required that both ends of the cylinder be fully clamped and the cylindrical surfaces be free. There is a singularity that can be expected to occur at the corner where the cylindrical surface meets the end. He did not say how many terms he had chosen; however, the paper was written before the advent of the digital computer, which would have greatly limited him. So one cannot say whether or not the solution would have converged with more terms. I recently attempted the solution of the vibrating cylinder, which is fully clamped at one end and free on the other surfaces. I also ran into convergence problems. The solution converged reasonably well for the fundamental frequency, but the higher frequencies did not converge well nor compare well with known results. The problem could have been in the formulation, the computer program, or the existence of the singularity. The next step will be to take a careful look at the mode shapes to see if that will shed any light on the problem. As far as I have been able to determine, convergence has not been a problem for any of the plate problems.

REFERENCES:

1. Mathieu, É., *Theorie de l'Élasticité Des Corps Solides*, Gauthier-Villars, Paris, 1890, pp. 140-181.
2. Taylor, G. I., "The Buckling Load for a Rectangular Plate With Four Clamped Edges," *Zeitschrift für Angewandte Mathematik und Mechanik*, Band 13, 1933, pp. 147-152.
3. Tomotika, S., "The Transverse Vibration of a Square Plate Clamped at Four Edges," *Philosophical Magazine*, Vol. XXI, 1936, pp. 745-760.
4. Timoshenko, S. P., "Bending of Rectangular Plates With Clamped Edges," *Proceedings of Fifth International Congress of Applied Mechanics*, Cambridge, Mass., 1938, pp. 40-43.
5. Pickett, G., "Applications of the Fourier Method to Solution of Certain Boundary Problems in the Theory of Elasticity," *ASME Journal of Applied Mechanics*, Vol.11, 1944, pp. A176-182.
6. Hutchinson, J. R., "Axisymmetric Vibrations of a Solid Elastic Cylinder Encased in a Rigid Container," *The Journal of the Acoustic Society of America*, Vol. 42, 1967, No. 2, pp. 398-402.
7. Gorman D. J. and Sharma, R. K., "A Comprehensive Approach to the Free Vibration Analysis of Rectangular Plates by use of the Method of Superposition," *Journal of Sound and Vibration*, Vol. 47, 1976, pp. 126-128.

Recent advances in asymptotic modeling in vibration analysis.

S. Ilanko

Department of Mechanical Engineering, University of Canterbury, Christchurch, New Zealand.

Background

The Rayleigh-Ritz and the Galerkin methods are widely used in the vibration analysis of continuous systems. They are approximate methods and require the displacement form to be expressed as a series of product of admissible shape functions and undetermined coefficients. In vibration analysis, the Rayleigh-Ritz method gives upperbound values for the natural frequencies. The proof of this bounded nature of the solution appears to have been first reported by Lord Rayleigh [1,2] and explained clearly by Gould [3]. Galerkin's method also yields upperbound results and gives rise to the same stiffness and mass matrices as the Rayleigh-Ritz method if the admissible functions used are the same. Although Rayleigh introduced the notion of minimising the expression for the frequency in the form of a quotient called the Rayleigh Quotient [1], it was Ritz [4] who presented the popular minimisation procedure in which the potential and kinetic energy terms as expressed as quadratic functions of undetermined displacement coefficients leading to a simple eigenvalue matrix equation.

An essential requirement of the Rayleigh-Ritz method is that the displacement functions used must not violate any geometric constraints such as that translation or rotation be zero at the supports or be continuous at connections. This limitation may be overcome by using the Lagrangian multiplier method but it involves two sets of equations: the constraint equations and the modified minimization equations. The formulation and solution of the resulting eigenvalue problem become more complicated. In addition, continuous constraints such as line supports do not result in explicit constraint equations that can be readily used, and need to be approximated by a series of point supports or by other means.

A more convenient method of handling constraints was introduced by Courant in 1943 [5] by replacing rigid supports with partial elastic restraints of very high stiffness. With partial restraints the admissibility requirements are relaxed and their effect in controlling the translation or rotation is considered through the strain energy terms associated with their deformation. This idea has subsequently been adopted into other mathematical procedures to solve problems in a vast range of disciplines due to the contribution of Zienkiewicz [6, 7] in what is now well known as the penalty function method. In vibration analysis, this method has also been extended by Yuan and Dickinson and others [8] for the analysis of connected systems and also plates with cracks.

One drawback with this approach is that it is not possible to determine the error caused by replacing a rigid constraint with a restraint of large stiffness. If the stiffness parameters used are not sufficiently large, the error due to the violation of the constraint may be too large, but a very high stiffness value could cause numerical problems such as ill conditioning. A suitable stiffness value is usually found by trial and error until the solution shows numerical convergence. In addition, the upper bound nature of the Rayleigh-Ritz solution would be lost by replacing a constraint with a restraint as the resulting solution is an upper bound to a lower bound model.

However, recent publications show that it is possible to overcome these problems by using positive and negative values for the stiffness of artificial restraints in asymptotic models [9-12]. It has been proven that by using a combination of large positive and negative stiffness values it is possible to determine the maximum possible error due to the modelling [9]. The proof is based on Rayleigh's theorem of separation [1, 3]. Although Lord Rayleigh [1] did not suggest the use of large stiffness to model constraints, he derived the theorem of separation by treating a constrained system as a special case of non-constrained system where either the kinetic energy or potential energy associated with the motion of the constrained coordinate was taken as infinite. The expression for the natural frequencies of the unconstrained system was determined by expanding a determinantal frequency equation. A simpler mathematical proof of the theorem of separation was presented by Gould [3]. The author was unaware of these when he first proposed the idea of using masses instead of stiffness to obtain true upper bound solutions to constrained systems at the First International Symposium on Vibration of Continuous Systems [13]. This idea did not receive much support because using large masses to enforce continuity of displacement at joints seemed awkward compared to using springs with large stiffness. While replacing a stiff spring support with a large inertial body could be easily visualised, rigidly connecting two elements by introducing a mass is harder to imagine. In order to do this, it is necessary to introduce a mass that vibrates

at the relative speed between the connected elements. Although one could think of a complicated pulley system to cause a mass to vibrate at such a relative speed, and the introduction of an artificial mass is only needed in a mathematical sense, this idea was not well received. During the informal discussion session, the author then proposed the use of restraints with negative stiffness and these too raised questions about the possibility of introducing instability. However, subsequent research has shown that this idea works well [9]. The work presented in [9] also came under constructive criticism at a seminar [14] for not having a theoretical proof as it was only a demonstration. Questions were still raised about potential problems with instability and the existence of natural frequencies of negatively restrained systems. The author subsequently arrived at a conditional proof that relied on their being a proof for the separation of natural frequencies of the constrained systems. Professor Hagedorn [15], who was at the University of Canterbury at that time, introduced this proof in Reference [3] to the author. The author then derived two theorems of existence and convergence of natural frequencies of systems with positive and negative restraints. The theorems in [10] could be inferred from Rayleigh's work but its effect on asymptotic modelling and the use of negative stiffness for this purpose are not readily obtainable from his work. Subsequently, the theorems in Reference [10] were used to derive another proof showing that the critical loads of structures could also be found using asymptotic modelling in the same way [11].

Existence and convergence of natural frequencies of systems carrying artificial stiffness or inertial restraints

The theorems presented in Reference [10] were derived assuming that each constraint resulted in the loss of one vibratory degree of freedom. That is to say, all constraints and asymptotic restraints were associated with a mass or inertia. However the bounding nature of the asymptotic models has been shown to be true even for systems subject to constraints that are not associated with any mass or inertia [12]. For example, a massless cantilever beam carrying a particle of mass m at a point is a single degree of freedom system. By introducing a prop at mid-span, the displacement form would be constrained but it would still be a one degree of freedom system. The theorems presented in [12] are as follows:

Theorem 1 (a): If h restraints of positive or negative stiffness are added to an n degree of freedom system (A) where $h<n$, along coordinates that are directly associated with a mass or inertia, then for the resulting system (A_h), there exist at least ($n-h$) natural frequencies and modes.

Theorem 1 (b): Furthermore, as the h stiffness parameters approach infinity, the ($n-h$) natural frequencies and modes of System A_h would asymptotically approach those of the n degree of freedom system subject to h constraints ($\tilde{A}_h$).

Theorem 2 (a): If h restraints of positive or negative stiffness are added to an n degree of freedom system (A), along coordinates that are not directly associated with a mass or inertia, then for the resulting system ($A_{(h)}$), there exist at least (n) natural frequencies and modes for all positive values of stiffness, and for very large values of negative stiffness, but for a finite range of negative stiffness values, in the vicinity of h specific critical values, some of the frequencies may not exist.

Theorem 2 (b): As the magnitudes of the h stiffness parameters approach infinity, the n natural frequencies and modes of System A_h would asymptotically approach those of the n degree of freedom system subject to h constraints ($\tilde{A}_{(h)}$), irrespective of the sign of the stiffness.

The proofs for the above theorems are given in References [10, 12]. Similar proof is given in Reference [11] to show that critical loads of linear structures with constraints are also bracketed and approached by the critical loads of the corresponding asymptotic model.

While the theorems of existence and convergence of natural frequencies of negatively or positively restrained systems justify the use of asymptotic modelling for vibration analysis, there still remains a practical problem: in any practical application the magnitude of negative stiffness values must be greater than the highest critical stiffness parameter to ensure that the correct modes are being traced. To overcome this problem, the use of positive and negative artificial mass or inertia has been proposed. The justification comes in the form of the following theorems which have recently been accepted for publication [16].

Theorem 3 (a): If h artificial inertial restraints of positive or negative mass are added to an n degree of freedom system A where $h<n$, so as to resist the motion along h coordinates each of which is already associated with a mass or moment of inertia, then for the resulting system A_h, there exist at least ($n-h$) natural frequencies and modes.

Theorem 3 (b): Furthermore, as the h inertial parameters approach infinity, $(n-h)$ natural frequencies and modes of System A_h would asymptotically approach those of the corresponding constrained system $\tilde{A}_h$, from above in the case of positive inertial terms, and from below otherwise.

Theorem 4 (a): If h artificial inertial restraints of positive or negative mass are added to an n degree of freedom system A, so as to resist the motion along h coordinates, none of which is already associated with a mass or moment of inertia, then for the resulting system $A_{(h)}$, there exist at least n natural frequencies and modes.

Theorem 4 (b): Furthermore, as the h inertial parameters approach infinity, n natural frequencies and modes of System $A_{(h)}$ would asymptotically approach those of the corresponding constrained system $\tilde{A}_{(h)}$, from above in the case of positive inertial terms, and from below otherwise.

Unlike the case of asymptotic modelling with artificial elastic restraints of positive and negative stiffness, the use of positive and negative inertial terms does not introduce instability at lower modes. Therefore asymptotic modelling with positive and negative terms may be conveniently employed in natural frequency calculations using the Rayleigh-Ritz procedure, without the need to select admissible functions which satisfy geometric constraint conditions.

Concluding Remarks

A brief review of the recent advances in modelling constraints with artificial restraints has been presented. Although the use of positive and negative stiffness values enables the determination and control of errors due to violation of the constraints, the introduction of instability through the negative restraints may cause difficulties. The use of large positive and negative masses has been proposed as an alternative route to asymptotic modelling.

References

1. Lord J.W.S. Rayleigh, *Theory of Sound* New York: Dover, First American Edition, 1945.
2. Lord J.W.S. Rayleigh, On the Calculation of the Frequency of Vibration in its Gravest Mode, with an Example from Hydrodynamics. *Philosophical Magazine*, 1899, pp 566-572.
3. S.H. Gould, *Variational Methods for Eigenvalue Problems* London: Oxford University Press, 1966.
4. Ritz, Walter. Über eine neue Methode zur Lösung genisser Variationsprobleme der Mathematischen Physik. *Journal für Reine und Angewandte Mathematix*, Vol. 135, No. 1, pp. 1-61, 1908.
5. R. Courant, Variational methods for the solution of problems of equilibrium and vibration, *Bulletin of the American Mathematical Society* 1943; **49**: 1-23.
6. Zienkiewicz OC, *The Finite Element Method*, Third Edition, Mc-Graw-Hill: London, 1977; 86, 284-287.
7. Zienkiewicz OC, *Constrained Variational Principles and Penalty Function Methods in the Finite Element Analysis*, Lecture Notes in Mathematics vol. 363, Springer: Berlin, 1974; 207-214.
8. J. Yuan and S.M. Dickinson, On the use of artificial springs in the vibration analysis of systems comprising several distinct components, *Proceedings of the 22nd Midwestern Mechanics Conference, Missouri-Rolla, 1991,* pp91-92.
9. S. Ilanko and S.M. Dickinson, Asymptotic modelling of rigid boundaries and connections in the Rayleigh-Ritz Method, *Journal of Sound and Vibration* 1999; **219(2)**: 370-378S.
10. S. Ilanko, Existence of natural frequencies of systems with imaginary Restraints and their convergence in asymptotic modelling, *Journal of Sound and Vibration* 2002; **255 (5)**: 883-898
11. S. Ilanko, The use of asymptotic modelling in vibration and stability analysis of structures, *Journal of Sound and Vibration* 2003; **263(5)**: 1047-1054
12. S. Ilanko, On asymptotic modelling of constraints that do not Change the degrees of freedom, Submitted to *Journal of Sound and Vibration*, 2004.
13. S. Ilanko, On the application of Rayleigh's Principle and the Ritz method - Some Points to Ponder, *Proceedings of the International Symposium on Continuous Systems*, Colorado, 1997, pp27-8.
14. S. Ilanko, Asymptotic modelling of rigid boundaries in the Rayleigh-Ritz analysis using imaginary masses and negative springs, Mechanical Engineering Seminar, University of Canterbury, 25 March 1999.
15. Private Communication with Professor Peter Hagedorn, Technical University of Darmstadt, Germany, 1999.
16. S. Ilanko, Introducing the Use of Positive and Negative Inertial Functions in Asymptotic Modelling, Royal Society Proceedings A: Physical, Mathematical and Engineering Sciences [in press]

Optimum Design of Prismatic Plate Assemblies with Spectral Gap Constraints

David Kennedy, Owen J. O'Leary and Frederic W. Williams
Cardiff School of Engineering, Cardiff University, Cardiff CF24 0YF, UK

When designing structures positioned close to an excitation source, the inclusion of spectral gap constraints (i.e. frequency ranges required to contain no natural frequencies) reduces the potentially destructive effects of resonance. Although spectral gaps can be created by the strategic addition of non-structural mass[1] or bracing[2], optimum design subject to multiple spectral gap constraints demands a more efficient use of mass within the optimisation process[3].

The software VICONOPT[4] covers the buckling and vibration analysis, and optimum design, of prismatic plate assemblies such as aircraft wing and fuselage panels. Although more general options are available, attention is here confined to the minimum mass design of isotropic stiffened panels with simply supported ends, such that the response varies sinusoidally with m half-waves along the length of the panel. Exact solution of the governing plate equations, without discretisation, results in a transcendental eigenproblem which is solved reliably and efficiently by the Wittrick-Williams (W-W) algorithm[5]. In vibration problems, this algorithm determines $J(f)$, the number of undamped natural frequencies exceeded by a trial frequency f.

Optimum design varies the plate widths and thicknesses in order to minimise the panel mass subject to buckling, frequency and other constraints. In the strategy of Fig. 1, the (outer) sizing cycle calculates the constraints and sensitivities (step 3), which are used (step 5) by the method of feasible directions[6] in the (inner) CONMIN cycle. The stabilisation procedure (steps 2 and 7), adjusts the resulting design to a "just stable" configuration in which the most critical constraint is just satisfied. In buckling problems this is achieved by multiplying all the thickness design variables by the same factor F (whose value is determined iteratively) and leaving the plate widths unchanged. However, because this process alters both stiffness and mass, natural frequencies are not guaranteed to vary monotonically with F. Theoretical and numerical studies[3] have established a stabilisation rule for fundamental natural frequency constraints whereby the plate thicknesses are multiplied by F and their widths by F^α, where $0.1 \le \alpha \le 0.4$. The examples below use $\alpha = 0.3$.

---

[1]   Initial analysis
[2]   Initial stabilisation *(0.1 ≤ α ≤ 0.4)*
        [3]   Constraint and sensitivity analysis
            [4]   Move limit calculation
            [5]   CONMIN optimisation
            [6]   If CONMIN design satisfies all constraints, go to [12]
            [7]   Stabilisation (0.1 ≤ α ≤ 0.4)
            [8]   If just stable design satisfies all constraints, go to [12]
                [9]   Additional stabilisation (0.1 ≤ α ≤ 0.4)
                [10]   If all constraints are satisfied, go to [12]
                [11]   Loop back to [9] for next spectral gap cycle
            [12]   Loop back to [4] for next CONMIN cycle
        [13]   Loop back to [3] for next sizing cycle
[14]   Final analysis

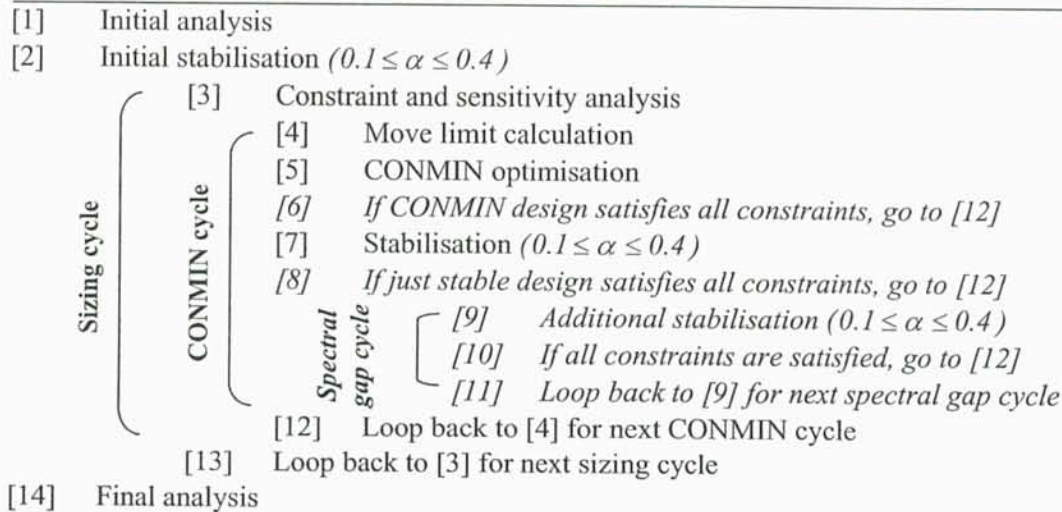*Sizing cycle* — *CONMIN cycle* — *Spectral gap cycle*

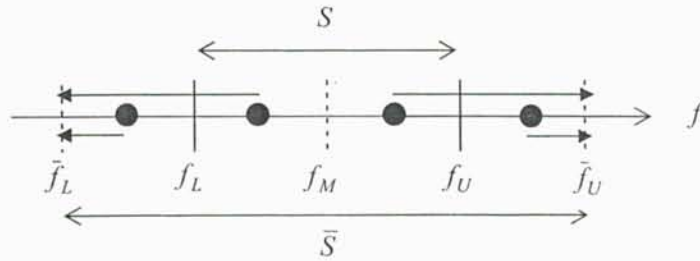Fig. 1. VICONOPT sizing strategy, with additional features for spectral gap clearance in italics.

Fig. 2. Clearance of natural frequencies ● from the spectral gap $S = (f_L, f_U)$.

Clearance of a spectral gap $S = (f_L, f_U)$ requires the removal of any natural frequencies f_i for which $f_L < f_i < f_U$, while ensuring that no other natural frequencies enter S. S is therefore widened to $\bar{S} = (\bar{f}_L, \bar{f}_U)$, where $\bar{f}_L = f_L - \beta(f_U - f_L)$, $\bar{f}_U = f_U + \beta(f_U - f_L)$, as illustrated in Fig. 2, with $\beta = 0.5$ for the examples below. $\bar{S}$ is cleared by imposing (at steps 3 and 5 of Fig. 1) the constraints $f_i < \bar{f}_L$ for all $\bar{f}_L < f_i \leq f_M$, $f_i > \bar{f}_U$ for all $f_M < f_i < \bar{f}_U$, where $f_M = (f_L + f_U)/2$. To establish whether S has been cleared, the W-W algorithm merely needs to check (at steps 6 and 8) that $J(f_L) = J(f_U)$.

In order to facilitate spectral gap clearance, during the first sizing cycle of Fig. 1 upper bounds are placed on the move limits for each design variable (at step 4). Also, the mass of the best feasible design found (at step 7) is permitted to exceed that of the initially stabilised design (step 2).

CONMIN (step 5 of Fig. 1) usually produces a design which fails to satisfy the fundamental natural frequency constraint, but this is remedied by stabilisation (step 7). Steps 6 and 8 determine whether the spectral gaps have been cleared. If not, additional 'spectral gap cycles' (steps 9-11) are initiated. Here the stabilisation factor F is successively increased (e.g. by increments of 0.05), until either all the spectral gaps have been cleared or it is decided to abandon the CONMIN cycle, e.g. because the panel mass is too high or too many natural frequencies remain in the spectral gaps.
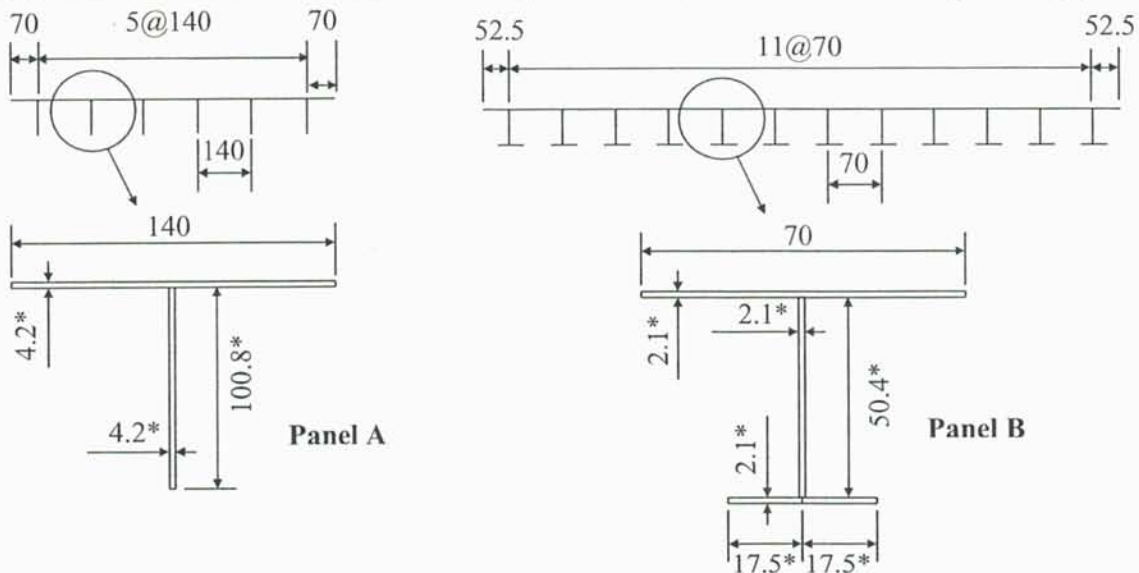

Fig. 3. Cross-sections of isotropic simply supported panels of length 1000 mm, Young's modulus 70 kNmm^{-2}, Poisson's ratio 0.3 and density 2710 kgm^{-3}. All dimensions are in mm. * denotes design variables, shown at their initial values.

The stiffened panels of Fig. 3 were optimised subject to fundamental frequency and spectral gap constraints, and the results are shown in Fig. 4. The results for panel A illustrate that natural frequencies can move in either direction during CONMIN optimisation, although all were increased during stabilisation. The single spectral gap was cleared by performing additional stabilisations in each of two spectral gap cycles, but with a heavy mass penalty (which was removed in subsequent sizing cycles). The results for panel B demonstrate successful clearance of all five spectral gaps for a problem having several regions of high modal density.

References

1. McMillan, A.J. and Keane, A.J., "Shifting resonances from a frequency band by applying concentrated masses to a thin rectangular plate", *Journal of Sound and Vibration*, Vol. 192, No. 2, 1996, pp. 549-563.
2. Lawther, R., "Altering structures to exclude multiple vibration frequencies", *Proceedings of EPMESC VII: International Conference on Enhancement and Promotion of Computational Methods in Engineering and Science*, Macao, 1999, pp. 475-484.
3. O'Leary, O.J. "Optimisation of prismatic aerospace structures with natural frequency constraints", *PhD thesis*, Cardiff University, U.K., 2000, pp. 71-187.
4. Butler, R. and Williams, F.W., "Optimum design using VICONOPT, a buckling and strength constraint program for prismatic assemblies of anisotropic plates", *Computers and Structures*, Vol. 43, No. 4, 1992, pp. 699-708.
5. Wittrick, W.H. and Williams, F.W., "A general algorithm for computing natural frequencies of elastic structures", *Quarterly Journal of Mechanics and Applied Mathematics*, Vol. 24, Part 3, 1971, pp. 263-284.
6. Vanderplaats, G.N. and Moses, F., "Structural optimization by methods of feasible directions", *Computers and Structures*, Vol. 3, No. 4, 1973, pp. 739-755.
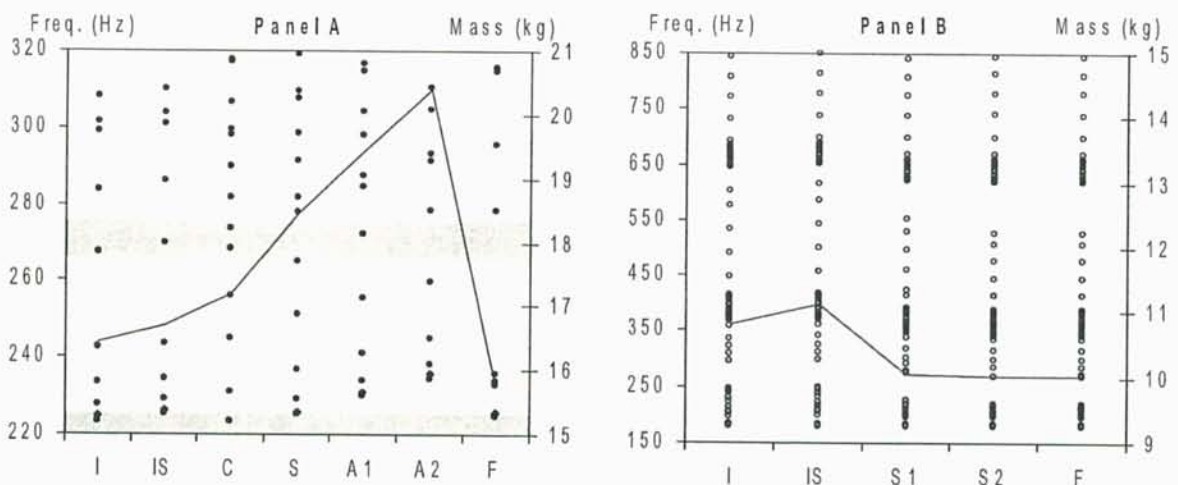
Fig. 4. Clearance of spectral gaps for panels A and B of Fig. 3, following: (I) initial analysis; (IS) initial stabilisation; (C) a typical CONMIN optimisation during the first sizing cycle; (S) the subsequent stabilisation; (A1/A2) additional stablisations in first/second spectral gap cycle; (S1/S2) end of first/second sizing cycle; (F) final analysis. Key: █ spectral gaps (including the region excluded by the fundamental natural frequency constraint); • natural frequency; ── panel mass.

Corrected Solvability Conditions for Non-linear Asymmetric Vibrations of a Circular Plate Revisited

W. K. Lee

School of Mechanical Engineering, Yeungnam University,

Gyongsan, 712-749, South Korea

H. D. Park

RMS Technology Co., Ltd.

Cheonan, 330-210, South Korea

This paper is intended to investigate further, responses of non-linear asymmetric vibrations of a perfect, clamped circular plate studied by Yeo and Lee [1]. For a numerical example, they considered the case of primary resonance, in which the frequency of excitation λ is near one of natural frequencies, say, ω_{11}, where the first subscript refers to the number of nodal diameters and the second one the number of nodal circles including the boundary. Then they derived a system of autonomous ordinary differential equations with dimension four given as follows:

$$a_{11}' = -c_{11}a_{11} + \frac{P_{11}}{2\omega_{11}}\sin\mu_{11}^a \tag{1a}$$

$$b_{11}' = -c_{11}b_{11} + \frac{P_{11}}{2\omega_{11}}\sin\mu_{11}^b \tag{1b}$$

$$a_{11}\mu_{11}^{a'} = \sigma a_{11} + \frac{\gamma_{1111}}{4\omega_{11}}a_{11}(a_{11}^2 + 2b_{11}^2) + \frac{P_{11}}{2\omega_{11}}\cos\mu_{11}^a \tag{1c}$$

$$b_{11}\mu_{11}^{b'} = \sigma b_{11} + \frac{\gamma_{1111}}{4\omega_{11}}b_{11}(b_{11}^2 + 2a_{11}^2) + \frac{P_{11}}{2\omega_{11}}\cos\mu_{11}^b, \tag{1d}$$

where a_{11}, b_{11} and μ_{11}^a, μ_{11}^b denote amplitude and phase variables, respectively. Parameters c_{11}, P_{11}, σ and γ_{1111} denote damping coefficient, excitation amplitude, external detuning and nonlinear coefficient, respectively. Each equilibrium solution ($a_{11}' = b_{11}' = \mu_{11}^{a'} = \mu_{11}^{b'} = 0$) corresponds to a steady-state response of the plate. We can write the steady-state response to the first order approximation as

$$w = \phi_{11}(r)\{a_{11}\cos(\lambda t - \mu_{11}^a + \theta + \tau_{11}) + b_{11}\cos(\lambda t - \mu_{11}^b - \theta - \tau_{11}) + O(\varepsilon), \tag{2}$$

where the forced response w is a superposition of the two traveling waves rotating clockwise and counterclockwise, respectively, $\phi_{11}(r)$ is the linear shape function corresponding to ω_{11} and ε is a small parameter introduced for the perturbation analysis [1]. When $a_{11} = b_{11}$ and $\mu_{11}^a = \mu_{11}^b$, form (2) is reduced to a standing wave [1].

It is found that there exist at most five stable responses: one standing wave and four traveling waves. Two of traveling waves lose their stability by Hopf bifurcations and have a sequence of period-doubling bifurcations leading to chaos. We consider the case of $\{v, \varepsilon, \varepsilon c, \varepsilon \sigma, \varepsilon P_{11}, \gamma_{1111}\}$={1/3, 0.001067, 0.01, 0.13278, 4, -772.046}, when the system has five attractors: three equilibrium solutions (one standing wave and two traveling waves) and two strange attractors (chaotic motions). Then the asymptotic behavior of the system depends on the initial condition. A set of initial states, the so-called domains of attraction, is attracted to one of attractors. The concept of the principal plane [2], which includes three equilibrium points of the system corresponding to one stable standing wave and two unstable traveling waves, is used to obtain the domains of attraction shown in Fig. 1. This figure shows the five domains of attraction represented by SS2 (standing wave), ST1-1, ST1-2 (two traveling waves) and UT2-1, UT2-2 (two chaotic motions), each of which is to attracted to each of five attractors. In order to examine more closely the domain of attraction of one of chaotic motions (UT2-1), we enlarge region Z4 to obtain Fig. 2. Consecutively enlarged results are shown in Fig. 3 and Fig. 4, from which we can see that the basin boundary of the chaotic motion is fractal.
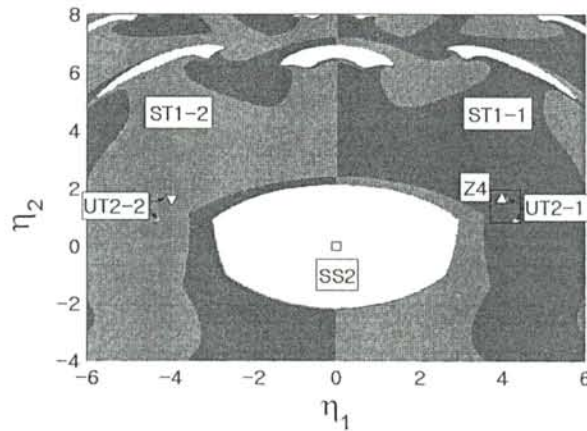

Fig. 1 The domains of attraction in the principal plane. □, The stable fixed point for SS2; △, the unstable fixed point for UT2-1; ▽, the unstable fixed point for UT2-2.
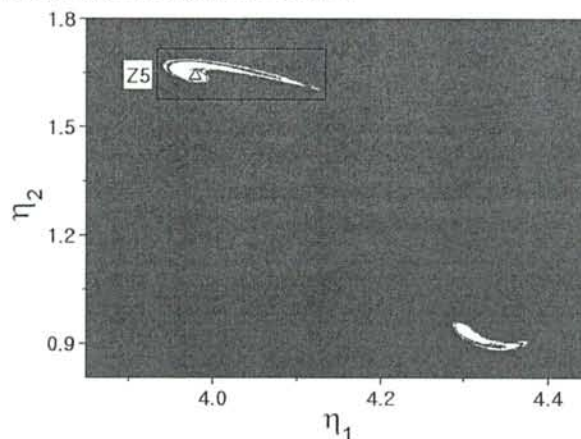

Fig. 2 The domains of attraction in the principal plane. The enlargement of Z4 in Fig. 1. △, The unstable fixed point for UT2-1.
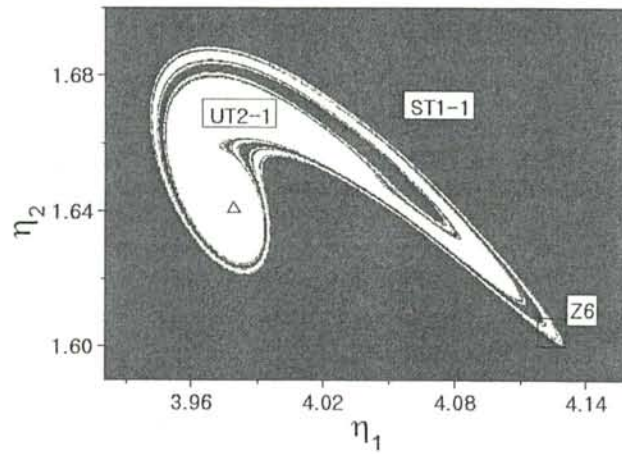
Fig. 3 The domains of attraction in the principal plane. The enlargement of Z5 in Fig. 2. △, The unstable fixed point for UT2-1.
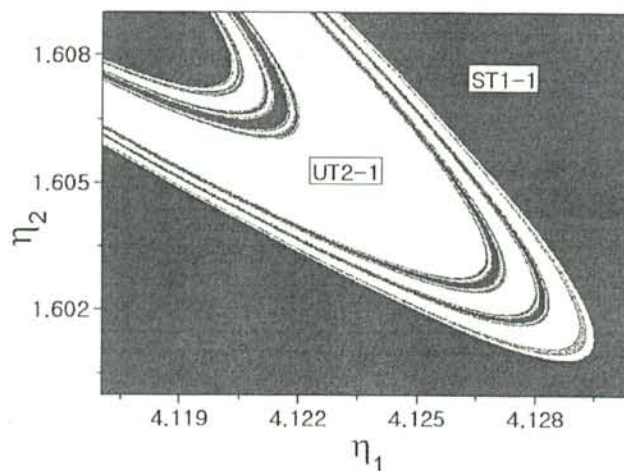

Fig. 4 The domains of attraction in the principal plane. The enlargement of Z6 in Fig. 3.

References

[1] M. H. Yeo and W. K. Lee, 2002, Corrected Solvability Conditions for Non-linear Asymmetric Vibrations of a Circular Plate, *Journal of Sound and Vibration*, Vol. 257, pp. 653-665.

[2] W. K. Lee and C. S. Hsu, 1994, A Global Analysis of an Harmonically Excited Spring-Pendulum System with Internal Resonance, *Journal of Sound and Vibration*, Vol. 171, pp. 335-359.

The Historical Bases of the Rayleigh and Ritz Methods

Arthur W. Leissa
Colorado State University
Fort Collins, Colorado USA

In 1877 the first edition of *Theory of Sound* by Lord Rayleigh [1] was published. (See the Historical Introduction by Lindsay, in the 1945 reprinting, for an excellent biographical sketch of Rayleigh and his work.) Volume I is devoted to vibration concepts, and the underlying mathematics, and also contains six chapters dealing with vibrations of strings, bars, beams, membranes, plates and shells. Volume II [2], published one year later, addresses problems in acoustics.

Most of the numerous problems dealt with in Volume I begin with the governing differential equation of motion, solving them by classical methods, and applying boundary conditions to obtain free vibration frequencies and mode shapes. But Rayleigh was also interested in the potential (V) und kinetic (T) energies of the system and, in some cases, attacked the problems from this perspective. In particular, in many cases, he assumed a mode shape, and calculated the corresponding free vibration frequency by equating V and T during a vibration cycle. This has generally become known as the Rayleigh method of solution. Its accuracy depends upon how closely the assumed mode shape fits the correct (exact) one.

In 1908 and 1909 Walter Ritz [3, 4] published two papers which thoroughly demonstrated a straightforward procedure for solving boundary value and eigenvalue problems numerically, to any degree of exactitude desired, also using energy functionals. For the free vibration eigenvalue problem, one assumes a displacement function in terms of a series of admissible displacement functions (that is, ones satisfying at least the geometric boundary conditions of the problem) having undetermined coefficients, and then minimizes an energy functional involving V and T to determine frequencies and mode shapes. The first paper [3] was extensive (61 pages), and laid out the method and its underlying concepts, discussed convergence, and applied it to some problems. The second one [4] used the method to present novel results for the vibrations of a completely free square plate. Tragically, Ritz died of consumption soon afterwards (cf. [5]). His complete scientific works were collected together and published posthumously [6].

Although the Rayleigh method is used frequently, the Ritz method has received tremendous usage during the past three decades to obtain accurate frequencies and mode shapes for the vibrations of continuous systems, especially for problems not amenable to exact solution of the differential equations. This is especially because of the increasing capability of digital computers to set up and solve the frequency determinants arising with the method. Even before that, the writer found 15 publications that used the Ritz method to solve classical rectangular plate vibration problems prior to 1966. These are described in Chapter 4 of his plate vibration monograph [7].

But in going through the 15 papers (as well as others, used elsewhere in the monograph for other shapes of plates, or non-classical ones), the author became aware that some researchers had also attached Rayleigh's name to the Ritz method, calling it "the Rayleigh-Ritz method". At that time he regarded this as simply a way of amalgamating the two methods, because the Rayleigh method may be regarded as a special case of the Ritz method when only a single admissible function is used to describe the vibration mode. But this is misleading, because then one would not bother to write the Ritz minimizing equation – the Rayleigh procedure is more direct.

As time went on the writer heard comments more than once that Rayleigh had used the Ritz method, and had written about it. But those who spoke could not cite references, saying that "they must be in Theory of Sound" The writer has looked through these volumes many times during the past forty years, and never found anything closely resembling the Ritz method. However, recently he was made aware of some additional published papers by Rayleigh, notably one [8] he published two years after Ritz' second paper, wherein he complained that Ritz had not recognized his own, similar work.

In the present work the methods of Rayleigh and Ritz are both briefly summarized. Then Rayleigh's 1911 paper [8] is studied in detail. Therein he said "---I am surprised that Ritz should have regarded the method as new". He then went on to say that he had himself investigated the vibrations of the completely free square plate in a manner similar to Ritz in his book [1] (Chapter 10, pages 372-383), and said also that he had used the method to determine:

1. the velocity at the open end of an organ pipe: [2], Appendix A
2. the fundamental frequency of a vibrating string: [1], Sections 88-91
3. the fundamental frequency of a cantilever beam: [1], Section 182
4. the fundamental frequency of an almost-square membrane: [1], Sections 209-210
5. acoustic resonance in a closed tube of variable cross-section: [2], Section 265
6. the fundamental sloshing frequency of a liquid in a rigid, circular cylindrical container: [9]

The writer has looked carefully at these examples cited by Rayleigh. He has recently gone through Rayleigh's two volumes [1, 2], looking for other possibly relevant examples, as well as another, earlier paper [10] on the square plate. Some of the above examples cited by Rayleigh do not even use a minimization process. Some involve minimization of a frequency (not a functional, as carried out by Ritz [3, 4]). That is, none of them use Ritz' method. Detailed examinations of the examples cited by Rayleigh [8], and a translation of the most important parts of Ritz' papers [3, 4] are available in [11].

Thus, the writer concludes that Rayleigh's name should not be attached to the Ritz method; that is, the "Rayleigh-Ritz method" is an improper designation.

REFERENCES

1. Lord Rayleigh 1877 *The Theory of Sound,* Volume 1. The Macmillan Company (reprinted 1945 by Dover Publications), New York.

2. Lord Rayleigh 1878 *The Theory of Sound,* Volume 2. The Macmillan Company (reprinted 1945 by Dover Publications), New York.

3. W. Ritz 1908 *Journal für Reine und Angewandte Mathematik* **135**, 1-61. Über eine neue Methode zur Lösung gewisser Variationsprobleme der mathematischen Physik.

4. W. Ritz 1909 *Annalen der Physik* **28**, 737-786. Theorie der Transversal-schwingungen einer quadratischen Platte mit freien Rändern.

5. R. Courant 1943 *Bulletin of the American Mathematics Society* **49**, 1-23. Variational methods for the solution of problems of equilibrium and vibrations.

6. W. Ritz 1911 *Oeuvres Complètes*. Paris: Gauthier-Villars.

7. A.W. Leissa 1969 *Vibration of Plates* (NASA SP-160). Washington: U.S. Government Printing Office (reprinted 1993 by The Acoustical Society of America)

8. Lord Rayleigh 1911 *Philosophical Magazine,* Sixth Series. **22**, 225-229. On the calculation of Chladni's figures for a square plate.

9. Lord Rayleigh 1899 *Philosophical Magazine*. 566-572. On the calculation of the frequency of vibration in its gravest mode, with an example from hydrodynamics.

10. Lord Rayleigh 1873 *Philosophical Magazine*, Series 4. **46**, 166-171. On the nodal lines of a square plate.

11. A.W. Leissa 2006 *Journal of Sound and Vibration* (to appear). The historical bases of the Rayleigh and Ritz methods.

High Frequency Vibration Analysis of Thick Shallow Shells using DSC-Ritz Method

C.W. Lim[1], A.Y.T. Leung[1], Z.R. Li[1] and G.W. Wei[2]

[1]Department of Building and Construction, City University of Hong Kong, Hong Kong

[2]Department of Mathematics and Department of Electrical and Computer Engineering, Michigan State University, East Lansing, MI 48824, U.S.A.

For decades, the vibration analysis of shell structures has been an important research topic due to their wide applications in structural, aerospace and mechanical engineering. One of the most successful theories for plates and shells is based on the Kirchhoff-Love hypothesis, which assumes that the thickness of the plate is very small compared to its shortest dimension. However, as the shell thickness increases, the classical Kirchhoff-Love theory loses its validity because of the transverse shear strain. To accommodate this effect, the Reissner-Mindlin plate theory, commonly used in thick plate analysis, has been extended to shell studies, which yields linearly varying transverse shear strain in contrast to the constant distribution. Since then, extensive research work has been conducted in the field.

Analytical solution to Reissner-Mindlin plates and shells is certainly valuable for basic understanding of dynamics of plate and shell structures. Unfortunately, exact solutions are scarce and limited to structures of simple geometries and support conditions. As a consequence, numerical solutions of Reissner-Mindlin plates and shells are indispensable for engineering prediction and design. There has been much achieved in computational methodology for shell analysis in the past two decades. Based on the Ritz extremum energy approach, a numerical procedure with geometrically compliant shape functions has been developed by Lim and his associates to solve the vibratory characteristics of thick shallow shells [1] subject to a variety of boundary constraints. Using this approach, shape functions are formed from the product of two-dimensional polynomials and appropriate basic functions which ensure the satisfaction of piecewise boundary geometric conditions. This method avoids the difficulty of global methods for implementing boundary conditions. However, like other standard global methods, this method fails to work for higher-order modes due to numerical round-off errors when the degree of polynomial is increased to a certain level. Nevertheless, a complete understanding of a number of very important engineering systems relies on accurate predictive capabilities of high-frequency response. For instance, such understanding is of crucial importance in aerospace structures, eg. aircraft, rotorcrafts, satellites and other space

vehicles.   There is a pressing need for the prediction and control of the high frequency vibration and noise levels at the structural design stage and this in turn requires the availability of analysis methods that are able to predict the structural response [2].

Recently, the discrete singular convolution (DSC) algorithm [3] has emerged as a novel approach for the computer realization of singular integrations.   The mathematical foundation of the DSC algorithm is the theory of distributions and wavelet analysis.   As wavelets are localized in both frequency and coordinate domains, they give rise to numerical schemes with optimal accuracy, stability and flexibility.   More recently the DSC has also been introduced to solve problems in structural mechanics for beams and plates.   In particular, it has been shown that extremely high frequency vibration modes can be predicted very accurately by using the DSC for plates with simply supported and clamped edges.   However, as the governing differential equation is discretized using a collocation approach in these analyses, further study is required for the collocation approach to be applicable to problems involving free edge supports.

In light of the various problems outlined above, this work intends to develop a new DSC-Ritz method which make use of DSC kernels of the Dirichlet type and the Ritz basic boundary functions to arrive at a new approach which is not only able to accommodate a variety of combinations of boundary conditions but also able to obtain accurate numerical solutions for high-mode vibration frequency parameters of Mindlin plates and shells.   Moreover, the present work introduces the DSC algorithm for the vibration analysis of shells with a variety of possible boundary conditions.   Two typical DSC kernels, regularized Shannon wavelet kernel and regularized de la Vallée Poussin kernel, are introduced to the DSC-Ritz scheme. Extensive numerical experiments are conducted to validate the convergence and test the accuracy of the proposed method.   Numerical results indicate that the new DSC-Ritz method provides accurate prediction of thousands of vibration modes, which, in shell analysis, have been hitherto unavailable to engineers.

A set of numerical studies is carried out for doubly-curved shells of square planform ($a/b = 1$) and shallowness ratio $b/R_x = 0.5$ with two different boundary conditions: SSSS, CCCC.   The curvature ratio R_y/R_x ranges from -2, -1 (negative Gaussian curvature corresponding to a hyperbolic paraboloidal shell) to 1, 2 (positive Gaussian curvature corresponding to a spherical shell).   The thickness ratio ranges from 0.02 (a thin shell) to 0.2 (a thick shell).   The first 500 mode frequencies are presented in Table 1.   In the calculation, de la Vallée Poussin kernel is adopted with a 32×32 grid.

Table 1. Frequency parameter $\lambda' = \omega a \sqrt{\rho / E}$ for a thick doubly-curved shallow shell with $\nu = 0.3$, $a/b = 1.0$ and $b/R_y = 0.5$.

Boundary Condition	R_y / R_x	Mode sequence number							
		1	10	50	100	200	300	400	500
SSSS	-2	0.55064	2.5102	7.5546	11.905	17.864	21.317	23.959	26.475
	-1	0.56587	2.5147	7.5543	11.906	17.864	21.314	23.958	26.471
	1	0.59448	2.5216	7.5723	11.910	17.858	21.328	23.965	26.471
	2	0.56666	2.5137	7.5662	11.904	17.861	21.325	23.963	26.474
CCCC	-2	1.0802	3.7695	9.6106	13.523	19.658	22.948	25.637	28.101
	-1	1.1248	3.7683	9.6136	13.518	19.654	22.948	25.637	28.093
	1	1.2101	3.8162	9.6236	13.542	19.657	22.953	25.644	28.118
	2	1.1256	3.7936	9.6161	13.537	19.659	22.949	25.640	28.114

With the new capability of predicting high-frequency parameters, the new DSC-Ritz gives us the privilege to reveal an important limitation of a formal analytical relationship [4] which converts frequency parameters of a Kirchhoff plate into those of a Mindlin plate. The present finding indicates that a family of shear deformable vibration modes in the Mindlin plate could be missing if the prediction is solely based on the relationship with the vibration modes computed from the Kirchhoff plate.

Reference

1. K.M. Liew and C.W. Lim, Vibration studies on moderately thick doubly-curved elliptic shallow shells, *Acta Mechanica*, **116**, 83-96, 1996.
2. R.S. Langley and N.S. Bardell, A review of current analysis capabilities applicable to the high frequency vibration prediction of aerospace structures, *The Aeronautical Journal*, **102**, 287-297, 1998.
3. G.W. Wei, Discrete singular convolution for the solution of the Fokker-Planck equations, *Journal of Chemical Physics*, **110**, 8930-8942, 1999.
4. C.M. Wang, J.N. Reddy and K.H. Lee, *Shear Deformable Beams and Plates: Relationships with Classical Solutions*, Elsevier: Singapore, 2000.

Acknowledgement

Non-smooth Resonant Vibrations of Delaminated Beam-type Structures

INGOLF MÜLLER and PETER VIELSACK

Institut für Mechanik, Universität Karlsruhe (TH), Germany

mechanik@ifm.uni-karlsruhe.de

Introduction

Oscillation properties of delaminated structures are governed by strongly nonlinear phenomena, which are associated with two major mechanisms, namely the presence of a unilateral constraint across the interface of the debonded zone and dissipative impact-like contacts in this region. Therefore, damage mechanisms will produce local sources of nonlinearity in a predominantly linear structure, that are detectable on a global basis [1]. Investigations of the arising nonlinear response, as will be addressed, are promising for reliable localisation of the involved delamination. As a general conclusion, it was found that a consideration of the damage-related nonlinearity is much more sensitive to structural alterations than any other method based on the investigation of linear system properties (e.g. modal characteristics [2]).

Delaminated Beam

The model problem for non-destructive damage analysis is a straight laminate beam with a distinct debonded zone. Harmonic resonant vibrations are induced at one end of the beam. In the stationary state of motion, the gap between both separated parts of the beam opens and closes. In the following, a delaminated beam as depicted in figure 1 is investigated by different mechanical models of increased complexity to obtain insight into the nonlinear oscillation behaviour of damaged structures. The outlined experimental investigations will provide both a possibility of judging the quality of the numerical models and the basis for the following damage identification procedure.
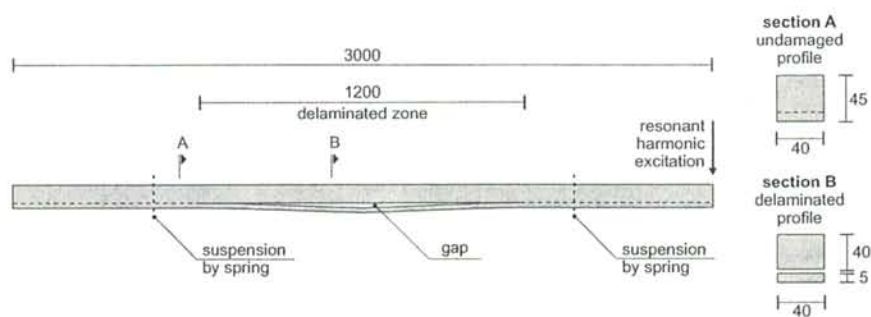

Figure 1: Delaminated beam with symmetric damage scenario.

Minimal Mechanical Models

The present major task, with a view to the damage identification, is the isolation of the predominant damage-related oscillation phenomena - the fingerprint of the flaw - and to prove

the robustness of these phenomena. Therefore, the investigation starts with two non-smooth rigid body models that allow the capturing of the most conspicuous effects. The dynamic contact-impact problem has as the simplest approximation two neighbouring linear oscillators (see figure 2 [a]). It is well known that externally excited vibro-impacting systems have no unique solutions [3]. Depending on the system properties as well as the amplitude and frequency of a harmonic excitation, a cascade of bifurcations up to chaotic motions may occur. The essential point in this scenario is its dependency on the amount of energy dissipation at each impact-like contact. Introducing a high contact dissipation according to the experiment, only one-periodic (non-bifurcated) oscillations exist [4]. On the basis of this knowledge, the distortion factor [1] can be employed to quantify the degree of response nonlinearity at each oscillator. As a result, it was found that the responses of both subsystems bear noticeable nonlinearity.
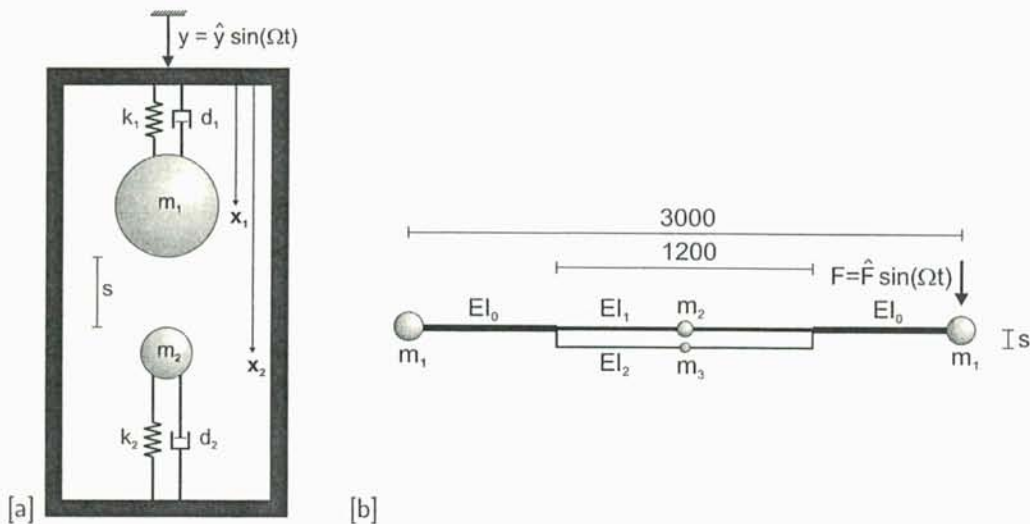

Figure 2: Minimal models: [a] 2 DOF model, [b] 4 DOF model.

A more detailed approach provides a 4 DOF beam model with lumped masses (see figure 2 [b]). For this purpose, two intact regions are added in regard to the afore considered system. The extended model additionally reveals the penetrative character of the local source of nonlinearity to all responses, even in the undamaged region. Finding the fingerprint of the damage on nearly arbitrary test points provides the key for the development of global methods (on a system level) for damage assessment.

Finite Element Model

Finally, a Finite Element model (fig. 3) is proposed that affords both a reliable prediction of all predominant oscillation phenomena as well as a qualitatively and quantitatively correct simulation of the system's response. For this purpose, the one-dimensional continuum problem (fig. 1) is discretised by EULER-BERNOULLI beam elements. Supplying the time harmonic excitation on the system with sufficiently large amplitude, coupling of the linear subsystems (remaining beam and delaminated layer) in the debonded region occurs due to impact-like contact events along the delamination. Two fundamental challenges appear: the appropriate time integration in regard to the non-smooth nature of the problem and the reliable capture

of the periodically appearing dynamic contacts within the stationary state of motion. The conception of the node-to-node contact description via impact law in combination with a penalty stiffness is adopted to tackle the special type of contact. The impact law mainly involves the distinct contact dissipation while the latter helps to capture states of permanent contact. This technique turns out to be very advantageous in regard to the robustness of the simulation results.
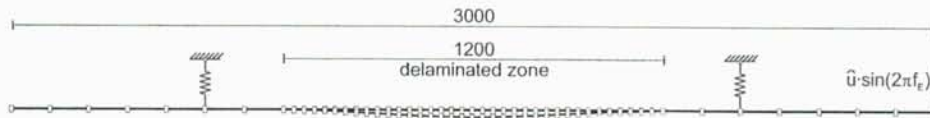

Figure 3: Finite Element model.

Inverse Analysis for Vibration-based Damage Identification

A nonlinear model-based approach for inverse damage identification can be established by parametric updating of the Finite Element model. Therefore, an error function is needed to control the iterative adaption of the damage scenario involved in the numerical model. Due to the distinct damage-related sensitivity of the nonlinear structural response, an appropriate error function shows great promise for overcoming the ill-posedness of the inverse problem without any mathematical augmentation (i.e. regularisation). Due to the nonlinear nature of the parameterised mapping the minimisation problem to be solved is, in general, non-convex and may imply in the majority of cases that several minima occur. Thus, a special optimisation technique with global character is required to overcome this difficulty and to achieve success in inverse damage identification.

References

[1] Müller, I.; Vielsack, P.: Identification of delaminations based on non-smooth vibrations. *Proceedings of EURODYN Conference 2005, Paris / France*, (2005).

[2] Zou, L.; Tong, L.; Steven G. P.: Vibration-based model-dependent damage (delamination) identification and health monitoring for composite structures. *Journal of Sound and Vibration*, **230**(2): 357–378, (2000).

[3] Vielsack, P.: A vibro-impacting model for the detection of delamination. *Journal of Sound and Vibration*, **253**(2): 347–358, (2002).

[4] Müller, I.; Konyukhov, A.; Vielsack, P.; Schweizerhof, K.: Parameter estimation for Finite Element analyses of stationary oscillations of a vibro-impacting system. *Engineering Structures*, **27**(2): 191–201 (2005).

corresponding author:

Ingolf Müller
Institut für Mechanik, Universität Karlsruhe (TH), Kaiserstr. 12, D-76131 Karlsruhe, Germany
Tel: +49-(0)721-608 3252, Fax: +49-(0)721-608 7990, e-mail: imueller@ifm.uni-karlsruhe.de

Experiments of Modal Interaction on Chaotic Oscillations of an Annular Plate with Initial Deflection

Ken-ichi NAGAI, Shinichi MARUYAMA and Takao YAMAGUCHI
Department of Mechanical Engineering, Gunma University,
1-5-1 Tenjin-cho, Kiryu, Gunma 376-8515, JAPAN
nagai@eng.gunma-u.ac.jp

1. Introduction Experimental results are presented on chaotic oscillations of a thin annular plate subjected to periodic acceleration. The plate is clamped at the internal boundary and is free along the outer circumference. Chaotic responses are examined by using the Poincaré maps and the Lyapunov exponents. The time responses on the multiple positions of the plate are inspected with principal components obtained by the Karhunen-Loève transformation.

2. Test Plate and Test Procedure As shown in Fig.1, a phosphor-bronze annular plate of thickness h=0.23 mm is clamped at the inner boundary with the cylindrical block of diameter $2b$=22.8mm. The outer boundary of diameter $2a$=115mm is free along the circumferential direction. The plate has initial deformation with the form of an umbrella and the maximum deflection is close to the plate thickness. The cylindrical coordinate-system is denoted by radial coordinate r, circumferential angle θ and axial coordinate z. In the experiment, the plate is shaken laterally with an electromagnetic exciter. The plate is subjected to the gravitational acceleration g and the periodic acceleration $a_d \cos 2\pi f\, t$, where f is the exciting frequency and a_d is the peak amplitude of acceleration. Dynamic responses of the plate are measured with a laser displacement sensor and recorded for signal processing and data analysis. The experiments were conducted as follows: first, the linear natural frequencies and the restoring force of the annular plate are examined. Next, under periodic lateral acceleration, chaotic responses are inspected with the frequency response curves, the Fourier spectra, the Poincaré projections and the maximum Lyapunov exponents. Finally, detecting the chaotic responses at multiple positions of the plate, mode contribution to the chaos is discussed with the principal component analysis.

3. Results and Discussion The results of the experiment are arranged with the following non-dimensional notations.

$$\xi = r / a, \ w = W / h, \ [p_s, p_d] = [g, a_d]\, \rho a^4 / D, \ q_s = Q_s a^2 / Dh, \ [\omega, \omega_i] = [f, f_i]\, 2\pi / \Omega_0, \ \tau = \Omega_0 t \quad (1)$$

where $\Omega_0 = a^{\pm 2}\sqrt{D / \rho h}$ is the coefficient corresponding to lateral vibration of the plate. Notation $D = Eh^3 / \{12(1 \pm v^2)\}$ is the bending rigidity of the plate, where E is Young's modulus and v is Poisson's ratio. In Eq. (1), ξ is the non-dimensional coordinate, w is the lateral displacement normalized by the plate thickness h. Notations p_s and p_d are the non-dimensional load intensities related to the gravitational acceleration g and the periodic peak acceleration a_d, respectively. When the restoring force of the plate is examined, static deflection under the static concentrated force Q_s is measured. Notation q_s is the non-dimensional force. Notations ω and τ are the nondimensional exciting frequency and the time, respectively. Non-dimensional exciting force is expressed as $p_s + p_d \cos \omega \tau$.

Figure 2 shows the static deflection w of the plate under the concentrated force q_s loaded at ξ=0.92 and θ=0. The deflections at ξ=0.76, θ=0 and ξ=0.76, θ=π are detected, which are indicated by a solid line and a dotted line, respectively. When the force increases from the stable equilibrium position to the positive z direction, the plate deflection at ξ=0.76, θ=0 shows the characteristics of a hardening spring. The deflection at the opposite side θ=π, turns to the negative direction. As the force is loaded to the negative z direction, the spring characteristics at θ=0 change to the softening-and-hardening type. The deflection at θ=π increases towards the positive direction at first, then turns back to the negative direction and finally returns to the positive direction. These complicated movement is due to the spring characteristics of softening-and-hardening type. Table 1 shows the linear natural frequencies ω_i where i denotes the number of nodal diameter. In the table, the lowest natural frequency ω_1=3.55 of the mode with one nodal diameter is close to the natural frequency ω_0=4.09 of the mode

with zero nodal diameter. The natural frequency $\omega_2=8.95$ of the mode with two nodal diameters is close to twice the frequency $\omega_0=4.09$. These relations imply possibilities of the existence of internal resonance.

Nonlinear response curves of the plate are presented in Fig. 3. The amplitude of response at the position $\xi=0.76$, $\theta=0$ is shown with the root mean square value. A chaotic response is denoted with the symbol $C(i, p)$, where index i represents a generated mode of vibration with the number of nodal diameters i and index p is the type of resonance. For example, $C(1, 1)$ and $C(1, 1/2)$ denote the chaotic responses of the mode of one nodal diameter generated from the principal resonance and from the sub-harmonic resonance of $1/2$ order, respectively. $C(i, p: j, q)$ represents the chaotic response involving the response of internal resonance. Non-stationary amplitude modulation is observed in a lower exciting frequency range. The large amplitude response $C(0,1:1,1)$ is generated from the principal resonance both of the lowest and second modes of vibration. The nonlinear response exhibits the characteristics of a hardening spring. At the exciting frequency $\omega=4.47$, the time progress, the Fourier spectrum and the Poincaré projection of the chaotic response $C(0,1:1,1)$ are shown in Fig.4. The time progress of the response w is presented by the number of excitation period τ_e. Irregular amplitude modulation of chaotic response is observed. In Fig. 4(b), broad band spectrum is observed. Dominant peaks of the spectrum correspond to the lowest and the second mode of vibration. In Fig. 4(c), the Poincaré projection shows the distributed dots in the space of deflection and velocity. When the exciting frequency increases to $\omega=4.87$, the response approaches the maximum amplitude which was shown in Fig. 3. The time progress is prevailed by the periodic response, although chaotic behavior exists. When the exciting frequency $\omega=8.77$ is close to the natural frequency ω_2, the chaotic response involves the sub-harmonic components both of the lowest and second modes of vibration. Because of the condition of internal resonance $\omega_2\approx2\omega_1$ and $\omega_2\approx2\omega_0$, multiple modes are generated simultaneously in the chaotic response. Figure 5 shows the maximum Lyapunov exponents λ_{max} related to the embedding dimension e of the chaotic responses of $C(0,1:1,1)$ at $\omega=4.47$ and $\omega=4.87$ and of the response $C(0,1/2:1,1/2:2,1)$ at $\omega=8.77$. As the embedding dimension e increases, the maximum Lyapunov exponents λ_{max} converges to positive constants, then these responses are confirmed as chaos. In the chaotic response $C(0,1:1,1)$ at $\omega=4.47$, the maximum Lyapunov exponents takes from $\lambda_{max}=0.05$ to $\lambda_{max}=0.09$. When the frequency is $\omega=4.87$, the exponent decreases around $\lambda_{max}=0.02$, because periodic components in the chaotic response are increased. For the response $C(0,1/2:1,1/2:2,1)$ at $\omega=8.77$, the amplitude is smaller than that of the chaotic response near the principal resonance $C(0,1:1,1)$. The maximum Lyapunov exponent takes a larger value from $\lambda_{max}=0.2$ to $\lambda_{max}=0.3$, because the amplitude of the chaotic response is within the range where the effects of the softening spring prevail.

The principal component analysis enables the estimation of the contribution of vibration modes to the chaotic response of the annular plate. The chaotic time histories of deflection are detected simultaneously at four positions of the plate. The positions are selected on the radius $\xi=0.76$ and the angles $\theta=0$, $\pi/2$, π and $3\pi/2$. Applying the principal component analysis to the data with length 4500 τ_e of the chaotic response of $C(0,1:1,1)$ at $\omega=4.47$, the contribution ratio and decomposed modal pattern are shown in Fig. 6. The mode with zero nodal diameter has the largest contribution ratio $\mu_1=44.1\%$. The second and third larger contribution ratios of $\mu_2=29.6\%$ and $\mu_3=19.6\%$ correspond to the modes with one nodal diameter. These modes have different angular orientation. The nodal lines are perpendicular to each other. The mode with two nodal diameters has smaller contribution ratio of $\mu_4=6.6\%$. Figure 7 shows the decomposed modal pattern related to the contribution ratio μ_i in the chaotic response. In the figure, the modal pattern is denoted by open circles calculated with the time data of length 4500 τ_e. The bold solid line represents the modal configuration constructed from the modal pattern by the least square method. In Fig. 7(a), the modal configuration of the zero nodal diameter indicates one side vibration at the position $\theta=0$. Figure 7(b) and 7(c) correspond to the mode with one nodal diameter. These modes have phase difference of $\pi/2$ along the circumference with each other. Figure 7(d) indicates the mode of two nodal diameters. To investigate the existence of a

traveling wave in the chaotic response, the principal components are calculated in the short interval 50 τ_e. In the figure, thin lines indicate the modal configuration with short time duration. Irregular movement appears in the modes with zero and one nodal diameter. For the mode with zero nodal diameter, the modal configuration is almost fixed along the circumference. On the contrary, the mode with one nodal diameter travels drastically in the circumferential direction.

4. Conclusion   The experiments are conducted on the annular plate with the initial deflection subjected to periodic excitation. The chaotic response is generated involving the internal resonance. The most significant modes that contribute to the chaos are the vibration modes with zero and one nodal diameter. Principal component analysis with the short time duration shows that: the mode with one nodal diameter travels violently in the circumferential direction. Two modes with one nodal diameter of different angular orientation coexists in the chaotic oscillation.

References
(1) Nagai, K., Maruyama, S., Oya, M. and Yamaguchi, T., "Chaotic oscillations of a shallow cylindrical shell with a concentrated mass under periodic excitation," Computers and Structures Vol.82,(2004),pp.2607-2619.

(2) Yamaguchi, T. and Nagai, K., "Chaotic vibration of a cylindrical shell-panel with an in-plane elastic-support at boundary," Nonlinear Dynamics Vol.13,(1997), pp.259-277.

(3) Nayfeh,T.A. and Vakakis, A.F., "Subharmonic traveling waves in a geometrically non-linear circular plate," International Journal of Non-Linear Mechanics Vol.29, No.2, (1994), pp.233-245.

(4) Azeez, M.F. and Vakakis, A.F., "Proper orthogonal decomposition (POD) of a class of vibroimpact oscillations," Journal of Sound and Vibration Vol.240, No.5, (2001), pp.859-889.
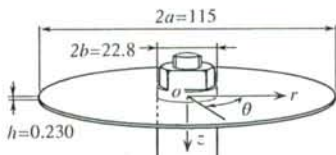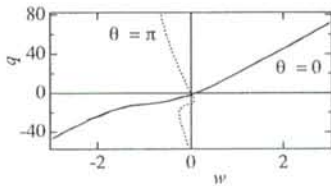
Fig.1 An annular plate

Fig.2 Deflection of the annular plate at $\xi=0.76$, $\theta=0,\pi$ under the concentrate load at $\xi=0.92$, $\theta=0$

Table.1 Natural frequencies and Natural modes of vibration

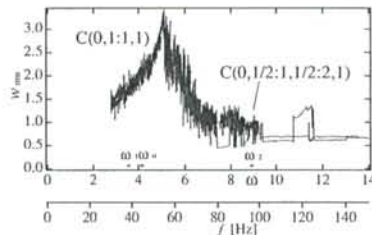| Number of nodal diameter i	1	0	2	3
Modal pattern				
ω_i	3.55	4.09	8.95	16.52
f_i [Hz]	38.28	44.25	96.50	178.25

Fig.3 Frequency response curve of the annular plate (p_d=16.7 measured at $\xi=0.76$, $\theta=0$)
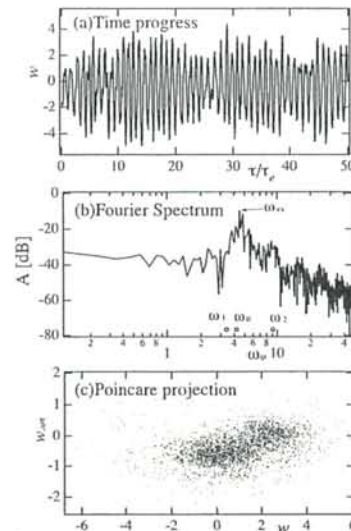

Fig.4 Chaotic response of the annular plate (measured at $\xi=0.76$, $\theta=0$, p_d=16.7, ω=4.47)
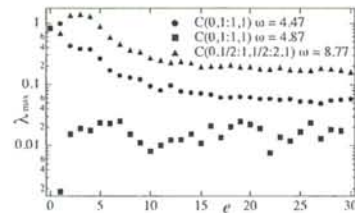

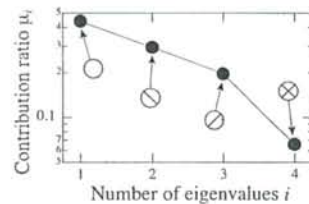Fig.5 Maximum Lyapunov exponent related to embedding dimension

Fig.6 Principal components obtained by Karhunen-Loève transformation (4500τ_e, p_d=16.7, ω=4.47)
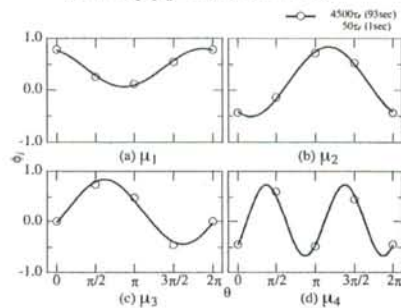

Fig.7 Modal pattern obtained by Karhunen-Loève transformation (p_d=16.7, ω=4.47)

LAYERWISE OPTIMIZATION VS. HEURISTIC GLOBAL OPTIMIZATION IN VIBRATION DESIGN OF LAMINATED COMPOSITE PLATES

Yoshihiro Narita

Department of Mechanical Engineering, Hokkaido University, Sapporo, 060-8628 Japan

e-mail: ynarita@eng.hokudai.ac.jp

1. Introduction

With the requirements for higher performance and lower operational cost, more composites are targeted toward structural applications in aerospace, marine and automobile engineering. Composite materials are mainly preferred in such applications because of their advanced elastic properties and tailoring capability, and have the potential for incorporating recent optimum design techniques into the design process. Among various relating problems, vibration design of laminated plates is one of the technically important problems, since vibration may cause serious fatigue damage to the composite structure.

This paper reviews the development of optimization techniques and applications to laminated composite plates in the past two decades. The recent progress made on a layerwise optimization (LO) approach is summarized, and a heuristic optimum approach is introduced to search for the globally optimum solutions in numerical experiments. The validity of the LO approach is demonstrated by comparing the optimum vibration frequencies with the global solutions determined by the heuristic optimum approach.

2. Problem Description and Optimization Approaches

2.1 Laminated plates considered

Consider a symmetrically laminated rectangular plate of dimensions $a \times b$ with thickness h. The direction of the fibers and the transverse direction to the fibers are denoted by L and T, respectively, and the fiber orientation angle between the x and L axes is denoted by θ. Each layer is considered to be macroscopically orthotropic and the total number of symmetric layers is defined as $2K$. The differential equation of equilibrium for such plates in free vibration state may be expressed as

$$D_{11}\frac{\partial^4 w}{\partial x^4} + 4D_{16}\frac{\partial^4 w}{\partial x^3 \partial y} + 2\left(D_{12} + 2D_{66}\right)\frac{\partial^4 w}{\partial x^2 \partial y^2} + 4D_{26}\frac{\partial^4 w}{\partial x \partial y^3} + D_{22}\frac{\partial^4 w}{\partial y^4} - \rho\omega^2 w = 0 \tag{1}$$

where w is the amplitude of the mid-plane, D_{ij} (i,j=1,2,6) are the bending stiffness and ρ is an average mass per unit area. A radian frequency ω is rewritten in the dimensionless frequency parameter

$$\Omega = \omega a^2 \left(\rho / D_0\right)^{1/2}, \text{ with } D_0 = E_T h^3 / 12\left(1 - \nu_{LT}\nu_{TL}\right) \text{ (reference bending rigidity)} \tag{2}$$

which is used as the object function to be maximized in the present problem.

2.2 Layerwise optimization (LO) approach

The design variables are taken to be a set of fiber orientation angles $[\theta_1/\theta_2/.../\theta_k/.../\theta_K]_S$ in the K layers, where θ_k is the fiber orientation angle in the k th layer (k=1:outermost, k=K: innermost) and the subscript "s" denotes symmetric lamination. The optimization problem is written in the standard form as

Find $[\theta_1/\theta_2/.../\theta_K]_S$, which maximizes Ω (frequency parameter)

$$\text{subject to constraints } -90° \le \theta_k \le 90° (k=1,2,...,K) \tag{3}$$

In the LO approach, use of a simple physical observation "*In the bending of plates, the outer layer has a greater stiffening effect than the inner layer and therefore has a greater influence on the frequencies*" is made and the following assumption to the problem is advocated:

The optimum stacking sequence $[\theta_1/\theta_2/.../\theta_K]_{S,opt}$ for the maximum vibration frequency of a laminated plate can be obtained by determining the optimum fiber angle for each layer sequentially in the order from the outermost to the innermost layer.

An algorithm is made from the above assumption and a set of layerwise steps 1-K (K is the same as the number of layers) is applied as one cycle in an iterative procedure. In the first cycle, the inner layers are assumed to have zero stiffness, and the fiber orientation angles determined at Step K in the first cycle, i.e. $[\theta_1/\theta_2/.../\theta_K]_{S,opt}$, are considered as a better initial approximation for the second cycle of Steps 1-K. The iterative cycles thus continue until a converged solution is obtained.

2.3 Heuristic global optimization approach

In optimization of laminated composites, it is known that a great number of *nearly optimum* solutions exist close to the *global* optimum. The conventional optimization methods that seek for only one optimum solution tend to be trapped in local solutions and may lose many nearly optimum solutions that are almost equivalent to the global solution. A basic approach for the global solution is to calculate the vibration frequencies corresponding to all the combinations of discrete fiber orientation angles, but this of course ends up with huge number of combinations. For example, when one gets 36 discrete fiber angles with an increment of 5 degree for $-90° \le \theta \le 90°$ in one layer of symmetric 8-layer plates, this yields 36^4=1679616 combinations that require vast computation time for vibration analysis.

A new computation technique is proposed here to remedy this situation by using the physically based branch and bound approach. The idea is partly based on the layerwise optimization in that very rough increments are used for fiber orientation angles in the inner layers while fine increments are used in the outer layers. Figure 1 presents an example of normalized distribution of fundamental frequencies versus reduced 20736 combinations of lay-ups for 8-layer square plates with SSSC boundary conditions. The next process is to limit the search band to the narrow band where the global solution apparently exists. This process is continued to pin down only one global solution with other nearly optimums.

3. Results and Discussions

The elastic constants used in the examples are taken for Graphite/epoxy as E_L= 138 GPa, E_T=8.96 GPa , G_{LT}=7.1 GPa and ν_{LT}=0.30. The frequencies were calculated by using the Ritz method to make use of its short computation time. The design variables are presented in the notation as $[\theta_1/\theta_2/\theta_3/\theta_4]_S$.
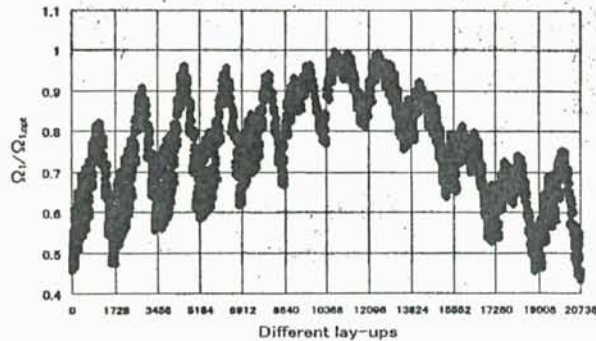
Fig.1 Normalized distribution of fundamental frequencies of an 8-layer square plate.

Table 1 presents the highest ten fundamental frequencies for the 8-layer plates obtained by the heuristic approach, where the results for square SCFF ($a/b=1$) and rectangular SSCF ($a/b=2$) plates are given in (a) and (b), respectively. These two cases are chosen because the optimum fiber orientation angles are not evident by the physical reason from the edge constraints, being different from cases such as $[0_4]_{S,opt}$ for CFCF plate. For SCFF square plate in (a), the LO solution (given in a frame) is listed in the second place among 36^4 combinations and virtually there is no difference between the first solution (global optimum) and the LO solution. The difference of the first and tenth frequencies is less than 0.004 %. In (b), when one of the worst cases is given, the LO solution is lower than the tenth solution, but still the difference between the first and the LO solution is less than 0.1 %. Thus the LO approach gives remarkably accurate solutions to the global optimum in 36^4 combinations, and advantage is obvious when one considers considerably short computation time of the LO approach.

Table 1 The highest 20 frequency solutions and the LO solution of symmetric 8-layer plates.

(a) SCFF ($a/b=1$)			(b) SSCF ($a/b=2$)		
rank	Ω_{opt}	$[\theta_1/\theta_2/\theta_3/\theta_4]_s$	rank	Ω_{opt}	$[\theta_1/\theta_2/\theta_3/\theta_4]_s$
1	16.403	[70/−45/65/70]s	1	64.896	[−10/−10/25/−10]s
2	16.403	[70/−45/70/65]s	2	64.895	[−10/−10/25/−5]s
LO sol.	16.403	[70/−45/70/65]s	3	64.894	[−10/−10/25/−15]s
3	16.402	[70/−45/70/70]s	4	64.893	[−10/−10/20/20]s
4	16.402	[70/−45/65/65]s	5	64.893	[−10/−10/25/0]s
5	16.401	[70/−45/70/60]s	6	64.893	[−10/−10/20/2]s
6	16.399	[70/−45/65/75]s	7	64.892	[−10/−10/20/15]s
7	16.399	[70/−45/70/75]s	8	64.891	[−10/−10/20/30]s
8	16.999	[70/−45/65/60]s	9	64.891	[−10/−10/25/5]s
9	16.398	[70/−45/65/80]s	10	64.891	[−10/−10/20/−5]s
10	16.396	[70/−45/70/80]s	LO sol.	64.842	[−10/0/−5/25]s

Dynamic Analysis of MEMS Resonators

Ali H. Nayfeh†, Mohammad I. Younis‡, and Eihab Abdel-Rahman†

†*Department of Engineering Science and Mechanics, MC 0219, Virginia Polytechnic Institute and State University, Blacksburg, VA 24061, USA*
‡*Department of Mechanical Engineering, State University of New York at Binghamton, Binghamton, New York 13902, USA*

We present a dynamic analysis and simulation of an electrically actuated clamped-clamped microbeam under primary-resonance excitations, Figure 1. The dynamics are governed by a nonlinear integral partial-differential equation and associated boundary conditions. We use the Galerkin procedure to reduce the problem to a finite-number of nonlinearly coupled ordinary-differential equations. We use this reduced-order model to simulate the local and global dynamic behavior of the resonators using a combination of a shooting technique and long-time integrations to predict periodic motions and their bifurcations. We use this analysis to investigate the dynamic pull-in instability and show three scenarios and mechanisms for its occurrence. The dynamic pull-in can occur through a saddle-node bifurcation, a period-doubling bifurcation, or homoclinic tangling, depending on factors such as the initial conditions of the device and the level and frequency of the electrostatic force.

The nondimensional equation of motion and boundary conditions that govern the transverse deflection of the microbeam can be expressed as

$$\frac{\partial^4 w}{\partial x^4} + \frac{\partial^2 w}{\partial t^2} + c\frac{\partial w}{\partial t} = \left[\alpha_1 \int_0^1 \left(\frac{\partial w}{\partial x}\right)^2 dx + N\right]\frac{\partial^2 w}{\partial x^2} + \frac{\alpha_2\left[V_{DC} + V_{AC}\cos(\Omega t)\right]^2}{(1-w)^2} \tag{1}$$

$$w(0,t) = w(1,t) = 0 \quad \text{and} \quad \frac{\partial w}{\partial x}(0,t) = \frac{\partial w}{\partial x}(1,t) = 0 \tag{2}$$

where x, t, and w are the nondimensional position, time, and transverse deflection, respectively. They are related to the dimensional variables (denoted by hats) as

$$w = \frac{\hat{w}}{d}, \quad x = \frac{\hat{x}}{\ell}, \quad t = \frac{\hat{t}}{T} \tag{3}$$

where $T = \sqrt{\frac{\rho bh\ell^4}{EI}}$ and ℓ is the microbeam length.

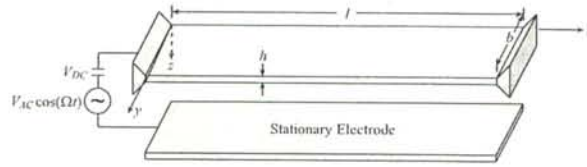Figure 1: A schematic of an electrically actuated microbeam.

The parameters appearing in equation (1) are

$$c = \frac{\hat{c}\ell^4}{EIT}, \quad \alpha_1 = 6\left(\frac{d}{h}\right)^2, \quad N = \frac{\hat{N}\ell^2}{EI}, \quad \alpha_2 = \frac{6\epsilon\ell^4}{Eh^3 d^3} \tag{4}$$

where A and I are the area and moment of inertia of the cross-section, E is Young's modulus, $\hat{N}$ is an applied tensile axial force, ρ is the material density, h is the microbeam thickness, d is the capacitor gap width, and ϵ is the dielectric constant of the gap medium.

Next, we generate a reduced-order model by discretizing equations (1) and (2) into a finite-degree-of-freedom system using the linear undamped mode shapes of the straight microbeam as basis functions. Thus, we express the deflection as

$$w(x,t) = \sum_{i=1}^{M} u_i(t)\phi_i(x) \tag{5}$$

We multiply equation (1) by $(1-w)^2$, substitute equations (5) into the resulting equation, multiply the result by $\phi_n(x)$, integrate the outcome from $x = 0$ to 1, and obtain a system of M nonlinearly coupled second-order ordinary-differential equations in time describing the dynamic behavior of an electrically actuated microbeam. We found that using three or more modes gives good convergence for the stable equilibria.
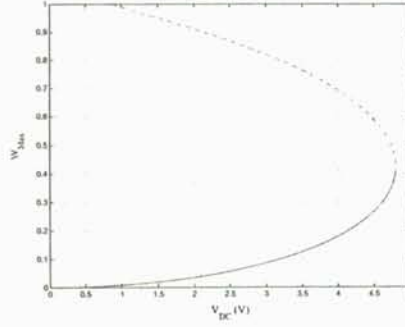
Figure 2: Equilibria of an electrostatically actuated microbeam, solid line: stable, dashed line: unstable.
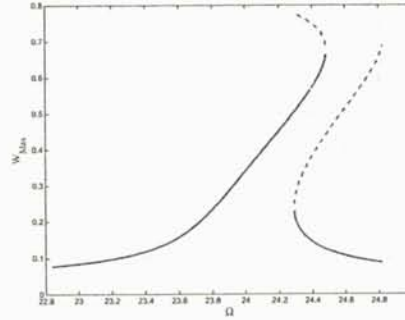

Figure 3: Frequency-response curves showing the onset of the dynamic pull-in.

We show in Figure 2 the equilibria of a microbeam under DC loading when $\ell = 510\mu m$, $h = 1.5\mu m$, $b = 100\mu m$, $d = 1.18\mu m$, and the nondimensional axial load $N = 8.7$. Figure 2 shows variation of the microbeam mid-point deflection W_{Max} with the DC voltage. The stable (lower) branch and the unstable (upper) branch collide in a saddle-node bifurcation at the static pull-in instability $V_{DC} \approx 4.8V$, resulting in the destruction of both branches. This static analysis shows that MEMS resonators should be designed to operate below this value to ensure stability.

Next, we simulate the dynamic behavior of a microbeam under an AC harmonic excitation in addition to the DC bias. Figure 3 shows variation of W_{Max} with Ω when $V_{DC} = 2V$, $V_{AC} = 0.1V$, and a quality factor $Q = 1000$. The solid curves denote stable branches and the dashed curves denote unstable branches. The dynamic pull-in instability is characterized by a slope approaching infinity, where a Floquet multiplier approaches unity. We note from the figure that the dynamic pull-in corresponds to a saddle-node bifurcation at $\Omega = 24.4857$, where a stable branch collides with an unstable branch leading to their destruction. Therefore, if the frequency of excitation is swept from low values to beyond the above value, so that the response follows the upper stable branch, the system will go to pull-in.

Figure 3 shows another saddle-node bifurcation at $\Omega \approx 24.2917$, where also a Floquet multiplier approaches unity. This bifurcation can lead to undesirable phenomena, such as jumps and hysteresis, in devices like resonant microsensors. If the solution jumps from the lower branch it either goes directly to pull-in or settles down on the upper stable branch corresponding to a stable periodic motion of larger amplitude. This depends on the transient dynamics of the system, which in turns depend on several factors, such as the sweeping rate of Ω, the ramping rate of V_{AC}, and any external disturbances in the system. In Figures 4a and 4b, we show time-history evolutions for a point that is initially close to the lower saddle-node bifurcation of Figure 3 ($\Omega \approx 24.2917$, $W_{Max} = 0.23$). In Figure 4a, $\dot{u}_1 = 0.2$; and in Figure 4b, $\dot{u}_1 = 0.23$.

Next, we describe another pull-in scenario. The time-history evolution in Figure 5a shows that dynamic pull-in occurs below $V_{AC} \approx 0.2819V$, resulting from a saddle-node bifurcation. In this case, the dynamic pull-in occurs when the stable periodic orbit around the stable equilibrium collides with the saddle (the unstable equilibrium solution at $W_{Max} \approx 0.91$) and its stable manifold. Figure 5b is generated from the same data of Figure 5a except that the sign of one of the initial condition states is changed from positive to negative. We note that the motion is stable, which indicates a fractal dynamical behavior that is sensitive to initial conditions.
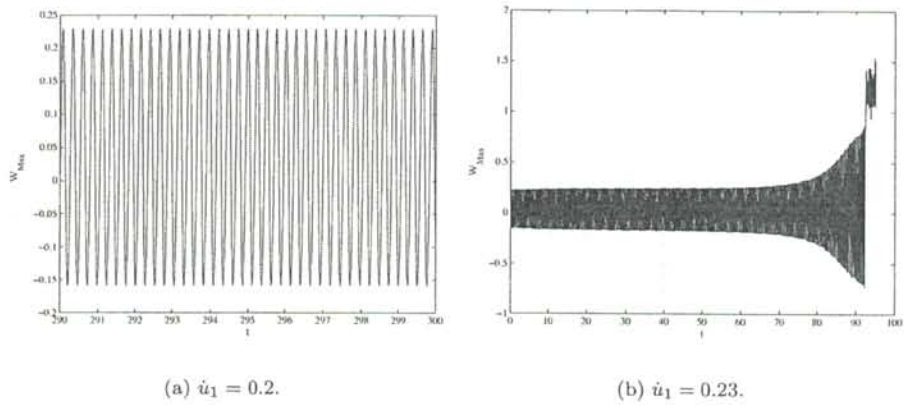
(a) $\dot{u}_1 = 0.2$.

(b) $\dot{u}_1 = 0.23$.

Figure 4: Long-time integration results for the lower saddle-node bifurcation of Figure 3 and two different initial velocities.
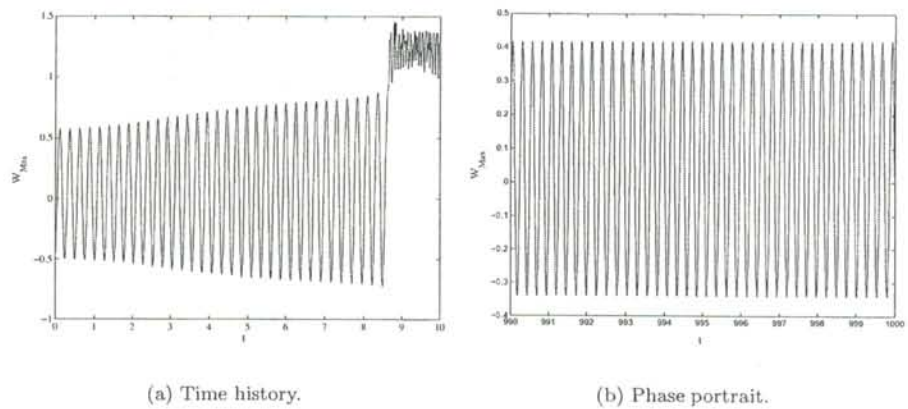

(a) Time history.

(b) Phase portrait.

Figure 5: Long-time integration results showing the onset of dynamic pull-in.

References

[1] Abdel-Rahman, E. M., Younis, M. I., and Nayfeh, A. H., "Characterization of the mechanical behavior of an electrically actuated microbeam," Journal of Micromechanics and Microengeering, Vol. 12, 2002, pp. 795–766.

[2] Younis, M. I. and Nayfeh, A. H., "A study of the nonlinear response of a resonant microbeam to an electric actuation," Nonlinear Dynamics, Vol. 31, 2003, pp. 91–117.

[3] Younis, M. I., Abdel-Rahman, E. M., and Nayfeh, A. H., "A Reduced-order model for electrically actuated microbeam-based MEMS," Journal of Microelectromechanical Systems, Vol. 12, 2003, pp. 672–680.

Vibration of an Atomising Disc Subjected to Growing Distributed Mass

Huajiang Ouyang

Department of Engineering, University of Liverpool, Liverpool L69 3GH, UK

Discs are a basic mechanical element commonly found in engineering. Examples are plentiful and include computer discs, circular saws, disc brakes, and so on. Frequently these discs are subjected to loading that moves relative to the discs and are treated as moving-load problems.

Mote [1] studied the vibration of a stationary disc subjected to a simple, point-wise rotating load. Iwan and Moeller [2] studied the vibration of a spinning disc subjected to a simple, point-wise stationary load. Since then, a large number of papers have been published on disc vibration excited by moving loads, which was reviewed by Mottershead [3]. Two types of moving-load problems have received much attention. They are the computer disc problem [4] and the wood saw problem [5]. In addition, Ouyang et al. [6] tackled disc brake vibration and squeal as a moving-load problem.

The vibration of atomising discs has not been studied in the open literature. This paper appears to be the first attempt to investigate this important problem. The centrifugal atomisation device at Liverpool generates large-amplitude vibration and creates a safety concern. The high-frequency vibration is also likely to cause premature fatigue failure.

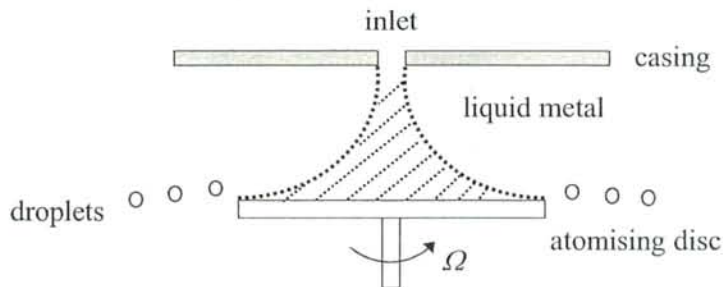A schematic view of centrifugal atomisation at Liverpool is shown in Figure 1 (adapted from [7]).

Figure 1. Schematic of powder production using atomising disc

The liquid metal stream flows down from an inlet and drops onto the surface of a flat metal (atomising) disc that is spinning at very high speed. Due to the centrifugal force acting on it, the liquid metal stream is broken into a spray of metal droplets that fly off the disc and become powder particles when cooled. This is an efficient way of producing high quality powder. As the molten metal descends on to the disc, it cools down and part of it gradually solidifies prematurely and accumulates on the disc. As the process goes on, more solid metal accumulates and forms a 'skull' on the disc. The skull hinders the flow of the metal stream and the flight of metal droplets as a barrier and thus reduces yield of powder and also produces unwanted vibration due to the imbalance. From the point of view of dynamics, the whole system has a time-dependent moving mass (growing mass). This paper studies the simple case of axially symmetrical mass distribution that grows and moves, which bears some resemblance to (but are more complicated than) the problem of a disc subjected to a radially moving load studied by Huang and Chiou [8].

As a first study conducted on the vibration of atomising discs, a number of rather restrictive assumptions have to be made. (1) The effect of temperature variation in the metal flow and in the

disc itself is not considered. (2) There is no thermal and mechanical coupling. (3) The shape and the rate of the metal flow are known a priori and are not influenced by the disc vibration. This latter assumption is probably not very true but the fact is not known yet. (4) The metal flow on the disc is axial-symmetrical. This assumption is largely true. However, a slight deviation from axial symmetry will result in extra excitation and further mathematical complication, which will be considered in the next investigation. (5) The metal flow on the disc provides only inertia, but no stiffness or damping to the system. (6) The disc vibration is initiated by the liquid metal descending onto the disc as an impact. (7) The disc is modelled as a flat, annular, thin (Kirchoff) plate of equal thickness with clamp-free boundaries. By removing any of the above assumptions, the system becomes more representative of reality but increasingly complex. In so doing a series of investigations of increasing sophistication can be made in future.

The dynamic model of the system is shown in figure 2.
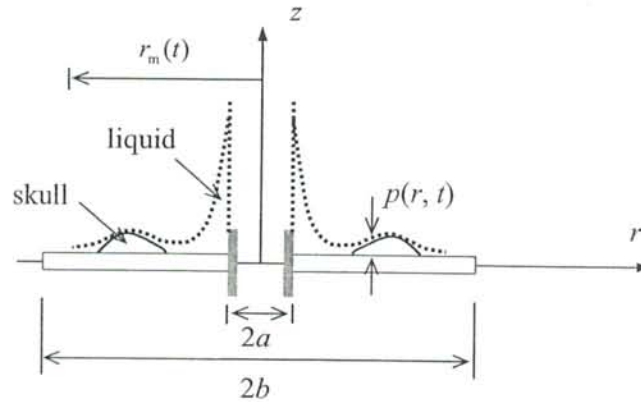

Figure 2. Dynamics model of the atomising disc

The equation of motion of the above-mentioned disc (with centrifugal force) cast in the space-fixed cylindrical coordinate system, is [2]

$$\rho h(\frac{\partial^2 w}{\partial t^2} + 2\Omega \frac{\partial^2 w}{\partial t \partial \theta} + \Omega^2 \frac{\partial^2 w}{\partial \theta^2}) + D\nabla^4 w - h\frac{\partial}{r \partial r}(r\sigma_r \frac{\partial w}{\partial r}) - h\frac{\sigma_\theta}{r^2}\frac{\partial^2 w}{\partial \theta^2} = p(r,t) \tag{1}$$

In the region where the metal stream is present on the disc surface, the distributed inertial load is $-\rho_m(r,t)h_m(r,t)\frac{\partial^2 w}{\partial t^2}$, where ρ_m is the density of the metal stream on the disc. Hence

$$p(r,t) = \begin{cases} -\rho_m(r,t)h_m(r,t)\dfrac{\partial^2 w}{\partial t^2} & a < r \le r_m(t) \\ 0 & r_m(t) < r < b \end{cases} \tag{2}$$

and the in-plane stresses due to the centrifugal force are [2, 4]

$$\sigma_r(r) = d_1 + \frac{d_2}{r^2} + d_3 r^2 \qquad \sigma_\theta = d_1 - \frac{d_2}{r^2} + d_4 r^2 \tag{3}$$

Suppose that the formation (the height h_m and radius r_m of the profile) of the metal stream on the disc surface is known. This information may be obtained through measurement, or through computer simulation as done by Ho and Zhao [7]. Then the distributed load p can be determined.

The solution of equation (1) can be written as

$$w(r,\theta,t) = \sum_{m=0}^{\infty} \sum_{n=-\infty}^{\infty} \phi_{mn}(r,\theta) q_{mn}(t), \qquad \phi_{mn}(r,\theta) = R_{mn}(r)\exp(in\theta) \qquad (4)$$

and the 'radial mode' is [9]

$$R_{mn}(r) = (a_{mn} + b_{mn} r + c_{mn} r^2)(r-a)^{m+2} \qquad (5)$$

where the coefficients a_{mn}, b_{mn} and c_{mn} can be determined at the free boundary of the disc where the shear force and the bending moment vanish, and from the normalisation condition [9].

Multiplying equation (1) after substituting equations (2) and (4) into it with $\bar{\phi}_{kl}(r,\theta)$ ($k = 0,1,2,...; l = 0,-1,1,-2,2,...$) and then integrate the resultant equation over the disc area (Galerkin's method) yields a system of simultaneous second-order differential equations of the complex-valued modal coordinates $q_{kl}(t)$ with time-dependent coefficients for the mass term. There is no closed-form solution for these complicated equations in general. Therefore numerical methods must be used to solve these equations. A fourth-order Runge-Kutta algorithm is developed to conduct numerical integration of these equations in the time-domain. From the numerical solutions, the influence of the metal flow and disc speed on the vibration of the disc can be determined. A numerical example of a real atomising disc is analysed. It is found from the numerical solutions that due to the radially growing mass the vibration of the system is non-stationary with multiple frequencies that decrease as time goes by and can exhibit flutter.

References

1. Mote, C. D., Jr. Stability of circular plates subjected to moving loads. *Journal of the Franklin Institute*, 1970, **290**, 329-344
2. Iwan, W. D. and Moeller, T. L. The stability of a spinning disc with a transverse load system. *ASME J. Appl. Mech.*, 1976, **43**, 485-490
3. Mottershead, J. E. Vibration and friction-induced instability in discs. *Shock Vib. Dig.*, 1998, **30**, 14-31
4. Ono, K., Chen, J. S. and Bogy, D. B. Stability analysis of the head-disk interface in a flexible disc drive. *ASME J. Appl. Mech.*, 1991, **58**, 1005-1014
5. Hutton, S. G., Chonan, S. and Lehmann, B. F. Dynamic response of a guided circular saw. *J. Sound Vib.*, 1987, **112**, 527-539
6. Ouyang, H., Mottershead, J. E. and Li, W. A moving-load model for disc-brake stability analysis. *ASME J. Vib. Acoust.*, 2003, **125**(1), 53-58
7. Ho, K. H. and Zhao, Y. Y. Modelling thermal development of liquid metal flow on rotating disc in centrifugal atomisation. *Materials Science and Engineering*, 2004, A365 336–340
8. Huang, S. C. and Chiou, W. J. Modeling and vibration analysis of spinning-disk and moving-head assembly in computer storage systems. *ASME J. Vib. Acoust.*, 1997, 119, 185-191
9. Chung, J., Oh, J.-E. and Yoo, H. H. Non-linear vibration of a flexible spinning disc with angular acceleration. *J. Sound Vib.*, 2000, **231**(2), 375-391

63

Modal Properties of Planetary Gears with an Elastic Continuum Ring Gear

Xionghua Wu and Robert G. Parker
Department of Mechanical Engineering
The Ohio State University

Planetary gears (Figure 1) are widely used in automotive and aerospace transmissions due to advantages such as compactness, high torque/weight ratio, low bearing load and high transmission ratio. Although planetary gears have a reputation of being quieter than parallel axis systems, their noise and vibration remain a key concern.

The elastic continuum vibration of the ring gear as shown in Figure 1 is significant for many practical applications of planetary gears, especially in aircraft engine, rotorcraft, and automotive applications [1]. Weight is a paramount concern in these systems, and use of thin ring gears maximizes the torque/weight ratio. Ring flexibility also introduces compliance that improves load sharing among the separate planet load paths and improves tolerance to manufacturing errors. In the limited literature on planetary gear dynamics, however, the analytical models use exclusively discrete models for all components in the planetary gear (sun, planets, carrier, and ring) [2, 3]. In such models each component is a rigid body with up to three planar degrees of freedom.

The present work adopts a continuum ring gear vibration model represented as a partial differential equation while all other components are modeled as discrete rigid bodies. Analytical study of this expanded hybrid discrete-continuous model shows that the modal properties and natural frequency spectrum are highly structured. All vibration modes are classified into one of four types according to their unique characteristics. The well-defined properties and natural frequency multiplicity of each mode type are proved analytically.

The discrete-continuous model of a planetary gear is shown in Figure 1. All gear meshes are represented by linear springs. The sun, carrier and planets are considered as rigid bodies, while the ring gear is modeled as a thin, inextensible, elastic ring. The bearings and supports of all bodies are modeled as linear stiffnesses. The planets are identical and equally spaced. All ring-planet mesh stiffnesses are equal, and all sun-planet mesh stiffnesses are equal. $u(\theta,t)$ is the tangential displacement of the ring, which is separated into the elastic deformation $v(\theta,t)$ and the rigid body motion $\mathbf{p}_r = (x_r, y_r, u_r)^T$. The translations and rotations of the sun and carrier are $\mathbf{p}_j = (x_j, y_j, u_j)^T$, $j = s,c$, and the deflections of the planets $\mathbf{p}_n = (\xi_n, \eta_n, u_n)^T$, $n = 1, \cdots, N$ are described by radial and tangential coordinates.

The dimensionless equation of motion for the ring gear is

$$M_e v_{,\tau\tau} + k_{bend} L_1 v + L_2 v + \sum_{n=1}^{N} L_3^n \delta_n = 0 \tag{1}$$

$$M_e = \frac{1}{2\pi}\left(1 - \frac{\partial^2}{\partial\theta^2}\right), \quad \bar{k}_{bend} = \frac{EJ}{R'(1-v^2)}, \quad L_1 = -\left(\frac{\partial^6}{\partial\theta^6} + 2\frac{\partial^4}{\partial\theta^4} + \frac{\partial^2}{\partial\theta^2}\right)$$

$$L_2 = -\sum_{n=1}^{N}\left[(\sin^2\alpha_r \frac{\partial^2}{\partial\theta^2} - \cos^2\alpha_r)\delta(\theta-\psi_n) + (\sin\alpha_r \frac{\partial}{\partial\theta} + \cos\alpha_r)\sin\alpha_r \frac{\partial\delta(\theta-\psi_n)}{\partial\theta}\right] + (\bar{k}_{rus}R - \bar{k}_{rhs}R\frac{\partial^2}{\partial\theta^2})/\bar{k}_{rp}$$

$$L_3^n = \cos\alpha_r \delta(\theta-\psi_n) - \sin\alpha_r \frac{\partial\delta(\theta-\psi_n)}{\partial\theta} \tag{2}$$

$$\delta_n = -x_r \sin\psi_m + y_r \cos\psi_m + u_r + \xi_n \sin\alpha_r - \eta_n \cos\alpha_r - u_n \qquad (3)$$

The equations of motion for the discrete elements are omitted for brevity. Coupling between the elastic ring vibration, rigid body ring vibration, and planet motions is evident in the last term of (1).

To provide mathematical structure, the displacement of the whole system is separated into two parts: $v(\theta,t)$ and $q(t)$. v is the elastic deformation of the ring gear and q is the vector of discrete component motions of the sun, planets, carrier, and ring. These elements are formed into the extended variable $a = (v, q^T)^T$. With $a(\theta,\tau) \to a(\theta)e^{i\omega t}$, the extended operator eigenvalue problem is

$$-\omega^2 Ma + Ka = 0 \quad a = \begin{bmatrix} v \\ q \end{bmatrix}, \; Ma = \begin{bmatrix} M_e v \\ \mathbf{M}q \end{bmatrix}, \; Ka = \begin{bmatrix} k_{bend}L_1 + L_2 & L_3 \\ L_4 & \mathbf{K} \end{bmatrix}\begin{bmatrix} v \\ q \end{bmatrix} \qquad (4)$$

where M and K are extended stiffness and inertia operators, $\mathbf{M}$ and $\mathbf{K}$ derive from the mass and stiffness matrices for the discrete planetary gear model [2], and L_4 is a linear operator from the space of $v(\theta)$ to the space of q that, along with L_3 which is an operator from the space of q to the space of $v(\theta)$, captures the coupling between continuum and discrete vibrations. The extended operators are self-adjoint with the inner product $<a_1, a_2> = \int_0^{2\pi} v_1 v_2 d\theta + q_1^T q_2$. This structure simplifies use of analytical methods.

In order to find all natural frequencies and vibration modes of the elastic-discrete model using perturbation analysis, two systems must be considered. In the first one, the unperturbed system is a discrete planetary gear having a rigid ring gear. The stiffness of the ring is perturbed from infinite to a finite number. The small quantity ε is the ring bending compliance. The discrete model has $3N+9$ eigensolutions, where N is the number of planets, so only $3N+9$ perturbed eigensolutions are obtained. To find the remaining eigensolutions, we examine a system where the sun-planet-carrier system is very stiff, and their displacements are small compared to the elastic ring deformation. The unperturbed system is an elastic ring having multiple springs representing the ring-planet gear meshes, and the perturbation parameter is $\varepsilon = 1/k_{sp}$. The eigensolutions from these two perturbations form the complete set of eigensolutions of the elastic ring planetary gear system with no redundancy. This process mathematically exposes the system's highly structured modal properties. The shortcoming is that there is an implicit assumption that the modal properties do not change as the perturbation parameters cease to be small. While this assumption is confirmed in all numerical results, the assumption is eliminated in an alternate approach.

The properties of all modes can be proven by first choosing a candidate mode guided by numerical results and the perturbation analysis. Direct substitution into the discrete-continuous eigenvalue problem and reduction of the results leads to reduced eigenvalue problems that confirm the modal properties. This process is conducted for each of the four mode types. The modal properties from this method and perturbation are identical. The candidate mode method places no restriction on the size of any parameters.

Four types of modes exist, and this list is exhaustive ($j = 1, 2, \ldots$ in all cases) (Figure 2):

- *Rotational modes* contain only the jN nodal diameter ring components. The sun, carrier and ring rigid body motion have only rotational motion, and all planets have the same motion. The natural frequencies are distinct.
- *Translational modes* contain only the $jN \pm 1$ nodal diameter ring components. The sun, carrier and ring rigid body motion have only translational motion; the planet motions are related by a rotation transformation. These all occur in degenerate pairs of modes with equal natural frequencies.
- *Planet modes* contain only the $jN \pm s$ nodal diameter ring components, where $s = 2, 3, \ldots, \text{int}(N/2)$. The translation and rotation of the sun, carrier and ring rigid body motion

are zero, and the deflection of any planet is proportional to the deflection of any other planet. These occur in degenerate pairs of modes except for even N, where one mode has a distinct natural frequency.

- *Ring modes* contain only a single nodal diameter of ring vibration. The deflections of the sun, carrier, and planets are zero. The natural frequencies are distinct.

With the ring gear deformation represented by a truncated Fourier series of J terms, the exact number of each mode type can be determined. For odd number of planets N, the number of rotational, translational, planet and ring modes are $J+6$, $4J+10$, $(2JN-6J)+(3N-9)$ and J, respectively. For even N, they are $J+6$, $4J+10$, $(2JN-7J)+(3N-9)$ and $2J$, respectively.

References

1. A. Kahraman and S. Vijayakar, Effect of Internal Gear Flexibility on the Quasi-Static Behavior of a Planetary Gear Set, Journal of mechanical Design, 123 (2001), 408-415.
2. A. Kahraman, Natural Modes of Planetary Gear Trains, Journal of Sound and Vibration, 173 (1994), 125-130.
3. J. Lin and R. G. Parker, Analytical Characterization of the Unique Properties of Planetary Gear Free Vibration, Journal of Vibration and Acoustics, 121 (1999), 316-321.
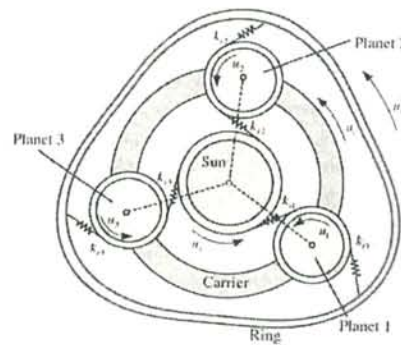
Figure 1. Elastic-discrete model of a planetary gear with a continuum ring gear.
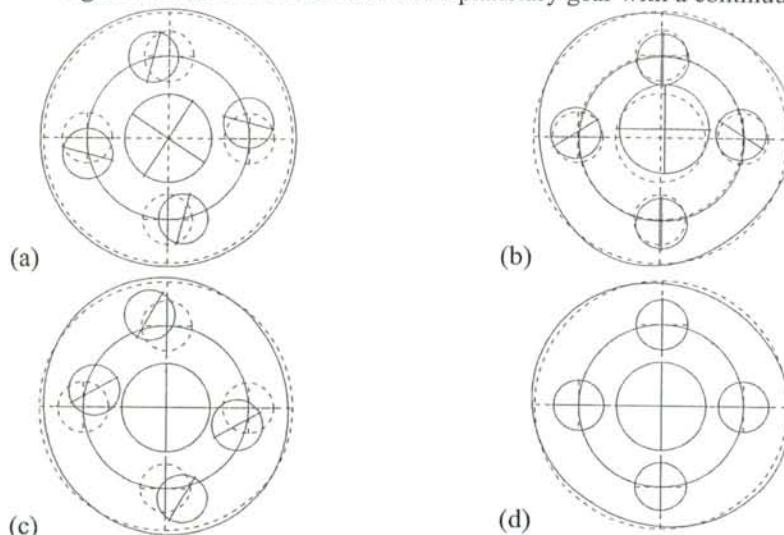

(a)

(b)

(c)

(d)

Figure 2. (a) rotational mode, (b) translational mode, (c) planet mode, and (d) ring mode.

DYNAMIC STABILITY OF SHELLS: THEORIES AND EXPERIMENTS

F. PELLICANO

Dip. di Ingegneria Meccanica e Civile, Università di Modena e Reggio Emilia, V. Vignolese, 905, Modena, I - 41100 ITALY
E-MAIL: francesco.pellicano@unimore.it

M. AMABILI

Dip. di Ingegneria Industriale, Università di Parma, Area delle Scienze, 181/A, Parma, 43100 ITALY, E-MAIL: marco@me.unipr.it

K. AVRAMOV

Dept. of Theoretical Mechanics, Faculty of Physics and Engineering, National Technical University "KhPI", Frunze St.21, Kharkov 61002, Ukraine, E-MAIL kvavr@kharkov.ua.

ABSTRACT

In the present paper the dynamic stability of circular cylindrical shells is investigated. Donnell's Nonlinear Shallow Shell and Sanders' Theories have been applied for numerical studies in order to evaluate the accuracy of methods. The effect of a contained fluid on the stability and the postcritical behaviour is analyzed in detail. Chaotic dynamics of pre-compressed shells is investigated by means of nonlinear time series techniques, extracting correlation dimension and Lyapunov exponents. The effect of a seismic excitation on the base of the shell is analyzed experimentally and numerically by means of a new model having mixed boundary conditions able to model the presence of a mass rigidly fixed on the top of the shell.

1. INTRODUCTION

The development of aerospace vehicles requires deep studies on light-weight, thin-walled structures. A wide branch of the technical literature in the past century was focussed on the analysis of thin-walled structures and tried to investigate their behaviour in many different operating conditions; i.e. under static or dynamic loads, either in the presence or absence of fluid-structure interaction. Both linear and nonlinear models have been developed to forecast the response of the structure under different excitations. Many studies were concerned with cylindrical shell structures that constitute main parts of aircraft, rockets, missiles and general aerospace structures.

The stability of thin circular cylindrical shells has been studied in an innovative way by Von Karman and Tsien [1] in the last century. Vijayaraghavan and Evan-Iwanowski [2] studied a parametrically excited shell both analytically and experimentally. The dynamic stability and the longitudinal resonance of simply supported cylindrical shells under axial load were analyzed by Koval [3]. Hsu [4], Nagai and Yamaki [5] developed models suitable for describing the parametric instability of shells. Popov et al. [6] Gonçalves and Del Prado [7, 8] analyzed the parametric instability of infinitely long circular cylindrical shells under static and dynamic loads.

Koval'chuk and Krasnopol'skaya [9] introduced the effect of geometric imperfections. Pellicano and Amabili [10] considered the dynamic behaviour of a cylindrical shell without imperfections; they outlined the fundamental role of both asymmetric and axisymmetric modes to predict the nonlinear response of the structure. A review of studies on the nonlinear dynamic stability and nonlinear vibrations of circular cylindrical shells is provided by Amabili and Païdoussis [11]. In [12] a full report of a NATO project related to shells dynamics and stability with fluid structure interaction can be found.

In the present work, the static and the dynamic behaviour of thin cylindrical shells is considered. Both Donnell's shallow-shell and Sanders' theories are used: Galerkin projections and Lagrange equations are used respectively to obtain a system of ordinary differential equations. Geometric imperfections are included in the model. The response of the system subjected to several kinds of loads is investigated: static and periodic axial external loads; seismic base excitation and added mass. Continuation techniques are applied to obtain static and periodic solutions of ODE (ordinary differential equations) varying one or more parameters of the system. Time histories and spectra of non-stationary responses are obtained by using direct simulations. Experimental modal analysis has been performed on a shell clamped-free having an added mass on the top.

2. GOVERNING EQUATIONS

A brief description of the Donnell Nonlinear Shallow Shell theory is given in the present section, Sanders' theory is not reported for the sake of brevity.

The equation of motion for flexural vibrations of a thin, circular cylindrical shell is given by

$$D \nabla^4 w + c h \dot{w} + \rho h \ddot{w} = f + p + \frac{1}{R} \frac{\partial^2 F}{\partial x^2} + \left(\frac{\partial^2 F}{R^2 \partial \theta^2} \frac{\partial^2 w}{\partial x^2} - 2 \frac{\partial^2 F}{R \partial x \partial \theta} \frac{\partial^2 w}{R \partial x \partial \theta} + \frac{\partial^2 F}{\partial x^2} \frac{\partial^2 w}{R^2 \partial \theta^2} \right), \tag{1}$$

with the compatibility equation

$$\frac{1}{E h} \nabla^4 F = -\frac{1}{R} \frac{\partial^2 w}{\partial x^2} + \left[\left(\frac{\partial^2 w}{R \partial x \partial \theta} \right)^2 - \frac{\partial^2 w}{\partial x^2} \frac{\partial^2 w}{R^2 \partial \theta^2} \right], \tag{2}$$

where $D = E h^3 / [12(1 - v^2)]$ is the flexural stiffness, E the Young's modulus, v the Poisson ratio, h the shell thickness, R the mean shell radius, ρ the mass density of the shell, c the damping coefficient, F is the in-plane stress function, p is the pressure acting on the shell surface due to the fluid-structure interaction and f is a distributed external load. Moreover, simply supported boundary conditions are considered and the continuity in θ is imposed. The axial load is: $\widetilde{N}_x(t) = -N + N_D \cos \omega t$.

The radial displacement w is expanded by using the linear shell eigenmodes as bases; in particular, the flexural response may be written as follows:

$$w(x,\theta,t) = \sum_{n_1=1}^{N_1} \sum_{m=1}^{N_1} \left[A_{m,(n_1 n)}(t) \cos(n_1 n\theta) + B_{m,(n_1 n)}(t) \sin(nn_1\theta) \right] \sin(\lambda_m x) + \sum_{m=1}^{M} A_{2m-1,0}(t) \sin(\lambda_{2m-1} x), \qquad (3)$$

where $\lambda_m = m\pi/L$, t is the time; $A_{m,j}(t)$, $B_{m,j}(t)$ and $A_{m,0}(t)$ are unknown functions of t and $j = n_1 n$. In the numerical calculations, N_1 and M will be assigned equal to 3 and 5, respectively. Expansion (3) is suggested by the presence of quadratic and cubic nonlinearities.

A similar expansion has been performed in the case of Sanders' theory; however, in this case both radial w and in-plane u, v displacement fields have been expanded.

The shell is assumed to be empty or completely fluid-filled. An incompressible inviscid fluid is considered and the effect of the dynamic pressure acting on the shell surface is linearized. The fluid velocity field can be described in terms of the velocity potential Φ, where $\mathbf{v} = -\nabla \Phi$, and $\nabla^2 \Phi = \dfrac{\partial^2 \Phi}{\partial x^2} + \dfrac{\partial^2 \Phi}{\partial r^2} + \dfrac{1}{r} \dfrac{\partial \Phi}{\partial r} + \dfrac{1}{r^2} \dfrac{\partial^2 \Phi}{\partial \theta^2} = 0$.

3. NUMERICAL RESULTS

A numerical analysis is performed on a test shell, studied in [6-8], having the following characteristics: $h = 2 \times 10^{-3}$ m, $R = 0.2$ m, $L = 0.4$ m, $E = 2.1 \times 10^{11}$ N/m^2, $v = 0.3$, $\rho = 7850$ kg/m^3; in the case of fluid-filled shell, $\rho_F = 1000$ kg/m^3. The fundamental frequency of the empty shell is equal to 2 $\pi \times 503.7$ rad/s and is obtained for $m=1$ and $n=5$. When the shell is excited by an axial periodic load, two kind of excitations are present on the modal equations: (i) a direct excitation of the axisymmetric modes due to the Poisson's effect; (ii) a parametric excitation of all modes. In Figure 1 the principal instability region is presented for $\zeta = 0.0008$ and no axial preload: regions obtained with Donnell's nonlinear shallow shell and Sanders' theories are very close; the effect of imperfection ($w_{1,5,c}^{(0)}/h = 0.15$) is a translation of the instability boundary, without changing the minimum value of P_D.
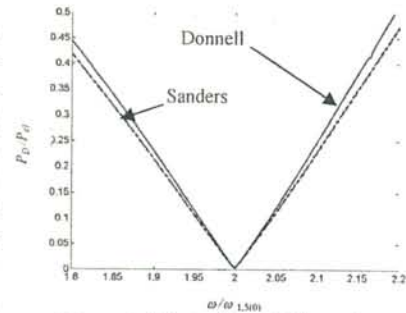

Figure 1. Principal instability region: comparison theories and effect of imperfections

$\dfrac{\omega_{1,5}}{\omega_{1,5(0)}}$	$\dfrac{w_{1,5,c}^{(0)}}{h}$	$\dfrac{w_{1,15,c}^{(0)}}{h}$	$\dfrac{w_{3,5,c}^{(0)}}{h}$	$\dfrac{w_{1,0}^{(0)}}{h}$	$\dfrac{w_{3,0}^{(0)}}{h}$	$\dfrac{P_{Dcr}}{P_{cl}}$
1	0	0	0	0	0	0.0038 (Donnell)
1	0	0	0	0	0	0.0035
0.99091	0.1	0	0	0.1	0.1	0.0033
1.02912	0.1	0.1	0.1	0.1	0.1	0.0036
0.99117	0	0	0	0.1	0.1	0.0033
1.03715	0.1	0.1	0.1	0	0	0.0038
1.7001	0.5	0.5	0.5	0.5	0.5	0.0077
1.04611	-0.1	-0.1	-0.1	-0.1	-0.1	0.004
1.00975	0	0	0	-0.1	-0.1	0.0037

Table 1. Dynamic buckling: effect of imperfections.

In Table 1 the effect of different imperfections is summarized: the general comment is that geometric imperfections are not quite effective on the parametric instability; the only case where the influence is evident regards a big imperfection (50% h) that gives rise to a growing of the critical dynamic load; this is mainly due to axial symmetric outward imperfections, that make the shell stiffer. Results presented in Table 1 are obtained by means of a two parametric continuation, which allows for finding the minimum dynamic load versus the excitation frequency.

In the case of axial preload, the parametric resonance can lead the structure to collapse, by jumping on buckled static configuration; this is due to the static bifurcation nature, which is strongly sub-critical. Furthermore, in the case of axial pre-compression, amplitude modulations and chaotic dynamics can appear. The analysis of strange attractors by means of nonlinear time series techniques, show that the correlation dimension of the chaotic attractor is about 3.5; moreover, a positive maximum Lyapunov exponent has been estimated, confirming the chaotic character of oscillation.

A numerical and experimental analysis has been performed on a PVC shell having the following characteristics: $h = 0.3 \times 10^{-3}$ m, $R = 0.043$ m, $L = 0.09$ m, $E = 2.65 \times 10^9$ N/m^2, $v = 0.4$, $\rho = 1370$ kg/m^3; the shell is clamped on the base and a mass is rigidly attached on the top, see figure 2. The fundamental mode is found experimentally at 92 Hz after a

modal identification performed by means of LMS CADA-X, which allowed the determination of damping (0.85%) and modal shape also, see Figure 3. The theoretical mode shape is shown in figure 4, which shows good agreement with experiments: the first mode of such a shell is a beam-like mode; the theory of Sanders predicts that the fundamental frequency is 89 Hz, i.e. very close to the experimental observation. Note that the shape of the fundamental mode is strongly influenced by the mass on the top. Numerical simulations show that such a model can undergo dynamic instability in the case of seismic excitation. Experimental validations will be performed in the next future.
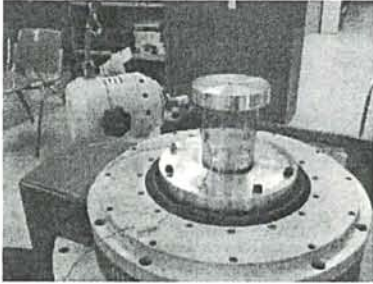

Figure 2. Experimental setup

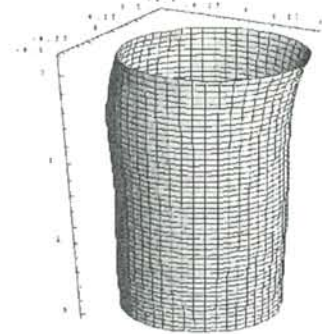Figure 3. First mode (experimental)

Figure 4. First mode (theory)

CONCLUSIONS

The parametric instability and the postcritical behaviour of a circular cylindrical shell subjected to dynamic axial loads are analysed. The Donnell's nonlinear shallow-shell and Sanders' theories have been compared: both theories show that the fluid gives a safety effect on the parametric instability and the geometric imperfection does not change the dynamic critical load. Sanders' theory has been applied to the case of a clamped free shell having an added mass on the top. Linear analyses show good agreement between experiments and theory.

ACKNOWLEDGEMENTS

REFERENCES

1. Von Kármán T, Tsien HS. The buckling of thin cylindrical shells under axial compression. J. of the Aeronautical Sciences 1941; 8(8): 303-312.
2. Vijayarachavan A, Evan-Iwanowski RM. Parametric instability of circular cylindrical shells. J. of Appl. Mech. 1967; 34: 985-990.
3. Koval LR. Effect of longitudinal resonance on the parametric stability of an axially excited cylindrical shell. J. of Acoustic Society of America 1974; 55(1): 91-97.
4. Hsu CS. On parametric excitation and snap-through stability problems of shells. In: Thin-Shell Structures; Theory Experiments and Design. Y.C. Fung and E.E. Sechler Eds. Englewood Cliffs, New Jersey: Prentice-Hall; 1974.
5. Nagai K, Yamaki N. Dynamic stability of circular cylindrical shells under periodic compressive forces. J. of Sound and Vibration 1978; 58(3): 425-441.
6. Popov AA., Thompson JMT, McRobie FA.. Low dimensional models of shell vibrations. Parametrically excited vibrations of cylindrical shells. J. of Sound and Vibration 1998; 209: 163-186.
7. Gonçalves PB, Del Prado ZJGN. The role of modal coupling on the non-linear response of cylindrical shells subjected to dynamic axial loads. In: Proc. of the Symp. on Nonlinear Dynamics of Shells and Plates, ASME Int. Mech. Eng. Congr. and Exp., Orlando, USA, 2000; AMD 238: 105-116.
8. Gonçalves PB, Del Prado ZJGN. Nonlinear oscillations and stability of parametrically excited cylindrical shells. Meccanica 2002; 37: 569–597.
9. Koval'chuk PS, Krasnopol'skaya TS. Resonance phenomena in nonlinear vibrations of cylindrical shells with initial imperfections. Soviet Applied Mechanics 1980; 15: 867-872.
10. Pellicano F, Amabili M. Stability and vibration of empty and fluid-filled circular cylindrical shells under static and periodic axial loads. International Journal of Solids and Structures 2003; 40: 3229-3251.
11. Amabili M, Païdoussis MP. Review of studies on geometrically nonlinear vibrations and dynamics of circular cylindrical shells and panels, with and without fluid-structure interaction. Appl. Mech. Rev. 2003; 56: 349-381.
12. Pellicano F, Mikhlin Y. and Zolotarev I., *Nonlinear Dynamics of Shells with Fluid-Structure Interaction*, published by Inst. of Thermomechanics AS CR, Prague, 2002.

Vibration Analysis of Postbuckled Elastica
Beams, Columns, Pipes, and Loops

Raymond H. Plaut[1] and Lawrence N. Virgin[2]

[1]Department of Civil and Environmental Engineering, Virginia Polytechnic Institute and State University, Blacksburg, Virginia 24061-0105, USA

[2]Department of Mechanical Engineering and Materials Science, Duke University, Durham, North Carolina 27708-0300, USA

Attention is focused on two-dimensional problems involving an elastica formulation. Beams, columns, pipes, and loops are considered. They are assumed to be slender, inextensible, unshearable, and elastic. In most cases the bending moment is assumed to be proportional to the curvature. The structures are subjected to loads that produce large static deflections, sometimes after buckling. Small vibrations about these equilibrium configurations are investigated.

The displacements are written as functions of the arc length along the structure and of time. At a given point on the structure, the relevant variables are the coordinates, the rotation, the bending moment, and the internal force components parallel to the two axes. The governing equations are two geometrical relationships, the moment-curvature relationship, and dynamic equilibrium of moments and force components. Transverse and axial inertias are included.

Both the equilibrium and vibration problems are boundary value problems, involving six first-order differential equations within the span and usually three boundary conditions at each end. They are solved as initial value problems, using a shooting method and the program Mathematica. The only approximation in the solution technique is in the numerical integration procedure used in the subroutine NDSolve in Mathematica. The unknown parameters (e.g., force components) and unknown boundary values at the initial end are guessed and then varied until the known boundary conditions at the other end are satisfied with sufficient accuracy.

This procedure yields the equilibrium shape first, and then vibration modes and frequencies for small motions about this shape. Different modes are obtained by guessing the vibration frequency in different ranges. In cases for which the solution involves complex vibration "frequencies," such as when damping is present or sometimes when Coriolis forces are active, the numerical computations are performed in complex form. In most of the problems, experiments are also carried out and their results are compared with those of the analysis.

In the first problem, a flexible strip is attached at its ends to a substrate comprised of two rigid plates connected with a hinge. One end of the strip is bonded to one of the plates, and the other end to the other plate. Initially the plates are flat and the strip has an upward (buckled) deflection. The right plate is rotated upward. This problem is motivated by an application of flexible electronic circuits in automobiles and possible debonding at the contact points with the substrate. If the system is symmetric, the strip contacts itself at a point when the rotation is sufficiently large. For an asymmetric system, as the rotation is increased, the strip jumps to a shape having point contact with one of the plates and line contact with the other. Even though the strip is inextensible, the second mode has no nodes [1].

The second problem is somewhat similar. In this case the weight is included, and the strip lies on a horizontal surface. Its ends are pushed together, causing the strip to buckle upward. The problem has applications involving fabrics and textiles. The strip is called "long" if the buckled region does not reach the pushed ends, and "short" if they do (i.e., there are no flat regions near the ends). As the ends are pushed together, initially the buckled region is symmetric about its center. In most cases, there is a bifurcation into a tilted stable equilibrium shape. Self-contact occurs at a certain value of end shortening, depending on a dimensionless parameter related to the weight and bending stiffness of the strip. As the ends are pushed, the fundamental vibration frequency increases and then decreases, reaching zero when bifurcation occurs. Cases of a heavy strip lying on an inclined or vertical surface also are considered, with relevance to buckling of drillpipes.

Longitudinal self-weight is the only load in the third problem, in which the postbuckling of a cantilevered column is examined. The critical height was determined by A. G. Greenhill in 1881. Here, linearly-elastic and softening constitutive laws are considered, and the bifurcation may be supercritical or subcritical. The effect of initial curvature is studied. For the softening material considered, which corresponds to a curtain wire consisting of a helical steel core surrounded by a plastic covering, the column suddenly jumps to a severely-drooped configuration as the length is increased past a certain value [2].

In the fourth problem, one end of a cable is attached to the tip of a cantilever and the other end is attached at or near the base. A turnbuckle within the cable is tightened. If the bottom end of the cable is at the base, buckling occurs at a critical load; if it is offset from the base, the column deflects as soon as the turnbuckle is tightened. Large deflections are computed, along with associated small vibrations [3].

Next, a thin strip is bent such that the two ends are brought together and clamped (pinched) to form a teardrop shape. The clamped end is held at various angles, with the loop either upright, horizontal, downward, or halfway between these positions. Self-weight provides the loading. The length of the loop is increased. When the loop is held upright, in-plane buckling occurs at a critical length. For the other orientations, except the hanging one, deflections also become large as the length is increased [4].

The sixth problem involves fluid-conveying pipes with supported ends, which buckle when the fluid velocity reaches a critical value. For higher velocities, the postbuckled equilibrium shape can be directly related to that for a column under a follower end load. However, the corresponding vibration frequencies are different due to the Coriolis force associated with the fluid flow. Clamped-clamped, pinned-pinned, and clamped-pinned pipes are considered. Axial sliding is permitted at the downstream end. The behavior is conservative in the prebuckling range and nonconservative in the postbuckling range. In conjunction with this problem, related columns are studied, first with a concentrated follower load at the axially-sliding end, and then with a distributed follower load. One case is particularly interesting, in which a supercritical bifurcation point is followed by a limit point on the postbuckling equilibrium path [5].

Finally, the use of slightly-buckled or pre-bent columns as vibration isolators is studied. The columns are designed to have a high axial stiffness under the weight that they support, so that the static displacement of the weight is not excessive, and then to have a low stiffness during excitation. The bases of the columns are subjected to vertical motion which is simple harmonic or a linear combination of two simple harmonic functions. The axial displacement transmissibility is computed, and the effects of external and internal damping, column stiffness, supported weight, and initial curvature are investigated. For the two-frequency excitation, the effects of the relative amplitudes and frequencies of the excitation

components are determined. Columns with pinned ends and with clamped ends are treated. A single column is considered first [6,7], and then a horizontal rigid bar supported by two columns is analyzed.

ACKNOWLEDGEMENT

REFERENCES

[1]   Plaut, R. H., Taylor, R. P., and Dillard, D. A., "Postbuckling and Vibration of a Flexible Strip Clamped at its Ends to a Hinged Substrate," International Journal of Solids and Structures, Vol. 41, No. 3, 2003, pp. 859-870.

[2]   Virgin, L. N. and Plaut, R. H., "Postbuckling and Vibration of Linearly-Elastic and Softening Columns Under Self-Weight," International Journal of Solids and Structures, Vol. 41, No. 18-19, 2004, pp. 4989-5001.

[3]   Holland, D., Virgin, L. N., and Plaut, R. H., "Postbuckling and Vibration of a Cantilevered Column Loaded by a Wire Passing Through the Base," presented at the Tenth Conference on Nonlinear Vibrations, Stability, and Dynamics of Structures, Blacksburg, Virginia, July 25-28, 2004.

[4]   Santillan, S., Virgin, L. N., and Plaut, R. H., "Equilibria and Vibration of a Heavy Pinched Loop," presented at the Tenth Conference on Nonlinear Vibrations, Stability, and Dynamics of Structures, Blacksburg, Virginia, July 25-28, 2004. Submitted for publication.

[5]   Plaut, R. H., "Postbuckling and Vibration of End-Supported Elastica Pipes Conveying Fluid and Columns Under Follower Loads," submitted for publication.

[6]   Sidbury, R. H., Plaut, R. H., and Virgin, L. N., "Analysis of Buckled and Pre-Bent Pinned Columns Used as Vibration Isolators," Proceedings of the 17th ASCE Engineering Mechanics Conference, June 13-16, 2004, Newark, Delaware.

[7]   Plaut, R. H., Sidbury, J. E., and Virgin, L. N., "Analysis of Buckled and Pre-Bent Fixed-End Columns Used as Vibration Isolators," Journal of Sound and Vibration, to appear.

Internally resonant dynamics of suspended cables: model validation, nonlinear normal modes, reduced order approximations

GIUSEPPE REGA AND NARAKORN SRINIL

Dipartimento di Ingegneria Strutturale e Geotecnica, Università di Roma "La Sapienza"
Via A. Gramsci 53, 00197 Roma, Italy

Nonlinear interaction effects characterizing the internally resonant finite amplitude dynamics of suspended cables have been a subject of considerable interest in the last fifteen years. With respect to system modelling, the following main situations have been considered: (i) horizontal and small sagged cables; (ii) condensed partial differential equations (PDEs) of planar motion obtained by linking the system longitudinal displacement field to the transversal one; (iii) low-order discretized models obtained from the PDEs of motion through an assumed mode Galerkin technique.

In turn, the solution of the ensuing ordinary differential equations (ODEs) has been accomplished through combined and comparative use of asymptotic and numerical procedures, which allowed the highlighting of many interesting nonlinear dynamic phenomena. At the same time, a number of meaningful experimental results have been obtained, and some recent purely numerical (finite difference based) investigations aimed at overcoming some of the above mentioned assumptions have been accomplished [1]. A comprehensive and updated review of the overall research activity on cable nonlinear dynamics has appeared very recently in the technical literature [2, 3].

Moving from the state-of-the-art in the field and attempting also to establish a link between analyses conducted in fairly different contexts [4], the present work deals, in principle, with the general class of arbitrarily inclined, sagged, and extensible cables for which no a priori assumptions are made as regards the order of displacement field components and the number of modes significantly contributing to system dynamics. With the perspective of still working in a basically analytical framework, which is deemed capable of enlightening the fundamental features of system nonlinear dynamics, approximate equations of motion valid for relatively small values of the cable sag-to-span ratio are considered, but a second-order asymptotic analysis of the ensuing approximate ODEs of free motion, capable of accounting for contributions from higher-order modes, is accomplished. In the background, as useful comparison elements for the analytical outcomes, "exact" numerical results of the original PDEs of motion provided by a companion multi-degree-of-freedom model are referred to.

Amongst various meaningful internal resonance conditions occurring in the actual planar and non-planar free vibrations of suspended cables, the planar 2:1 resonance is addressed. As a matter of fact, it describes a dynamic scenario typically occurring in both horizontal and inclined cables, while at the same time being a resonance case where it makes sense to develop an asymptotic analysis accounting for the higher-order effects of system quadratic nonlinearities.

An infinite-dimensional Galerkin discretization of the solution of the PDEs of motion is performed, and a second-order asymptotic analysis of the ODEs is accomplished through the method of multiple scales. Frequency-amplitude relationships and space-time dependent coupled configurations associated with the resonant nonlinear normal modes of the system are determined.

By accounting for also the effect of the assumed continuum model, the results of systematic parametric analyses made to investigate the actual activation of the considered internal resonance are discussed for both horizontal and inclined cables having different system parameters and involving different resonant modes in the interaction (see Fig. 1, $\lambda/\pi \approx$ 1.28, 2.95, 3.23, 5.48). Remarkably qualitative differences are seen to occur between horizontal and inclined cables as regards the nonlinear interaction effects of a characterizing issue of the relevant planar linear dynamics, namely the modification from crossover to avoidance (veering) in the natural frequency spectrum along with the associated transition from purely symmetric/anti-symmetric (S/A) mode shapes to hybrid (asymmetric, H) mode shapes, as shown in Fig. 1.
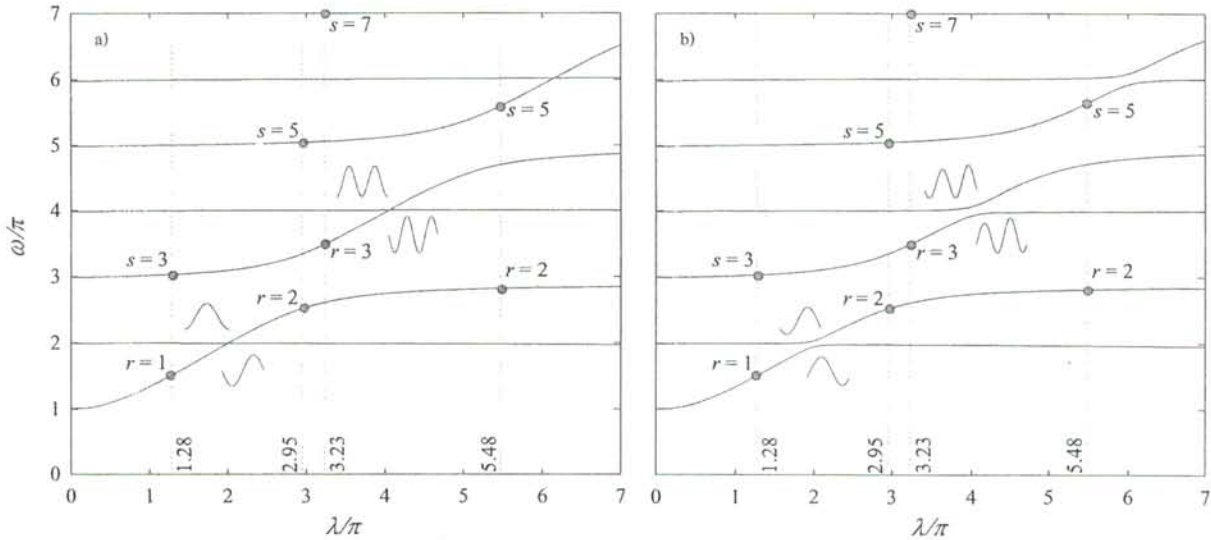
Figure 1 Crossover (S, A) and avoidance (H) phenomena (mode shapes) for a) horizontal and b) inclined cables, respectively: dotted lines denote non-crossover/avoidance resonant cable parameters λ/π and modes (r, s).

As a matter of fact, owing to the asymmetry effect of inclined equilibrium and to the associated asymmetrical modal functions, the nonlinear orthogonality condition of the modes is never satisfied and the pertinent resonance activation is nearly always possible, occurring over a wide range of the λ/π parameter. As an example, both analytical predictions and numerical results highlight that the nearly tuned 2:1 resonance involving the low-frequency (nearly) anti-symmetric first mode is activated around second avoidance ($\lambda/\pi \approx 4$) regardless of the involved high-frequency, hybrid, third or fourth mode. This outcome enlightens on the distinguishing dynamic characteristics of the inclined cable at second avoidance with respect to those of the horizontal cable at corresponding second crossover ($\lambda/\pi \approx 4$), whose 2:1 resonance is activated only when the high-frequency mode, out of the two coexisting modes, is symmetric.

The significant effects of cable sag, cable inclination and cable extensibility on the asymptotic solutions as well as on the system nonlinear behaviour are investigated, and the meaningful contribution from longitudinal displacement dynamics is highlighted. The space-time variability of the system dynamic configuration and the nonlinear dynamic tension is addressed. When considering a finite number of modes in the Galerkin expansion, analysis of the modal convergence properties of the asymptotic solutions allows us to discuss the important issue of the proper selection of a reliable reduced-order model of the actual continuum system.

Specifically, the work aims at contributing on the following main aspects of cable nonlinear dynamics: (i) *model validation* at the continuum level, (ii) characterization of the *nonlinear normal modes* in a meaningful condition of internal resonance, and (iii) identification of proper - and possibly minimal - *reduced-order models* to be reliably referred to in finite-dimensional analyses.

The first issue is addressed by comparing the results obtained analytically for the horizontal cable with either the condensed or the full (non-condensed) model (namely, by considering dependent *vs* independent cable longitudinal displacement fields), and by validating them through independent, purely numerical investigations. Also the outcomes of using either approximate or exact non-condensed PDEs for the inclined cable are compared. This allows us to obtain basic information about whether and when it is actually necessary/possible to consider full/condensed or exact/approximate sets of PDEs.

The second issue is dealt with by referring to the full continuum model of either horizontal or arbitrarily inclined cables, and by considering different values of the cable elasto-geometric parameter (which accounts for the variability of its sag-to-span ratio, extensibility and angle of inclination). Frequency-amplitude and dynamic configuration relationships characterizing cable steady motion are obtained analytically, and are compared with the numerical results of companion finite difference investigations aimed at confirming the analytically detected features as regards internal resonance activation, internally resonant softening/hardening behaviour of the structural system, modal interaction features, and space-time evolution of the response.

Finally, the third issue is addressed by performing systematic modal contribution and convergence analyses of the main dynamic characteristics of system response. These are aimed at distinguishing between (i) cases in which suitably reduced-order models, possibly accounting for even the solely two modes entering the reference 2:1 internal resonance, can be considered in a finite-dimensional analysis of cable dynamics without running the risk of withdrawing meaningful nonlinear phenomena, and (ii) cases wherein accounting for contributions from other, possibly higher-order, modes non-modelled in the theoretical analysis becomes mandatory to the aim of reliably describing the nonlinear dynamics.

Overall, as regards this aspect, it can be said that: (i) accounting for contributions from (higher-order) non-resonant modes is very important, unless a very low-sagged cable is considered; (ii) it may be enough to account for them in the nonlinear amplitude and frequency equations only, thereby developing a so-called improved first-order solution (or incomplete second-order solution), for relatively low-sagged cables; (iii) it is necessary to take them into consideration also in the nonlinear dynamic displacements (full second-order solution), as the effects of cable sag and/or cable inclination (asymmetry) become significant.

1. Srinil, N., Rega, G., Chucheepsakul, S., Large amplitude three-dimensional free vibrations of inclined sagged elastic cables, *Nonlinear Dynamics*, **33**, 129-154, 2003.
2. Rega, G., Nonlinear vibrations of suspended cables. Part I: Modeling and analysis, *Applied Mechanics Reviews*, **57**, 441-476, 2004.
3. Rega, G., Nonlinear vibrations of suspended cables. Part II: Deterministic phenomena, *Applied Mechanics Reviews*, **57**, 477-511, 2004.
4. Srinil, N., Large-amplitude three-dimensional dynamic analysis of arbitrarily inclined sagged extensible cables, Ph.D. Dissertation, King Mongkut's University of Technology Thonburi, Bangkok, Thailand, 2004.

Wire-screen belt vibrations in a paper machine

Yuichi SATO and Takuo NAGAMINE
Department of Mechanical Engineering
Saitama University
Saitama, Saitama, Japan
ysato@mech.saitama-u.ac.jp

In a paper machine, the fiber and water mixture flows onto a wire-screen belt as shown in Fig.1.   As the wire-screen belt travels horizontally, water is dripped through the screen and fibers are left on the screen. In some operating conditions large lateral vibrations of the wire-screen belt occurred.   The mechanism of this phenomenon is investigated.

The experimental apparatus is shown in Fig.2.   A sheet moves to the right at a constant speed v. Water flows out onto a sheet from a spout, which is 94 mm in width.   The displacement of the sheet is measured at the center of the span as shown in the figure.   Measured data are shown in Fig.3.
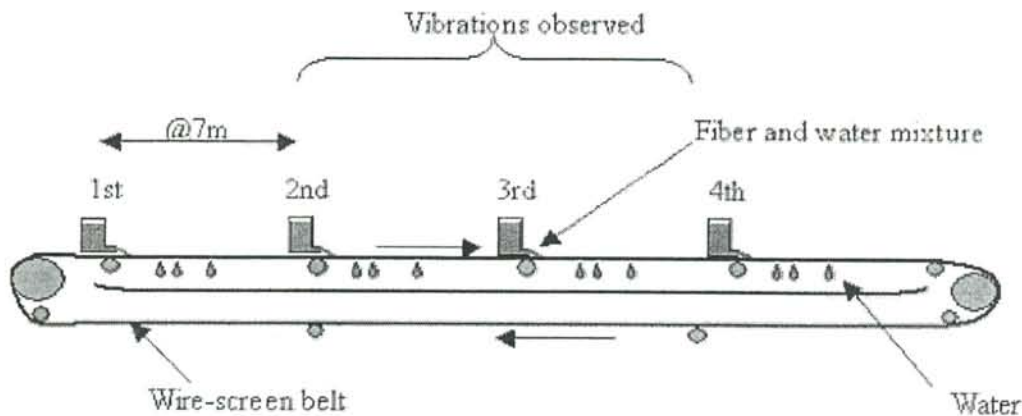
Fig.1   Schematic of a paper machine

Figure 3(a) shows the displacement measured at the mid-span of the traveling sheet when no water is fed.   The observed vibration is small.   When water is fed onto the sheet, the vibration became larger as shown in Fig.3(b).   Its dominant frequency is about 7 Hz lower than that of Fig.3(a) since the mass was increased by feeding water onto the sheet.   In Fig.3(c) vibration is shown when the sheet traveling speed is zero and the rate of water fed on the sheet was the same as in Fig.3(b).   Observed vibration is as large as Fig.3(b).   From these figures we note that feeding water causes sheet vibration whether the sheet travels or not.
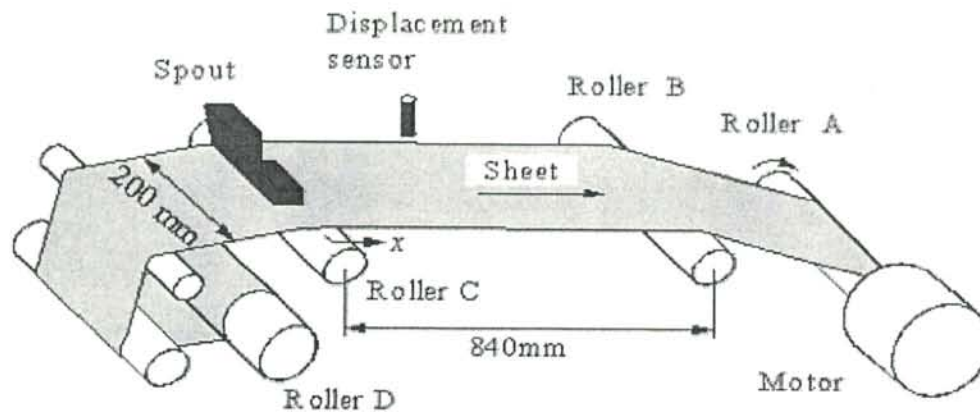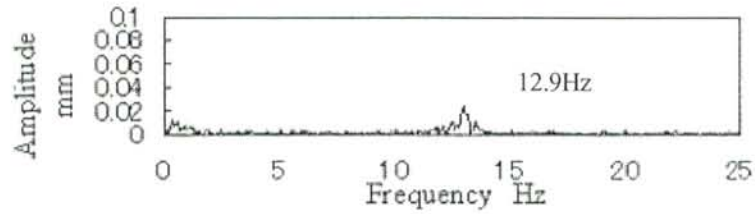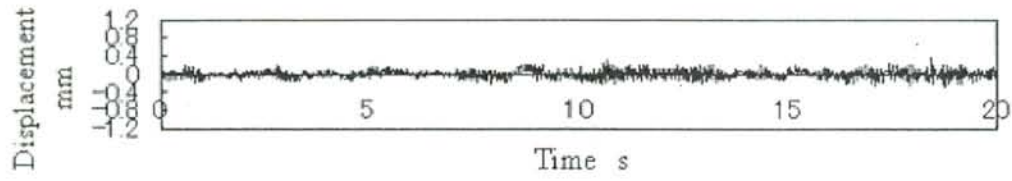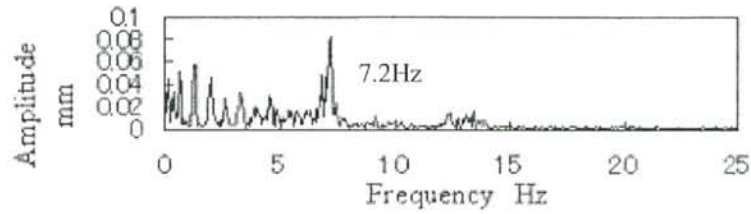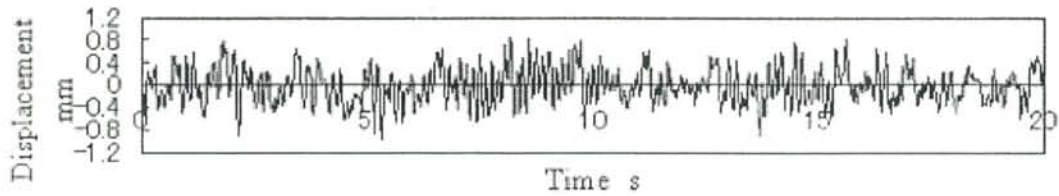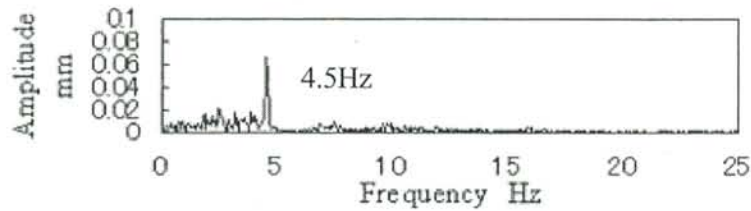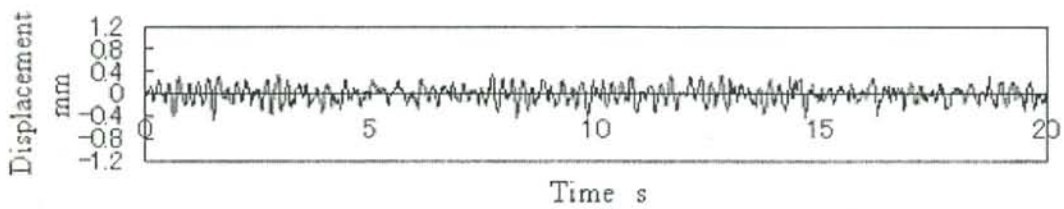

Fig. 2   Experimental apparatus

(a) Flow velocity = 0 mm/s, Sheet velocity = 164 mm/s

(b) Flow velocity = Sheet velocity =164 mm/s

(c) Flow velocity = 164 mm/s, Sheet velocity = 0 mm/s
Fig. 3 Experimental results of sheet displacement at x=420 mm

The equation of motion for sheet motion is expressed as,

$$\frac{\rho}{b}\left(\frac{\partial^2 u}{\partial t^2}+2v\frac{\partial^2 u}{\partial t\partial x}+v^2\frac{\partial^2 u}{\partial x^2}\right)-\frac{T}{b}\frac{\partial^2 u}{\partial x^2}-p-g\frac{\rho}{b}=0 \tag{1}$$

where

u : vertical displacement of the sheet, v : traveling speed of the sheet, T : tension of the sheet, b : width of the sheet, p : the pressure of the water acting on the sheet, ρ : sheet density. From experiment the rate of water dripping through the sheet is proportional to the pressure p acting on the sheet. Therefore the relation is expressed as,

$$-\rho_w\left(\frac{\partial h}{\partial t}+v\frac{\partial h}{\partial x}\right)=C_D p \tag{2}$$

where C_D is the permeability.

The pressure acting on the sheet consists of gravitational and inertial forces expressed as

$$p=\rho_w\left\{g-h\left(\frac{\partial^2 u}{\partial t^2}+2v\frac{\partial^2 u}{\partial t\partial x}+v^2\frac{\partial^2 u}{\partial x^2}\right)\right\} \tag{3}$$

where ρ_w is water density. The boundary conditions are

$$x=0 \ : \ u=0, h=h_* \tag{4a}$$
$$x=L \ : \ u=0. \tag{4b}$$

We assume the solutions of the equations (1)-(3) are expressed as

$$u=u_0(x)+\varepsilon u_1(x,t) \tag{5a}$$
$$h=h_0(x)+\varepsilon h_1(x,t) \tag{5b}$$

Using the following quantities,

$$U_i=u_i/u_*, \ \ H_i=h_i/h_* \ (i=1,2), \ \ X=x/L, \ \ \tau=\omega_* t \tag{6}$$

where $\omega_*=c_0/L$, $c_0=\sqrt{T/\rho}$, u_* and h_* are quantities for normalization.

Figure 4 shows the calculated sheet displacement at the mid span of the sheet and dimensionless water depth variation. We note that the phase of water depth variation is 90 degrees ahead of the sheet displacement. Therefore, sheet vibration is induced by the pressure variation of the water on the sheet.
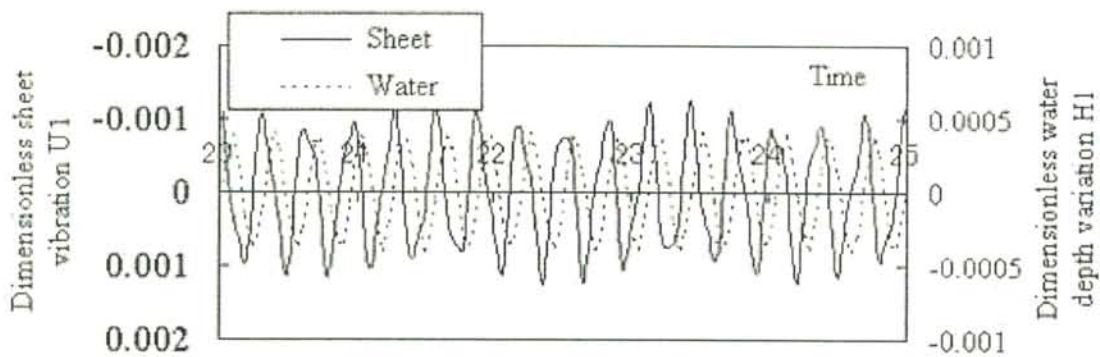

Fig. 4   Calculated sheet displacement $U_1=u_1/u_*$ at the mid-span of the sheet and dimensionless water depth variation $H_1=h_1/h_*$ where u_* and h_* are quantities for normalization

Ultrasonic motor based on longitudinal and torsional vibration

Wolfgang Seemann
Institut für Technische Mechanik
Universität Karlsruhe
Germany

Birgit Sauter, Youping Yi, Rainer Gausmann

In recent years several types of ultrasonic motors have been realized and used in industrial applications. The most common type is the traveling wave motor, in which a bending wave in a beam or plate is used to generate the motion of the rotor due to frictional forces. Other types of motors may be realized by a superposition of bending vibration and longitudinal vibration in a beam. Both in the traveling wave motor and in the other types of ultrasonic motors the vibration of the system is generated by piezoceramics, in which electrical fields are coupled with mechanical stress or strain. An overview can be seen for example in [1].

The aim of this presentation is to investigate an ultrasonic motor which is based on a superposition of longitudinal vibration and torsional vibration. This type of hybrid motor is supposed to have a high torque and a good efficiency. The working principle can be seen in figure 1. The voltages to excite the torsional vibration and the longitudinal vibration are shown in the upper part of the figure. The time at which the linetype changes from solid to dashed is the time which is shown below the voltage diagram. This figure also shows that the motor is constructed in such a way that it consists of one rotor and a stator on each side of the rotor. Two voltages are used to excite the vibration of the system: One is exciting the longitudinal vibration, the other voltage for the generation of the torsional vibration has a temporal phase shift of 90 degrees so that surface points of the stator move on elliptic orbits, figure 2. Each stator is driven by one piezoceramic ring in the longitudinal direction and another ring is used to excite the torsional vibration.
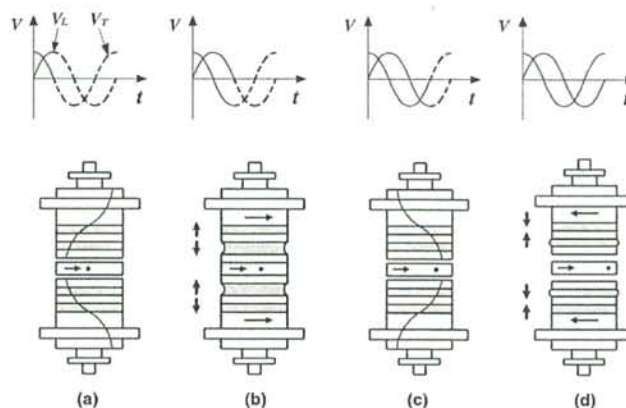

Figure 1: Working principle

For a good operation of the motor the amplitudes of the vibration may not be too small. Therefore, both the longitudinal and the torsional vibration should be excited in resonance
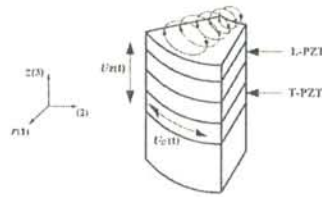
Figure 2: Trajectories of surface points of one of the stators

if possible. Thus the goal is that the eigenfrequencies of the corresponding modes coincide. However, as we know that the speed of longitudinal waves and the speed of torsional waves are quite different, it is necessary to have some additional design steps, which have to be undertaken. In this presentation a ring is attached to the stator which adds both inertia to the longitudinal motion and also to the torsional motion of the stator. The magnitude of influence, however, is different for varying diameters or lenghts of the ring. In order to get a first estimation of the eigenfrequencies of the stator an analytical approach in the form of an eigenvalue problem for both vibrations is used. As the system is symmetric with respect to the rotor it is sufficient to consider only one half of the system. As can be seen in figure 3 the model consists of six sections which are bonded together. The first section begins at the rotor and is characterized by the local coordinate z_6 in figure 3. The second section is the ceramic ring described by local coordinate z_5, which excites the longitudinal vibration, the third section (z_4)is the metallic part between the two ceramic rings, the fourth part is the ceramic which excites the torsional vibration. The corresponding coordinate is z_3. The sixth section with local coordinate z_2 is the metallic part between the ceramic and the metallic ring and the last part with coordinate z_1 is between the ring and the end of the stator. Each of these sections with corresponding length ℓ_i is modeled with a rod theory which takes also into account the piezoelectric effect in the ceramics. One ceramic ring is poled in the axial direction to excite the longitudinal direction. The other ceramic is poled in the circumferential direction to generate the torsional vibration. In reality a ring cannot be poled in circumferential direction so that it has to be approximated by several segments which are poled in a direction normal to the electrodes. In addition, for the eigenvalue problem the transition conditions between the segments are important. They are given by a continuity of displacement and rotational angle and by force or moment equilibrium. Especially the piezoelectric excitation and the influence of the rigid ring enter through these transition conditions. Also the boundary conditions are important. For the longitudinal vibration it is supposed that at the end towards the stator we have a rigid boundary whereas the other end is supposed to be free. For the torsional vibration both ends are assumed to be free.

Results are obtained for different variations of all parameters. For example, in figure 4 the eigenfrequencies for longitudinal vibration and torsional vibration are plotted as a function of the position of the ring. Other parameter variations may be done similarly.

[1] S. Ueha, Y. Tomikawa, *Ultrasonic Motors: Theory and Applications*, Clarendon Press, Oxford, 1993

[2]Youping Yi, W. Seemann, R. Gausmann, Jue Zhong, *A method for matching the eigenfrequencies of a hybrid piezoelectric motor*, Ultrasonics, to appear.
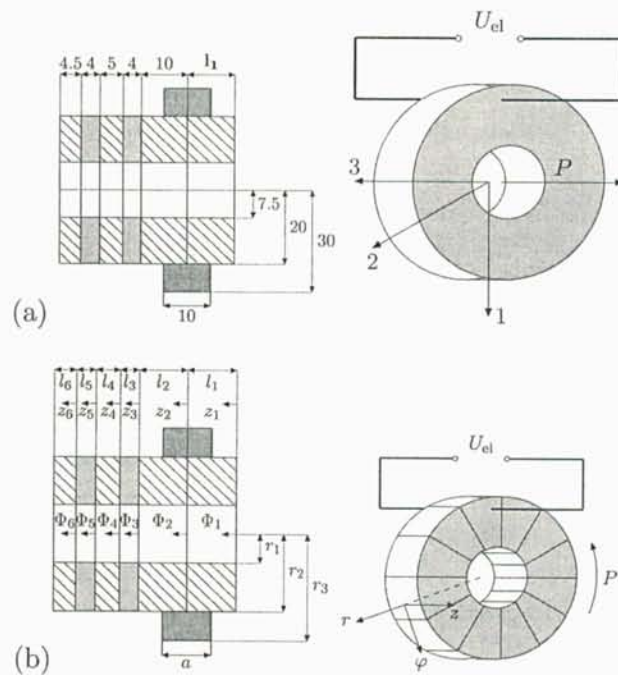
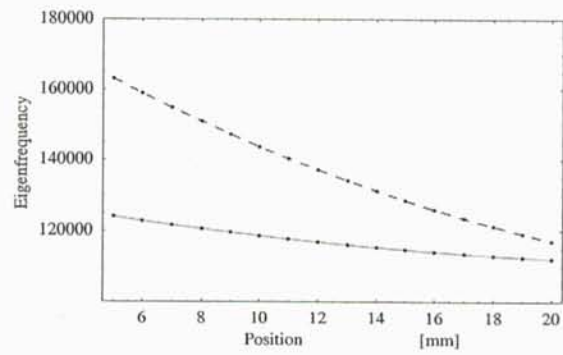Figure 3: Models for longitudinal (a) and torsional (b) vibrations

Figure 4: Eigenfrequencies of torsional and longitudinal vibrations for changing position ℓ_2 of the ring

NATURAL FREQUENCIES OF ROTATING AND NON-ROTATING FGM CIRCULAR CYLINDRICAL SHELLS

C.B. Sharma and M.N. Naeem

Department of Mathematics, UMIST, Manchester, M60 1QD, UK.

Introduction

The study of vibration characteristics of thin circular cylindrical shells is unarguably a very important branch of research in structural dynamics. In this paper vibration frequencies of rotating as well as non-rotating cylindrical shells are analysed. The shells are made out of a simplest form of functionally graded material (FGM) with only two common material constituents (stainless steel and nickel) which gradually change from one to another through the shell thickness. Apart from the simply supported conditions, where the closed form solutions are available, approximate solutions are sought for some other commonly occurring boundary conditions. The well established Rayleigh-Ritz method is adopted along with relevant Ritz polynomials (introducing axial dependence) to study the vibratory behaviour of non-rotating FGM shells. [1] The frequency spectrum of rotating FGM shells is analysed by utilizing Hamilton's principle. Budiansky and Sanders [2] shell equilibrium equations which include centrifugal and coriolis forces are considered here for rotating shells. To introduce the FGM characteristics, a volume fraction law is utilised to take into account the variation in constituent materials composition. In this case, axial modal dependence is characterized by the characteristics beam functions. Circumferential dependence of modal forms is assumed to be of harmonic type. The eigenvalue problem is formulated using Galerkin's procedure. Frequency parameters calculated here are compared, where possible, with corresponding results available in contemporary literature. Very good agreement is found to exist between various sets of results.

FGM Concept (Volume Fraction Law)

Like many biological materials found in nature which have FGM properties based on environmental conditions, the FGMs considered are fabricated from two or more material constituents according to the prevailing conditions such as high temperature conditions, a highly corrosive environment, and requirements like toughness, durability and machinability etc.

For a FGM fabricated from k constituent materials a particular property P can be expressed in the form

$$P = P_i V_i \qquad (i = 1, 2..., k) \tag{1}$$

where P_i and V_i are the material property and volume fraction of the ith constituent and for the repeated index i in equation (1) summation convention is implied. It is also obvious from the volume fraction assumption

$$\sum_{i=1}^{k} V_i = 1.$$

The volume fraction for a cylindrical shell is defined by the expression

$$V = \left((2z + h)/2h\right)^p \tag{2}$$

where h is the uniform thickness of the shell with the reference middle surface and p is the power law exponent, $0 \le p \le \infty$. Here, a circular cylindrical shell fabricated using the simplest FGM consisting of two material constituents is considered. The material properties, E ν and ρ of the FGM are expressed as the functions of E_1, E_2, v_1, v_2 and ρ_1, ρ_2, which are Young's moduli, Poisson's ratio and mass densities for the materials 1 and 2 respectively:

$$E = (E_1 - E_2)((2z + h)/2h)^p + E_2, \quad v = (v_1 - v_2)((2z + h)/2h)^p + v_2 \tag{3}$$
$$\rho = (\rho_1 - \rho_2)((2z + h)/2h)^p + \rho_2$$

The material properties of the shell vary continuously from the material 2 at the inner surface to material 1 at the outer surface. It is obvious that at the inner surface $z = -h/2$, $E = E_2$, $v = v_2$ and $\rho = \rho_2$ (material 2) and at the outer surface $z = h/2$, $E = E_1$, $v = v_1$ and $\rho = \rho_1$ (material 1), where $z = 0$ corresponds to the middle surface of the shell. A cylindrical shell fabricated of functionally graded material is essentially an inhomogeneous shell consisting of a mixture of isotropic materials. Unlike shells laminated of fibre-reinforced material where transverse shear deformation effects can be significant, for a FGM shell, a classical thin shell theory is applicable if radius-to-thickness ratio is ≤ 20.

Outline of Solution Procedure

In this piece of research, the theoretical formulation is based on the *best* first order thin shell theory [2] adapted for a FGM shell. Strain and kinetic energy expressions are derived taking into account asymmetry of material properties about the shell mid-surface due to the presence of coupling stiffnesses, which are zero for homogeneous isotropic shells. In this case of a rotating shell, the kinetic energy expression also includes the terms pertaining to centrifugal and coriolis actions. The initial hoop tension, a product of the centrifugal force, is included here. Hamilton's principle is then employed to derive the governing equations of motion. These are then written in terms of displacement functions for a rotating shell. For the resulting partial differential equations a general travelling wave solution is sought by the *product method*. In the modal forms, axial modal dependence is assumed in the form of characteristic functions of a vibrating beam, to facilitate the study of the influence of boundary conditions on shell vibration characteristics. Subsequently, Galerkins procedure is applied to derive the ensuing eigenvalue problem. This then is solved using a MATLAB software. As usual, eigenvalues and eigenvectors correspond to frequency parameters and modal forms respectively.

Results and Discussion

The influence of boundary conditions, rotating speed, shell geometrical and material parameters and circumferential wave numbers on the shell vibration characteristics are studied but, due to the space limitation, only the frequency parameter is discussed here. In order to check the accuracy of the present method, comparisons of natural frequencies are made with those found in the contemporary literature. Some of these were presented for non-rotating FGM shells in [1] for different boundary conditions and excellent agreement was noted between the two sets of results. In Table 1, a comparison of frequency parameter Δ for an infinitely long rotating isotropic cylindrical shell of given parameters is made with the results given in Chen et al [3]. Here Δ_b and Δ_f denote the frequencies of backward and forward travelling waves respectively for rotating velocity, $\Omega = 0.05$ cps. Clearly excellent agreement between the two sets of results is observed. Table 2 corresponds to the data identical with those in Table 1 except that the rotating velocity, $\Omega = 1$ cps. Once again the two sets of frequencies agree very well with each other.

The difference in the corresponding results of Tables 1 and 2 is due to the difference in rotating velocities. It is seen that Δ_b is slightly increased while Δ_f is slightly decreased due to the increased rotating velocity, Ω. It may be remarked that the value of the frequency for *backward* wave is slightly higher than that for a *standing* wave whereas for *forward* wave the reverse is the case. Also the variation of *backward* and *forward* frequency parameters with the circumferential wave number, n, is found to be of a similar nature as for a non-rotating shell.

Table 1 Comparison of frequency parameters Δ for an infinitely long rotating isotropic shell: ($R/h = 500$, $E = 1.83 \times 10^{11}$ N/m^2, $v = 0.3$, $\rho = 7492 kg/m^3$, $m = 1$, $\Omega = 0.05$ cps)

n	Chen et al [3]	Present	Chen et al [3]	Present
	Δ_b		Δ_f	
2	0.0015569	0.0015569	0.0015415	0.0015414
3	0.0043876	0.0043876	0.0043760	0.0043760
4	0.0084062	0.0084062	0.0083971	0.0083971
5	0.0135910	0.0135910	0.0135836	0.0135836
6	0.0199355	0.0199354	0.0199292	0.0199292

Table 2. Comparison of frequency parameters Δ for an infinitely long rotating isotropic shell: ($R/h = 500$, $E = 1.83 \times 10^{11}$ N/m^2, $v = 0.3$, $\rho = 7492 kg/m^3$, $m = 1$, $\Omega = 1$ cps)

n	Chen et al [3]	Present	Chen et al [3]	Present
	Δ_b		Δ_f	
2	0.0017127	0.0016897	0.0014039	0.0013808
3	0.0045012	0.0044911	0.0042695	0.0042595
4	0.0084945	0.0084888	0.0083128	0.0083071
5	0.0136628	0.0136591	0.0135144	0.0135107
6	0.0199958	0.0199932	0.0198706	0.0198680

Figures 1 and 2 show the variation of natural frequency Ω with the circumferential wave number n for a rotating FGM shell with radius to thickness ratio $R/h = 500$, axial wave number $m = 1$ and the power law exponent $p = 1$. These two sets of figures correspond to rotation speed $\Omega = 5, 15 cps$ respectively. The upper and lower curves (shown by solid and dotted lines) correspond to the frequencies for backward and forward travelling waves respectively.
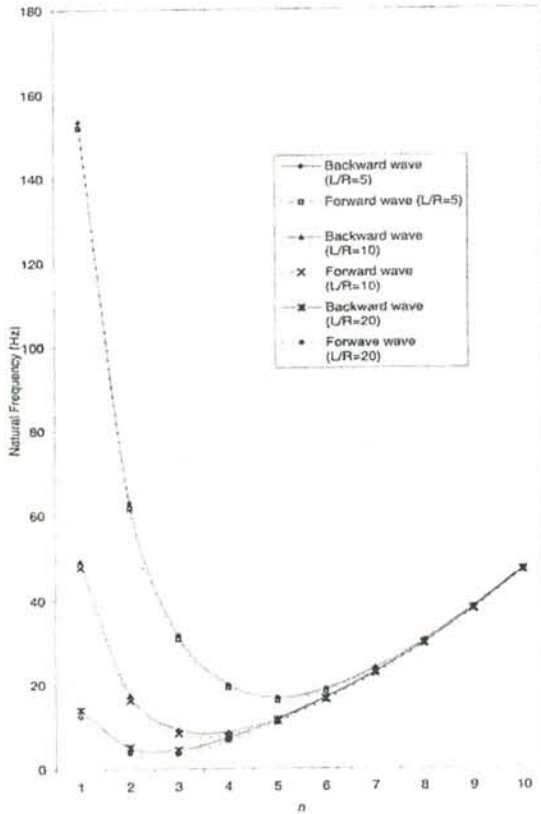

Fig. 1 Variation of natural frequency (Hz) with circumferential wave number n
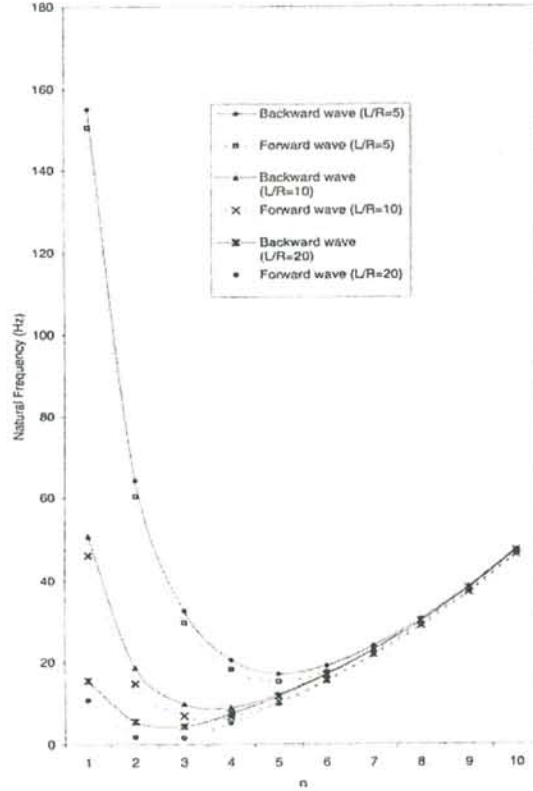$(R/h = 500, m = 1, p = 1, \Omega = 5)$

Fig. 1 Variation of natural frequency (Hz) with circumferential wave number n
$(R/h = 500, m = 1, p = 1, \Omega = 15)$

From these two figures, it is apparent that for a rotating shell the trend of frequency variation with circumferential wave number n resembles that observed for a stationary cylindrical shell. However frequencies for backward travelling waves are in general on a higher side than those for a stationary cylindrical shell, whereas the converse is true for the frequencies for forward travelling waves. It is also seen that the difference in frequencies between the corresponding backward and forward frequency curves is more noticeable for low $n - values$ and it decays gradually with increasing n. The two sets of curves appear to coincide with each other for higher $n - values$. This behaviour is also a *function* of parameters L/R and Ω. The frequency curves appear far more separated for higher values of L/R than for its lower values. This separation between two sets of frequency curves is also enhanced with rotating speed Ω. It may further be remarked that, as for a non-rotating shell, the frequency parameters for a rotating shell also decrease with p, the power law exponent. This decrement in frequency parameters is mainly the result of the arrangement of the constituent materials forming a FGM shell.

References

1. Sharma C B, Natural frequencies of thin FGM cylindrical shells. Proceedings ICCE-10, July 20-26, 2003, New Orleans, LA, USA, pp 645-646.
2. Budiansky B, Sanders J L, On the *best* first order linear shell theory, Progress in Applied Mechanics (The Prager Anniversary Volume), **192**, MacMillan Inc. pp 129-140, 1963.
3. Chen Y, Zhao H B and Shen Z P, Vibrations of high speed rotating shells with calculations for cylindrical shells, Journal of Sound and Vibration, **160**, pp 137-160, 1993.

VIBRATION AND BUCKLING OF PLATES BY P-TYPE METHOD

A. V. Singh[*] and T. Muhammad
Department of Mechanical and Materials Engineering
The University of Western Ontario
London, Ontario, Canada, N6A 5B9

* Corresponding author. Tel.: + 1-519-661-2111; fax: + 1-519-661-3030
E-mail address: avsingh@eng.uwo.ca (A. V. Singh)

This paper presents an application of p-type numerical method to the vibration and buckling analyses of first order shear deformable doubly connected plates as shown in the following figure. The middle plane of an arbitrarily shaped plate with an opening is divided into three quadrilateral sub-regions as an example. The thickness (h) of the plate is assumed to be uniform and small in comparison with the other in-plane dimensions.
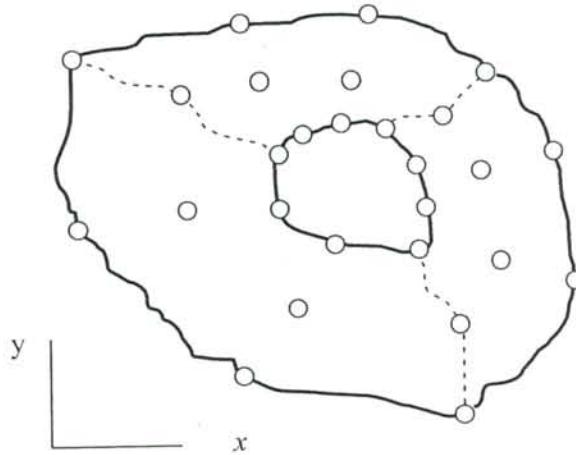

Figure. Middle plane of a doubly connected plate divided into three quadrilateral sub-regions.

The coordinates (x, y) of an arbitrary point inside the quadrilateral region are interpolated using polynomials in the natural coordinates ξ and η, [$-1 \leq (\xi,\eta) \leq +1$] which are very specific to the sub-region in which they are defined. The orders of the interpolating functions will depend upon the four boundaries of the quadrilateral sub-region and the geometric nodes that are selected to define the geometry accurately. The number of geometric points used to define a sub-region will depend upon the type of curvilinear edges it has and the points can lie on the boundary as well as in the interior. By using the prescribed coordinates (x_i, y_i) of the geometric points and the shape function $N_i(\xi,\eta)$ with $i = 1,2,3,\cdots,n$, the coordinates can be represented as shown below(Weaver and Johnson [1]).

$$x = \sum_{i=1}^{n} N_i(\xi,\eta)x_i \; ; \; y = \sum_{i=1}^{n} N_i(\xi,\eta)y_i \tag{1}$$

In the first order shear deformable plate bending theory, the primary unknowns are the three displacement components (u, v, w) at the middle plane in the (x, y, z) directions respectively and the two components (β_1, β_2) of the rotation of the normal to the middle surface. These primary variables are also interpolated, in the manner similar to the coordinates of an arbitrary point on the middle plane.

$$u = \sum_{i=1}^{p} f_i(\xi, \eta) U_i \; ; \; v = \sum_{i=1}^{p} f_i(\xi, \eta) V_i \; ; \; w = \sum_{i=1}^{p} f_i(\xi, \eta) W_i \; ;$$

$$\beta_1 = \sum_{i=1}^{p} f_i(\xi, \eta) \theta_i \; ; \; \beta_2 = \sum_{i=1}^{p} f_i(\xi, \eta) \phi_i \tag{2}$$

In the above equations, $f_i(\xi, \eta)$ is the displacement shape function and $U_i, V_i, W_i, \theta_i,$ and ϕ_i correspond to $u, v, w, \beta_1,$ and β_2 respectively at the *ith* displacement node. It should be noted here that much higher order polynomials are used for displacement components than the interpolation of the coordinates and the displacement nodes are defined separately from the geometric nodes. If ℓ and m denote respectively the orders of the polynomials in ξ and η, the number of displacement nodes required is: $p = (\ell + 1)(m + 1)$.

Using the standard procedure of the Rayleigh-Ritz method, the stiffness matrix $[K]$ and mass matrix $[M]$ can be derived for each sub-region of the plate and then assembled appropriately to obtain the matrix equation of motion, $[M]\{\ddot{\Gamma}\} + [K]\{\Gamma\} = 0$, for the free vibration. The numerical results are then obtained for the dimensionless frequency $\lambda = \omega a^2 \sqrt{\rho h / D}$ for various plates. Here, $\{\Gamma\}$ = displacement vector, a = length of the square plate, ρ = mass density, ω = circular frequency and D = flexural rigidity of the plate. In the analysis of a plate problem by the present method, the defined geometry will consist of a pre-selected number of quadrilaterals and remain fixed. The accuracy in the results is improved by increasing the orders of the polynomials interpolating the displacement components $u, v, w, \beta_1,$ and β_2. A convergence study is normally performed before getting results for different cases. By this method, a plate without the hole can also be analyzed using only one quadrilateral domain.

Table. Dimensionless natural frequency $\lambda = \omega a^2 \sqrt{\rho h / D}$ for a square plate with a circular hole at the center.

Mode	CCCC		CFCF		SFSF	
	P-M	I-DEAS	P-M	I-DEAS	P-M	I-DEAS
1	37.52	37.41	22.39	22.39	9.29	9.29
2	125.22	125.25	43.34	43.30	35.67	35.66
3	145.77	144.97	118.56	118.61	87.58	87.58
4	230.77	230.33	137.48	137.29	122.37	122.43
5	290.11	289.89	159.48	158.70	140.72	139.93

As a numerical example, the natural frequencies of a square plate with a circular hole at the centre are calculated using only one quarter of the geometry and two quadrilateral sub-

regions. The use of symmetry conditions with regards to geometry, boundary and loading has been made in the analysis. Second order polynomials are used to define each of the two quadrilateral segments of the plate and tenth order polynomials are used to describe the displacement fields given by Eq. (2). The parametric values used for this example include: Poisson's ratio (v) = 0.3, thickness to length ratio (h/a) = 0.01, and hole diameter to length ratio (d/a) = 0.25. Three combinations of the boundary conditions, namely all sides clamped (CCCC), clamped-free-clamped-free (CFCF) and simply supported-free-simply supported-free (SFSF), have been used for the analysis of the plate. The values of the frequencies were also calculated by the finite element method using the computer codes I – DEAS [2]. Eight – node parabolic elements were used to perform the FE analysis. The table shows excellent agreement between the results from the two methods.

Buckling analysis of plates and shells can also be performed using the present method. In the case of a plate buckling problem, the linear stiffness and load matrices are required. It is assumed here that the plate is divided into few quadrilateral regions, subjected to an in-plane compressive load, and analyzed first to obtain the in-plane stresses σ_x, σ_y and τ_{xy} which are then known for all locations on the middle plane of the plate. The expression for the work done on the plate under in-plane load for its bending is used to calculate the buckling load matrix $[L]$ (Bulson[3]).

$$T = \frac{1}{2} h \iint_{Area} \left\{ \frac{\partial w}{\partial x} \quad \frac{\partial w}{\partial y} \right\} \begin{bmatrix} \sigma_x & \sigma_{xy} \\ \sigma_{xy} & \sigma_y \end{bmatrix} \left\{ \begin{array}{c} \frac{\partial w}{\partial x} \\ \frac{\partial w}{\partial y} \end{array} \right\} dxdy \tag{3}$$

While integrating for $[L]$, the state of in-plane stress at each integration point in each of the quadrilateral region is known from the analysis mentioned above using only the displacement fields for u and v. Taking the variation of the potential energy, one can easily derive the following equilibrium equation $([K] + P_{cr} [L])\{\Gamma\} = 0$, which is an eigen-value problem. The symbol P_{cr} = the critical in-plane load applied to the edge of the plate. It is a standard practice to calculate the values of the buckling coefficient $k = P_{cr} b / (\pi^2 D)$ for plate buckling problems. The buckling coefficient has been calculated for rhombic and square plates subjected to different boundary and loading conditions and will be presented.

References

[1] W. Weaver, Jr. and P. R. Johnston, 1984, Finite Elements for Structural Analysis, Prentice Hall Inc., Englewood Cliffs, NJ.

[2] I-DEAS Master Series™, Structural Dynamics Research Corporation, Milford, OH .

[3] P. S. Bulson, 1970, The Stability of Flat Plates, Chatto and Windus, London, GB.

A NEW RELATIONSHIP BETWEEN LINEAR AND TRANSCENDENTAL EIGENPROBLEMS

F.W. Williams[*], D. Kennedy[*], M.S. Djoudi[*], S. Yuan[**]

[*]Cardiff School of Engineering, Cardiff University, Cardiff CF24 3AA, U.K.
[**]Department of Civil Engineering, Tsinghua University, Beijing 100084, China

Exact solutions are often available for natural frequency, critical buckling and wave propagation problems, i.e. the discretisation errors and other approximations of methods such as FEM are avoided. The same is true for many related problems in other disciplines, although this paper is simplified by giving detail only for the vibration of rigidly jointed plane frames. Exact solutions can be obtained because uniform members of frames have differential equations which can be solved to obtain member equations which relate the amplitudes of the sinusoidally varying forces and displacements at their ends. The member equations [1] involve transcendental functions of the eigenparameter λ, i.e. of frequency squared, and of the mass per unit length of the member. Thus a dynamic overall stiffness matrix $\mathbf{K}(\lambda)$ results when such members are assembled to form a frame and there is no need for the separate mass matrix $\mathbf{M}$ of the finite element method (FEM). Hence *the linear (algebraic) eigensolvers used by FEM and other approximate methods cannot be applied and so it is necessary to use instead the Wittrick-Williams (or W-W) algorithm [1]*, which is theoretically proven to always give the number of eigenvalues exceeded by any trial value of λ and so has yielded many secure methods for converging on the eigenvalues. The use of the W-W algorithm is essential as otherwise there will certainly be structures for which some (very exceptionally all!) of the eigenvalues will be missed, e.g. when performing the computational equivalent [2] of finding the zeros of a plot of $\mathrm{Det}\{\mathbf{K}(\lambda)\}$.

Hypothetically, the same exact results could alternatively be obtained by solving an appropriately formulated FEM problem of infinite order on a computer of infinite accuracy and this idea was used in an early alternative proof of the W-W algorithm [3]. However, although methods of varying sophistication [4,5] have been developed for finding the eigenvectors, i.e. the modes of vibration, of the transcendental eigenproblem a complete analogy with this hypothetical linear eigenproblem appears never to have been presented and used for this purpose. This is one reason why only very recently [6] has it been possible to obtain the eigenvectors with matching degrees of certainty, reliability and accuracy to those that the W-W algorithm has always given for the associated eigenvalues. Briefly, this paper indicates an inverse iteration method based on the above analogy and which hence probably gives the closest relationship that it is possible to obtain between linear and transcendental eigensolvers, one consequence being that it shares the almost machine accuracy mode finding ability of the recent method just mentioned [6], which can be interpreted as being a much simplified form of the method presented here.

The hypothetical linear eigenproblem is

$$(\mathbf{K} - \lambda \mathbf{M})\, \mathbf{D} = 0 \tag{1}$$

where $\mathbf{K}$, $\mathbf{M}$ and $\mathbf{D}$ are, respectively, the static stiffness matrix, the mass matrix and the displacement amplitude vector, with $\mathbf{K}$ and $\mathbf{M}$ being symmetric and with $\mathbf{K}$ additionally being positive definite.

Linear eigensolvers, e.g. inverse iteration, can involve computations close to, rather than exactly at, an eigenvalue so that the null right hand side of Eq. (1) becomes suitably non-null, see

Eq. (2) for which $(\mathbf{K} - \lambda\mathbf{M})$ can be partitioned as in Eq. (3). (Early mode finding for the transcendental equivalent of Eq. (2), i.e. when $(\mathbf{K} - \lambda\mathbf{M})$ is replaced by $\mathbf{K}(\lambda)$, solved it for a single randomly chosen value of $\mathbf{P}$ and so was called the random force vector method [4,5].)

$$(\mathbf{K} - \lambda\mathbf{M})\,\mathbf{D} = \mathbf{P} \tag{2}$$

$$\mathbf{K} = \begin{bmatrix} \mathbf{K}_{ii} - \lambda\mathbf{M}_{ii} & \mathbf{K}_{ic} - \lambda\mathbf{M}_{ic} \\ \mathbf{K}_{ic}^T - \lambda\mathbf{M}_{ic}^T & \mathbf{K}_{cc} - \lambda\mathbf{M}_{cc} \end{bmatrix} \begin{array}{l} \}\text{order } N, \to \infty \\ \}\quad \text{order } n \end{array} \tag{3}$$

Here the subscript c indicates degrees of freedom at the joints of the frame, while i indicates interior freedoms of the members, i.e. all other freedoms.

Members are only connected to joints at their two ends. Hence the $\mathbf{K}_{ii} - \lambda\mathbf{M}_{ii}$ of Eq. (3) is block diagonal, with one block per member. Similarly, $\mathbf{K}_{ic} - \lambda\mathbf{M}_{ic}$ also receives one block per member, which is uncoupled from the block from any other member, but is not diagonal, not least because it is not square. It is physically obvious that as $N \to \infty$ the mass within $\mathbf{M}_{ii}$ approaches the total mass of all of the members. Therefore the effect of $\mathbf{M}_{ic}$ becomes infinitesimal and so it can be ignored without loss of accuracy. Similarly, $\mathbf{M}_{cc}$ receives infinitesimal contributions from the members and so consists solely of any lumped masses attached at the nodes. Hence Eqs. (1) and (2) give

$$\begin{bmatrix} \mathbf{K}_{ii} - \lambda\mathbf{M}_{ii} & \mathbf{K}_{ic} \\ \mathbf{K}_{ic}^T & \mathbf{K}_{cc} - \lambda\mathbf{M}_{cc} \end{bmatrix} \begin{bmatrix} \mathbf{D}_i \\ \mathbf{D}_c \end{bmatrix} = \begin{bmatrix} \mathbf{P}_i \\ \mathbf{P}_c \end{bmatrix} \tag{4}$$

Hence eliminating $\mathbf{D}_i$ by the arrested form of Gauss elimination, usually used when computing, gives

$$\begin{bmatrix} (\mathbf{K}_{ii} - \lambda\mathbf{M}_{ii})^U & \mathbf{K}_{ic}^* \\ \mathbf{0} & \mathbf{K}_c(\lambda) \end{bmatrix} \begin{bmatrix} \mathbf{D}_i \\ \mathbf{D}_c \end{bmatrix} = \begin{bmatrix} \mathbf{P}_i^* \\ \mathbf{P}_c(\lambda) \end{bmatrix} \tag{5}$$

where superscripts U and $*$ respectively denote the upper triangular form and the modified form of matrices given by the Gauss elimination. Hence when $\mathbf{P}_i = \mathbf{0}$, so that $\mathbf{P}_c(\lambda) = \mathbf{P}_c$, i.e. in free vibration problems, for which the members do not carry sinusoidally time dependent forces, the second row of Eq. (5) gives

$$\mathbf{K}_c(\lambda)\mathbf{D}_c = \mathbf{P}_c \tag{6}$$

Equation (6) gives the exactly correct $\mathbf{P}_c$ (i.e. without discretisation errors) for any of the infinitely large number of possible choices of $\mathbf{D}_c$. Hence, because the transcendental formulation gives an equation identical to Eq. (6) except that $\mathbf{K}(\lambda)$ replaces $\mathbf{K}_c(\lambda)$, it follows that $\mathbf{K}(\lambda)$ must be identical to $\mathbf{K}_c(\lambda)$. Therefore the transcendental eigenproblem and the hypothetical infinite order linear eigenproblem are analogous, in the sense that if they were both to be solved with equal care they would yield identical eigenvalues and eigenvectors. However a crucial difference is that

the transcendental eigenproblem is solvable in the real world, whereas the hypothetical infinite order linear eigenproblem is not. Importantly, this enables inverse iteration to be applied to the transcendental eigenproblem to obtain essentially the same near machine accuracy modes as would be given by solving the hypothetical infinite order FEM problem on a computer of infinite accuracy. Space limitations prevent the method being given in full, but it is indicated as follows.

Using r as the iteration counter, the key equation when inverse iteration is applied to the hypothetical linear eigenproblem of Eq. (1) (see also Eq. (4)) is

$$\begin{bmatrix} \mathbf{K}_{ii} - \lambda^r \mathbf{M}_{ii} & \mathbf{K}_{ic} \\ \mathbf{K}_{ic}^T & \mathbf{K}_{cc} - \lambda^r \mathbf{M}_{cc} \end{bmatrix} \begin{bmatrix} \mathbf{D}_i^{r+1} \\ \mathbf{D}_c^{r+1} \end{bmatrix} = \begin{bmatrix} \mathbf{M}_{ii} & \mathbf{0} \\ \mathbf{0} & \mathbf{M}_{cc} \end{bmatrix} \begin{bmatrix} \mathbf{D}_i^r \\ \mathbf{D}_c^r \end{bmatrix} \qquad (7)$$

in which the RHS is known and consists of two vectors, which can be written as

$$\mathbf{P}_i^r = \mathbf{M}_{ii} \mathbf{D}_i^r, \qquad \mathbf{P}_c^r = \mathbf{M}_{cc} \mathbf{D}_c^r \qquad (8)$$

It was explained above that in the transcendental method (and in the hypothetical linear eigenproblem) $\mathbf{M}_{cc}$ consists solely of any lumped masses at the nodes and so $\mathbf{P}_c^r$ is readily computed when using the transcendental method. Then $\mathbf{P}_i^r$ is computed by numerical integration based on the mass per unit length that is equivalent to $\mathbf{M}_{ii}$.

The transcendental inverse iteration method briefly indicated above has been evaluated via problems chosen to be demanding and works well for all of them. A selection of these results will be presented.

References

1. Williams, F. W. and Wittrick, W. H., "An automatic computational procedure for calculating natural frequencies of skeletal structures", *Int. J. Mech. Sci.*, **12**, 1970, 781-791.
2. Williams, F.W., Yuan, S., Ye, K.S., Kennedy. D. and Djoudi, M.S., "Towards deep and simple understanding of the transcendental eigenproblem of structural vibrations", *J. Sound Vib.*, **256**, 2002, 681-693.
3. Wittrick, W. H. and Williams, F. W., "New Procedures for structural eigenvalue calculations", *Fourth Australasian Conf. on the Mechanics of Structures and Materials*, U. of Queensland, Brisbane, 1973, 299-308.
4. Hopper, C. T. and Williams, F. W., "Mode finding in nonlinear structural eigenvalue calculations". *J. Struct. Mech.*, 5, 1977, 255-278.
5. Ronagh, H. R., Lawther, R. and Williams, F. W., "Calculation of eigenvectors with uniform accuracy". *J. Eng. Mech. ASCE*, **121**, 1995, 948-955.
6. Yuan, S., Ye, K. S., Williams, F. W. and Kennedy, D., "Recursive second order convergence method for natural frequencies and modes when using dynamic stiffness matrices", *Int. J. Num. Meth. Engng.*, **56**, 2003, 1795-1814.